A STUDY OF THE COMPOUND NUCLEUS ^{7}Be

Thesis by
William Douglas Harrison

In Partial Fulfillment of the Requirements
For the Degree of
Doctor of Philosophy

California Institute of Technology
Pasadena, California
1966
(Submitted May 13, 1966)

ACKNOWLEDGMENTS

It is a pleasure to acknowledge the assistance of the Kellogg Radiation Laboratory faculty, staff, visitors, and students. The $^{6}Li(p, p)^{6}Li$ work was actually begun by Dr. A. Bruce Whitehead, and only the latter stages were a co-operative effort. The patient advice and encouragement of my advisor, Professor Charles A. Barnes, are appreciated, as are several useful discussions with Professors William A. Fowler and T. Lauritsen, and the invaluable assistance on several matters given by Professor T. A. Tombrello. On the theoretical side, considerable help was given by Professors Hans A. Weidenmueller, F. C. Barker, and J. Humblet. The assistance of staff, students, and a friend, in the form of advice, techniques, programs, design, and labor, has been so extensive that it must remain unheralded, but not unappreciated.

This work was supported by the Office of Naval Research [Nonr - 220(18) and Nonr - 220(47)].

ABSTRACT

Measurements were made of the differential cross section for the $^{6}Li(p, p)^{6}Li$ and $^{6}Li(p, p')^{6}Li(2.184\ MeV)$ reactions, of both the differential and the total cross section for the $^{6}Li(p, p'')^{6}Li^{**}(3.562$ MeV) reaction, and of the total cross section for the $^{4}He(^{3}He, p'')^{6}Li^{**}$ reaction. The ranges of incident particle laboratory energies were from 2.4 to 12.0 MeV, 3.6 to 9.4 MeV, 4.3 to 9.4 MeV, and 13.8 to 18.4 MeV respectively. Other measurements were made to determine the consistent relative normalization of these data and the data obtained by other investigators on ^{7}Be-forming reactions, and to determine the correct overall absolute normalization. The $^{6}Li(p, p)^{6}Li$ data indicate the existence of a broad state at about 10-MeV excitation energy in ^{7}Be and the possible existence of extremely broad structure at roughly 13 MeV, but do not support the existence of a proposed state at 14.6 MeV. The $^{6}Li(p, p')^{6}Li^{*}$ data indicate that the broad state is located at about 10.0 MeV and has a width of about 1.8 MeV. This is consistent with the $^{6}Li(p, p'')^{6}Li^{**}$ and $^{4}He(^{3}He, p'')^{6}Li^{**}$ data. These data exhibit an interference-like feature, which has been associated with the existence of another ^{7}Be state located at about 11.0 MeV and with a total width of about 0.4 MeV. On the basis of an analysis with complex eigenvalue resonance theory the assignments $J^{\pi} = \frac{3}{2}^{-}$ for both the 10.0- and the 11.0-MeV states have been made, and the existence of an extremely broad $J^{\pi} = \frac{1}{2}^{-}$ state at roughly 10 MeV or higher has been suggested. The isotopic spin assignments $T = \frac{1}{2}$ for the 10.0-MeV state and $T = \frac{3}{2}$ for the 11.0-MeV state have been made. Possible values for some of the partial widths, the results of other experiments, and the evidence relating to the usefulness of different versions of complex eigenvalue theory are discussed.

TABLE OF CONTENTS

PART		PAGE
I	INTRODUCTION	1
II	DISCUSSION OF THE EXPERIMENTS	4
	A. THE ELASTIC SCATTERING $^{6}Li(p, p)^{6}Li$	4
	(1) Apparatus	4
	(2) Procedure	6
	(3) Results	9
	B. THE INELASTIC SCATTERING $^{6}Li(p, p')^{6}Li^{*}$	10
	(1) Apparatus	10
	(2) Procedure	13
	(3) Results	14
	(4) Legendre Polynomial Fit	14
	C. THE INELASTIC SCATTERING $^{6}Li(p, p'')^{6}Li^{**}$: GAMMA-RAY MEASUREMENTS	17
	(1) Apparatus	17
	(2) Procedure	17
	(3) Results	20
	COINCIDENCE MEASUREMENTS	21
	(1) Apparatus	21
	(2) Procedure	22
	(3) Results	24
	PARTICLE MEASUREMENTS	24
	(1) Apparatus and Procedure	24
	(2) Results	25
	(3) Legendre Polynomial Fit	25

TABLE OF CONTENTS (cont.)

PART		PAGE
	D. THE REACTION $^{4}He(^{3}He, p'')^{6}Li^{**}$	26
	(1) Apparatus	26
	(2) Procedure	28
	(3) Results	31
	E. NORMALIZATION	31
III	THEORETICAL INTERPRETATION OF THE DATA	35
	A. OUTLINE OF THE ANALYSIS	35
	B. RESULTS OF SCATTERING AND RESONANCE THEORIES	36
	(1) Scattering Theory	36
	(2) Resonance Theories	40
	C. THE ELASTIC SCATTERING $^{6}Li(p, p)^{6}Li$	52
	D. THE INELASTIC SCATTERING $^{6}Li(p, p')^{6}Li^{*}$	54
	E. THE INELASTIC SCATTERING $^{6}Li(p, p'')^{6}Li^{**}$	58
	F. THE REACTION $^{4}He(^{3}He, p'')^{6}Li^{**}$	64
	G. REACTIONS STUDIED BY OTHER INVESTIGATORS	67
IV	SUMMARY	68
APPENDIX A - $^{6}Li(p, p)^{6}Li$ REACTION		72
APPENDIX B - $^{6}Li(p, p')^{6}Li^{*}$ REACTION		73
APPENDIX C - $^{6}Li(p, p'')^{6}Li^{**}$ REACTION		76
APPENDIX D - $^{4}He(^{3}He, p'')^{6}Li^{**}$ REACTION		79
REFERENCES		81
TABLES		83
FIGURES		125

I. INTRODUCTION

The experiments to be described were undertaken to shed light on the structure of the ^{7}Be nucleus at an excitation energy above 8 MeV. Little was known about this energy region prior to 1960. With the advent of the tandem electrostatic accelerators it became possible to form ^{7}Be as the compound nucleus up to an excitation energy of about 16 MeV through the ^{6}Li + p channel, and up to about 12 MeV through the ^{4}He + ^{3}He channel. At these energies many reaction channels are open (Figure 1):

$$\left.\begin{matrix} ^{6}\text{Li} + \text{p} \\ ^{4}\text{He} + ^{3}\text{He} \end{matrix}\right\} \rightarrow \begin{matrix} ^{6}\text{Li} + \text{p} \\ ^{6}\text{Li}^{*} + \text{p}' \\ ^{6}\text{Li}^{**} + \text{p}'' \\ \text{Higher } ^{6}\text{Li states} + \text{p} \\ ^{4}\text{He} + ^{3}\text{He} \\ ^{5}\text{Li} + \text{d} \\ ^{6}\text{Be} + \text{n} \\ ^{4}\text{He} + \text{p} + \text{d} \\ ^{4}\text{He} + \text{p} + \text{p} + \text{n} \\ ^{7}\text{Be} + \gamma \end{matrix}$$

The large number of open channels allows an interesting variety of decay modes of the compound nucleus to be studied. On the other hand, it complicates the analysis of elastic scattering

experiments, and what is more serious, causes the compound states to be short lived and hence broad. These difficulties, and those caused by the non-zero spins of most of the reaction particles, are characteristic of a study of this region of ^{7}Be.

Nevertheless, the present study of the reactions

$$^{6}\mathrm{Li}(p, p)^{6}\mathrm{Li}$$

$$^{6}\mathrm{Li}(p, p')^{6}\mathrm{Li}^{*} \ (2.184 \ \mathrm{MeV})$$

$$^{6}\mathrm{Li}(p, p'')^{6}\mathrm{Li}^{**} \ (3.562 \ \mathrm{MeV})$$

$$^{4}\mathrm{He}(^{3}\mathrm{Hc}, p'')^{6}\mathrm{Li}^{**}$$

has yielded considerable information about states in this region of ^{7}Be, particularly below about 11 MeV. The information is of theoretical interest because of the predictions of increasingly sophisticated nuclear models. The most recent calculations, those of Barker (1966), employ the intermediate-coupling shell model and predict four states between 8 and 11 MeV. These are three $T = \frac{1}{2}$ states close to the L-S coupling limit which are predominantly $^{4}D_{\frac{7}{2}}$, $^{4}P_{\frac{3}{2}}$, and $^{4}P_{\frac{1}{2}}$ states, and one $T = \frac{3}{2}$ state which is predominantly a $^{2}P_{\frac{3}{2}}$, $^{2}D_{\frac{3}{2}}$ mixture. States having several of the expected properties of the second and the fourth of these states were found at about 10 and 11 MeV. Some evidence for the existence of a very broad $J^{\pi} = \frac{1}{2}^{-}$ state, which might correspond to the third of these states, was also found.

The experiments are discussed in Part II, and the measured cross sections are given in a series of tables. The theoretical interpretation of the data is considered in Part III. This interpretation is summarized in Part IV, which also includes the numerical values of most of the resonant parameters obtained. Rough estimates of the numerical values of partial widths are discussed in a series of appendices.

II. DISCUSSION OF THE EXPERIMENTS

A. THE ELASTIC SCATTERING $^{6}Li(p, p)^{6}Li$

(1) Apparatus

The proton beam was supplied by the ONR-CIT tandem accelerator. After passing through the target, the beam was stopped on an insulated tantalum disk and integrated with an Eldorado Model CI-110 current integrator.

For some preliminary measurements a 13-cm diameter scattering chamber was used. However, most of the measurements were made with the 25.4-cm diameter chamber shown in Figure 2. The chamber was designed so that three independently movable detectors could be used simultaneously. Each detector was mounted on an arm which was, in turn, secured to one of the three stacked ring gears. Each ring gear was driven by a small pinion wheel located to mesh with the teeth on the inner radius of the gear. The gear ratio was 18:1 and the face of the dial which was mounted on the pinion axis was inscribed with 20 equally spaced divisions. Thus, a rotation of one dial division produced a detector rotation of 1^{o} about the target. Each detector viewed a solid angle determined by a limiting aperture 0.32 cm in diameter located 10 cm from the target.

Six accessory ports were located around the side of the chamber at 45^{o} intervals. In one of these ports was mounted a device for inserting a small quartz disk into the center of the chamber without breaking the vacuum. This was used to view the beam while it was being focused on the target. A vacuum gauge was mounted in a second port. For some measurements a fixed monitor

detector was mounted in a third. The remaining ports, containing lucite windows, were used for viewing the target and the detectors.

Targets were made by evaporating separated ^{6}Li (isotopic abundance 99%) onto thin carbon foils or, in later experiments, thin nickel foils. The carbon foils tended to extend and wrinkle during evaporation. The area being irradiated by the beam then tended to contract, producing a gradually thickening target. Most of the angular distributions were taken using targets on the carbon backings. The nickel backings, most of which were 5000 Å thick, were subsequently found to be more reliable and were used for all of the excitation functions.

Even with the nickel backings it was found that the lithium thickness often tended to change when the target was first irradiated. However, the thickness tended to stabilize within the first hour of irradiation. Targets made in apparently the same fashion varied widely in quality, some being unsuitable for taking excitation functions, while others showed essentially no thickness change after several days of use.

Lithium evaporation took place in a separate vacuum system accessible through the bottom of the target chamber. When the target holder was extended down into the furnace chamber, the target rod sealed the opening to the scattering chamber. This arrangement permitted access to the scattering chamber without destroying the target, or alternatively, the convenient replacement of targets without breaking the vacuum to the scattering chamber.

The targets were positioned with their surfaces at an angle of about 45^{o} to the beam axis, with the lithium side facing the beam. The thickness of lithium traversed by the beam ranged from 30 to 300 $\mu g/cm^{2}$ for the various targets used. Usually the beam

energy broadening due to target thickness was considerably less than 20 keV. Thickness was measured by comparing the proton yield from the $^{6}Li(p, p)^{6}Li$ reaction with the known absolute differential cross section at low energy (McCray 1962).

Impurities of ^{16}O, ^{12}C, and ^{1}H were present in all the targets even before irradiation. The ^{12}C content increased appreciably with irradiation, while the ^{16}O and ^{1}H contents were relatively stable.

The spectrum of particles emitted from the target was observed with silicon solid-state detectors. Both surface-barrier and lithium-drifted detectors were used. The surface-barrier detectors, made according to the technique of Dearnaley and Whitehead (1961), had a maximum depletion depth of about 500 microns, sufficient to stop protons of about 8 MeV, and a resolution better than 100 keV (full width at half maximum). The lithium-drifted detectors, made according to the technique of Cusson and Nordberg (1961), had a depth between 1000 and 1500 microns, sufficient to stop protons of at least 12 MeV, and a resolution of about 200 keV. The detectors were followed by Tennelec Model 100A preamplifiers and Hamner Model N328 non-overloading amplifiers. Spectra were recorded with a Radiation Instrument Development Laboratory Model 34-12 400-channel pulse-height analyzer and with a Nuclear Data Model ND 150-FM 1024-channel analyzer.

(2) Procedure

Some preliminary measurements of the differential cross section for the $^{6}Li(p, p)^{6}Li$ reaction were made using the 13-cm diameter scattering chamber. Excitation functions over

part of the energy range were taken at 3 angles in intervals of about 50 keV. Other crude data were taken at one angle in 20-keV intervals in the regions 3.0 to 5.0 and 6.0 to 12.0 MeV.

A more careful set of measurements was made using the 25.4-cm diameter scattering chamber. Angular distributions were taken in 200-keV intervals from 2.4 to 6.0 MeV, and in 1.0-MeV intervals from 6.0 to 12.0 MeV. The most backward angle that could be obtained was 160.0°. The most forward angle was determined by the ability of the detectors to resolve the ^{6}Li elastic protons from those due to ^{12}C, ^{16}O, and the Ni target backing. The most forward angle at which good data were obtained was 33.8°.

It was found that the simultaneous use of the three movable detectors presented normalizing and data handling problems. Consequently, only one movable detector was used for most of the work, although another detector was used at a fixed angle to monitor target thickness and beam integration during the taking of each angular distribution.

At each angle and energy the spectrum of charged particles emitted from the target was recorded in the first half of the 400-channel analyzer memory and used to estimate the background under the elastic proton group. The number of counts in this group was obtained by setting the Hamner amplifier single-channel differential discriminator to include the portion of the spectrum containing the group, and counting the discriminator output pulses with a scaler. The discriminator output could also be used to route the portion of the spectrum on which the discriminator was set to the second half of the analyzer memory (Pearson 1963). This arrangement facilitated the proper setting of the discriminator.

The background under the elastic proton group was mainly caused by the unsatisfactory beam collimator seen in Figure 2. Considerable stray beam was scattered from the collimator into the chamber. In addition, the beam spot size on target was ill-defined and varied considerably with beam focus.

At some energies and angles 0.008- mm aluminum foil was used over the detector to separate the proton group from the ^{3}He and ^{4}He groups.

Excitation functions were taken at the two lab angles 80.5^{o} and 160.0^{o}, each with a target whose thickness was checked repeatedly at a fixed energy and found not to fluctuate. These excitation functions were used to obtain the relative normalizations of the angular distributions. As a check, many points distributed throughout the energy and angle range were remeasured using a particularly uniform target.

Some spectra were taken at high energy with the lithium-drifted detectors in a search for protons inelastically scattered from highly excited states of ^{6}Li. One of these spectra is shown in Figure 3.

The data were normalized to the absolute differential cross sections obtained by McCray (1962). His data were interpolated to give 18 values of the differential cross section at 2.4, 2.6, and 2.8 MeV. These were compared with smooth curves drawn through the angular distributions obtained at the three energies, and a single normalization factor determined. McCray's points at the lab angles 70^{o} 41' and 90^{o} 45' fell consistently below the smooth curves, although agreement at other, more backward, angles was good. The standard error of the normalization factor was estimated to be about 1%. The results are shown in Figure 4.

(3) Results

Some of the preliminary data, with an approximate normalization, are shown in Figure 5. In these data, and in the other preliminary data taken in 20-keV energy intervals, there is no evidence for sharp structure in the compound nucleus, ^{7}Be. In particular, there is no evidence supporting the existence of a previously reported state at 14.6-MeV excitation energy (Ajzenberg-Selove and Lauritsen 1959).

In none of the spectra was there any clear evidence of protons inelastically scattered from any but the first two excited states of ^{6}Li. The spectrum in Figure 3 is an example.

The complete set of the best data, expressed in terms of center-of-momentum differential cross section, is given in Table 1. These data have already been published (Harrison and Whitehead 1963). Sample angular distributions and excitation functions are plotted in Figures 6 and 7 respectively.

The error given for each point was estimated from the statistics of the measurement, the magnitude of the background subtracted, and the accuracy with which the data from the particular target used could be normalized. Although the standard error is given, the distinction between standard and probable error is not particularly meaningful, because of the poor accuracy with which the errors are known. However, the relative sizes of the errors of any two points should be fairly well represented by the ratio of the given errors.

B. THE INELASTIC SCATTERING $^{6}Li(p, p')^{6}Li^{*}$ (2.184 MeV)

(1) Apparatus

The apparatus was similar to that used in the study of the $^{6}Li(p, p)^{6}Li$ reaction, although several modifications to the beam-defining system and target chamber were made.

The beam collimator of Figure 2 was replaced by two sets of adjustable tantalum slits located in the beam pipe. The first set, located about 125 cm from the target, was adjusted to define a 2.54-mm square aperture. The second set, located about 25 cm from the target, was adjusted to define a 0.89-mm square aperture. With this collimating arrangement the maximum beam spot size on target was a 1.75-mm square. In actual operation the slits were opened up to facilitate the initial stages of steering the beam onto the target, and adjusted as the beam was focused.

One anti-scattering baffle, consisting of a 2.18-mm diameter aperture in a tantalum disk, was installed at the entrance to the chamber. With this hole size, and the slit settings used, no unscattered beam could strike the baffle. On the other hand, beam scattered from the slits was constrained by the baffle to enter the chamber in a cone of angle sharp enough to pass through the target. Since the targets were thin, re-scattering into the detectors was very small.

An improved collimator was installed on the movable detector. It contained two apertures defined by fixed slits made of 0.5-mm thick tantalum. The entrance aperture, located about 6 cm from the target, was 4.8-mm wide and 7.9-mm high. The solid-angle defining aperture, located about 11 cm from the target and about 5 mm from the detector face, was 0.76-mm wide and 4.8-mm

high. This collimator eliminated the possibility of detecting particles scattered either from the beam-defining slits and subsequently from the baffle, or from the beam stopper.

These beam-defining and detector-collimating systems effectively removed the effects of stray beam from the spectra. A system of detector mounting slightly different from that shown in Figure 2 permitted observations at lab angles from 15^{o} to 165^{o}.

A target rod different from that in Figure 2 was installed. Immediately above the target holder a portion of the rod was milled away and a small quartz disk mounted with its face containing the axis of the rod, which was marked with a length of fine wire. During the alignment of the chamber the rod was lowered, and the wire viewed with a telescope through the beam defining slits. This permitted the axis of the scattering chamber to be located properly with respect to the beam-defining slits. In addition, with the target rod removed, the 0^{o} position of the detector could be determined. During normal operation the target rod could be lowered and the quartz used to determine the beam focus at the target position.

On one of the movable arms were suspended a foil holder and another small quartz disk, the centers of which were in the plane defined by the detector and the beam axis. This movable quartz disk, with its center marked by fine wire crosshairs, provided a method of checking the chamber alignment during operation. By placing it in the 0^{o} and 180^{o} positions, the path of the beam through the chamber could be traced. Both the beam-entrance and the beam-exit ends of the chamber were connected to the beam line with bellows couplings, permitting alignment changes if necessary.

The movable foil holder could be positioned in a small slot between the detector face and the detector solid-angle defining aperture. It was found that foils positioned on the other side of the aperture tended to cause changes of several percent in the solid angle.

The ^{6}Li targets were similar to those used in the study of the $^{6}Li(p, p)^{6}Li$ reaction, except that 500 Å nickel foils were used for the target backings. These were mounted over 7.9-mm diameter holes punched in 0.18-mm thick tantalum. The tantalum was clamped to a stainless steel target holder, which was fastened to the target rod with screws. Targets were positioned with their surfaces at an angle of 30^{o} to 45^{o} to the beam axis, lithium side facing the beam. The thickness of lithium traversed by the beam ranged from 70 to 300 $\mu gm/cm^{2}$ for the various targets that were used. Usually targets were made as thick as was possible without causing appreciable energy broadening of the $^{6}Li(p, p')^{6}Li^{*}$ proton group.

The spectrum of particles emitted from the target was observed with silicon surface-barrier detectors made by Molechem. Two detectors, each with a resolution of about 40 to 50 keV, were used. These had maximum depletion depths of about 500 and 700 microns, sufficient to stop protons of about 8 MeV and 9.5 MeV respectively. The experimental full width at half maximum of the $^{6}Li(p, p')^{6}Li^{*}$ proton group was typically about 70 keV. This includes a contribution from the natural width of the $^{6}Li^{*}$ state, about 30 keV. The electronic circuits were similar to those used in the study of the $^{6}Li(p, p)^{6}Li$ reaction.

(2) Procedure

Measurements of the differential cross section for the $^{6}Li(p, p')^{6}Li^{*}$ reaction were made at 12 values of the incident proton lab energy between 3.6 and 9.4 MeV. Angular distributions over a range of lab angles between about 20^{o} and 165^{o} were taken at each energy. The data were taken with a single movable detector, although a detector at a fixed lab angle was used as a monitor.

At each energy and angle the portion of the scattered particle spectrum containing the $^{6}Li(p, p')^{6}Li^{*}$ proton group was recorded in the first half of the 400-channel analyzer memory, printed out, and plotted. The sum of the counts in the proton group and in the background was determined, the background estimated from the plot, and the background subtraction performed. The resulting number of counts in the proton group was corrected for the small analyzer dead-time. The background counts, coming from the many-body reactions $^{6}Li + p \rightarrow {}^{4}He + d + p$ and $^{6}Li + p \rightarrow {}^{4}He + n + p + p$, were typically about 20% of those in the proton group, although this correction depended somewhat upon energy and angle.

At some energies and angles 10^{4} Å nickel foil was used in front of the detector to separate the $^{6}Li(p, {}^{3}He)^{4}He$ α-particle group from the $^{6}Li(p, p')^{6}Li^{*}$ proton group. At a few forward angles the proton group was obscured by protons scattered from the always-present hydrogen contamination in the targets.

At most energies complete spectra were taken at the lab angles 80.5^{o} and 160.0^{o}. They were used to obtain the relative normalization of the data from the $^{6}Li(p, p')^{6}Li^{*}$ and $^{6}Li(p, p)^{6}Li$ reactions. A typical spectrum is shown in Figure 8.

(3) Results

The results, expressed in terms of center-of-momentum differential cross section, are given in Table 2. The angular distributions are plotted in Figures 9 to 14.

The dominant source of error was the background, and the error given for each point in Table 2 was obtained from an estimate of the precision with which the background could be subtracted. Although an effort was made to obtain a random standard error, the results were not completely successful, and the error obtained undoubtedly contains some systematic error in background subtraction. Consequently, smooth curves pass within the given errors of somewhat more than 2/3 of the points in the angular distributions. The standard error in the normalization of each angular distribution relative to the correct $^{6}Li(p, p)^{6}Li$ cross section was also estimated, and is given in Table 2. In addition, there were systematic errors caused by geometrical inaccuracies in the scattering chamber, and in some cases, by relative normalization errors in data taken with different targets. The systematic error introduced by these effects was estimated to be 3% or less.

(4) Legendre Polynomial Fit

The series of Legendre Polynomials

$$c_1P_0 + c_2P_1 + \text{---} + c_{IMAX}P_{(IMAX - 1)}$$

was fitted to each angular distribution by evaluating the coefficients c_1, c_2, --- c_{IMAX}. The notation P_L stands for the polynomial of

order L with argument $\cos\theta$, where θ is the center-of-momentum scattering angle. The coefficients were determined by the method of least squares, with each data point weighted by the reciprocal of the square of its error. The data and errors were taken from Table 2, and the calculations done by the CIT IBM 7090 computer using a Fortran code. IMAX, the number of polynomials fitted to each angular distribution, was varied from 1 to 11. For each of these values the following quantities were obtained: the coefficients (IMAX in number), their errors, χ^2 divided by the number of degrees of freedom, and the angular distribution calculated from the coefficients. The addition of higher order polynomials to the series made only slight difference to the values obtained for the lower order polynomials.

The main problem was the determination of the number of polynomial terms required to fit each angular distribution. A helpful estimate of the significance of the first 4 or 5 polynomials could be obtained without calculation by estimating the number of powers of $\cos\theta$ occurring in each experimental angular distribution plot. This was possible because $\cos\theta$ was used as abscissa. However, detailed calculations were necessary for higher polynomials, and it was for this reason that IMAX, the number of polynomial terms in the series, was varied. In principle, information about the correct number of terms to use can be extracted with the help of χ^2 distribution tables from the χ^2 obtained at each value of IMAX, but the success of the procedure requires a better knowledge of the errors than was available. Therefore a more practical approach was followed. When it was necessary to choose a value of IMAX from several possibilities, the corresponding calculated angular distributions were plotted with the data, and with the magnitude of

possible systematic errors and the limitations of the accuracy of the random errors in mind, the value of IMAX corresponding to the simplest angular distribution thought to fit the data was chosen.

The angular distributions at the lowest incident proton lab energy, 3.60 MeV, can be fitted with a series containing terms up to P_2 only. However, this is the angular distribution with the greatest errors. It is necessary to use series with terms up to at least P_3 for all other energies. A P_4 term may be present for energy $\geq$ 4.20 MeV, and is definitely present for energy $\geq$ 6.60 MeV. For energy $\geq$ 7.00 MeV, a P_5 term may be present.

The calculated angular distributions are plotted in Figures 9 to 14. The difficulty in determining the significance of the P_4 term in the energy interval 4.20 to 6.60 MeV is illustrated by the plots in Figure 10b for 5.00-MeV energy, where the P_4 term, if significant, appears to assume its largest value in the interval. The difficulty in determining the significance of the P_5 term is illustrated by the plots in Figure 13b for 7.80-MeV energy, where the P_5 term, if significant, appears to be at its maximum.

The coefficients of the Legendre Polynomials and their errors are given in Table 3 and plotted in Figure 15. The standard errors were calculated from the random standard errors assumed for the data and from the normalization error of each angular distribution.

C. THE INELASTIC SCATTERING $^{6}Li(p, p'')^{6}Li^{**}$ (3.56 MeV): GAMMA-RAY MEASUREMENTS

(1) Apparatus

Much of the apparatus was the same as that used in the study of the $^{6}Li(p, p')^{6}Li^{*}$ reaction. However, in the first experiments the γ-ray yield from the decay of the second excited state of ^{6}Li was measured rather than the proton yield itself. It was therefore possible to use rather thick targets. These were about 700 $\mu gm/cm^{2}$, giving a beam energy broadening of about 40 to 55 keV.

The γ rays were observed with NaI(Tl) scintillation detectors. Two detectors, both of the Harshaw "Integral Line" series and with resolutions of 5 or 6%, were used. These were a 5.08-cm long by 5.08-cm diameter crystal mounted on an RCA 6342-A photomultiplier, and a 7.62-cm long by 7.62-cm diameter crystal mounted on a DuMont 6363 photomultiplier. The 5.08-cm detector was followed by a Kellogg Laboratory preamplifier and the internal amplifier of an RIDL 400-channel analyzer. The 7.62-cm detector was followed by a Kellogg Laboratory preamplifier and a Hamner amplifier. The γ-ray spectra were recorded with the 400-channel analyzer.

(2) Procedure

The total cross section for the $^{6}Li(p, p)^{6}Li^{**}$ reaction was determined over a range of proton energies by measuring the yield of the 3.56-MeV de-excitation γ rays. Because the 3.56-MeV state has spin zero, the γ radiation is isotropic in the system of the

decaying particle. Moreover, practically all of the decays occur before the recoiling $^6Li^{**}$ particles move out of the target. Therefore, the γ-ray yield at any laboratory angle is proportional to the total cross section σ for the $^6Li(p, p'')^6Li^{**}$ reaction, except for an effect of order V/c, where V is the recoil velocity and c the velocity of light. More exactly,

$$\text{(Yield at lab angle } \theta_\ell) \propto \sigma \frac{(1 - \frac{V}{c}\cos\theta_\ell \cos\psi)(1 - \frac{V^2}{c^2})}{[1 - 2\frac{V}{c}\cos^2\theta_\ell\cos^2\psi + \frac{V^2}{c^2}(\cos\theta_\ell^2\cos^2\psi - \sin^2\theta_\ell\sin^2\psi)]^{3/2}}$$

where ψ is the laboratory angle of the recoil. The yield was measured at 90°, where the V/c terms vanish. The error introduced by the V^2/c^2 terms was negligible because V/c was less than about 3.1% at all energies.

Two independent sets of measurements were made. The 5.08-cm detector was used for the first set; the 7.62-cm detector for the second. The measurements were made at different times with different targets, although the procedures followed were quite similar. In both cases the detector was located outside the chamber at 90° to the beam, its face about 17.5 cm from the target. The sides of the detector were surrounded by a cylindrical lead shield about 5 cm thick. Additional shielding from the beam-defining slits and the beam stopper was provided.

The incident proton lab energy was varied between 4.26 and 6.98 MeV in the first set of measurements, and between 4.80 and 7.80 MeV in the second. A γ-ray spectrum was recorded

at each energy. Changes in gain were usually negligible. Most of the spectra contained the 4.433-MeV γ ray from the de-excitation of the first excited state of ^{12}C. Its subtraction was straightforward, however, using a 4.433-MeV γ-ray spectrum obtained by proton bombardment of a carbon foil.

In both sets of measurements the subtraction was done by the CIT IBM 7090 or 7094 computers using a Fortran code. The procedure consisted of normalizing the photopeak of the 4.433-MeV spectrum to the same peak in each complete spectrum, allowing for a small continuum background, and performing a channel-by-channel subtraction. In the analysis of the second set of measurements a parameter representing the gain for the 4.433-MeV spectrum was varied, a normalization for each gain value determined, and a χ^2 representing the goodness of fit to the peak in the complete spectrum calculated. Then the normalized 4.433-MeV spectrum corresponding to the gain value giving the minimum χ^2 was subtracted from the complete spectrum. A typical spectrum, before and after subtraction of the 4.433-MeV γ ray, is shown in Figure 16.

The corrected spectra were plotted and the counts in the photopeak summed. The continuum neutron background was subtracted and a small correction made for analyzer dead time. The background was small at all except the highest energies, when it amounted to about 20% of the counts in the photopeak.

One of the particle detectors used in the study of the $^6Li(p, p')^6Li^*$ reaction was used to monitor target thickness and beam integration. This was done by comparing the proton yield from the $^6Li(p, p)^6Li$ reaction with the previously determined cross section. A several percent uncertainty in the monitoring was caused by the considerable energy broadening of the proton group by the large target thickness.

The normalization of the γ-ray data was determined from a particle angular distribution obtained later at 5.80 MeV. This angular distribution, normalized in turn to the $^{6}Li(p, p)^{6}Li$ cross section, was integrated to give total cross section, to which the γ-ray yield data were normalized.

(3) Results

The results are given in Table 4 and plotted in Figure 23. They are expressed in terms of center-of-momentum total cross section divided by 4π, which is equal to the coefficient of the Legendre polynomial P_0. The energy scale given was corrected for target thickness.

The standard error given for each point is a predominantly random error estimated from the accuracy of background and contaminant γ-ray subtraction, from the effect of possible small gain changes, and at low energies, from the statistics. Also included are uncertainties in correcting for small changes in target thickness. There is an additional error of about 3 1/2% in the normalization of these γ-ray data relative to the particle data for the same reaction obtained later.

The beam energy distribution was about 40 to 55 keV wide in the lab system. The error in the energy scale caused by the uncertainty in the location of the center of the energy distribution was estimated to be about 10 keV in the lab system.

COINCIDENCE MEASUREMENTS

(1) Apparatus

Most of the apparatus used in the p-γ coincidence measurements was the same as that used in the study of the $^6Li(p, p')^6Li^*$ reaction. The location of the solid-angle defining aperture of the movable detector was changed to about 8.5 cm from the target. The lithium target thickness traversed by the beam was about 50 $\mu gm/cm^2$. With this rather thin target there was no appreciable broadening of the proton group from the $^6Li(p, p'')^6Li^{**}$ reaction.

The γ rays were observed with a Harshaw 10.16-cm long by 10.16-cm diameter cylindrical NaI(Tl) crystal mounted on a CBS 7819 photomultiplier tube. The detector was located to subtend a large solid angle at the target. For this purpose a thin-walled aluminum can was made to replace the furnace and the cold trap at the bottom of the scattering chamber. With the can projecting into the chamber, the detector could be mounted with its face about 1.5 cm from the target beam spot. The sides of the detector were surrounded by a cylindrical lead shield about 2.5-cm thick.

Much of the circuitry was similar to that used in the experiments previously described. Both the γ ray and the particle preamplifiers were followed by Hamner Model N328 amplifiers equipped with Model N670 crossover pickoff gates and with single-channel differential discriminators. The intermediate-speed pulses from the pickoff gates and the slow pulses from the discriminators were fed to a Hamner Model N680 two-speed coincidence mixer. When a coincidence between the intermediate-speed pulses was

recorded simultaneously with a coincidence between the slow pulses, an output pulse was produced by the mixer.

(2) Procedure

The angular distribution for the $^{6}Li(p, p'')^{6}Li^{**}$ reaction was determined at 5.80-MeV incident proton lab energy by requiring at each angle a coincidence between the protons from the reaction and the 3.56-MeV de-excitation γ rays. The procedure is valid because of the absence of angular correlation between the reaction protons and the γ rays from this spin zero state of ^{6}Li. This approach, rather than the direct measurement of the proton yield, was adopted because of the small reaction yield and the large continuum background from many-body reactions. It was found later that careful direct measurement gave comparable results, and that technique was adopted in subsequent measurements.

After the target was made in the usual fashion with the furnace and cold trap in place, the chamber was vented with helium. Then the furnace and cold trap were removed and quickly replaced by the aluminum can, and the helium was pumped out. The procedure prevented appreciable chemical deterioration of the target.

The discriminator of the particle amplifier was set on the portion of the particle spectrum containing the $^{6}Li(p, p'')^{6}Li^{**}$ proton group. The discriminator of the γ-ray amplifier was set on the portion of the 3.56-MeV γ-ray spectrum containing the photopeak and the first and second escape peaks. These discriminators were set in the same way as used in the study of the $^{6}Li(p, p)^{6}Li$ reaction. With the γ-ray discriminator setting and the detector geometry used,

γ-ray coincidences were recorded for about 7% of the protons from the $^{6}Li(p, p'')^{6}Li^{**}$ reaction entering the particle detector.

The pulses from one of the pickoff gates were passed through a variable length of delay line which was used to provide the correct relative timing of the pulses from the two pickoff gates, to determine the number of random coincidences, and to measure the resolving time. The resolving time was about 125 nsec, and appeared to be constant.

A fixed-angle particle detector was used to monitor target thickness and beam current integration. The beam current was about 0.1 μA, and the charge collected, 300 μC.

The number of coincidences was obtained by counting the output pulses from the coincidence mixer with a scaler. The beam current was kept small in order to limit the number of random coincidences. These depended upon angle, but on the average were about 13% of the true coincidences. To determine the number of random coincidences, the pulses from one of the pickoff gates were delayed by an amount greater than the coincidence resolving time, making all coincidences random. These were counted for 60 μC of beam collection, normalized to 300 μC, and subtracted from the total number of coincidences. This procedure was followed at each angle.

At lab angles greater than about 130^{o} the proton groups from the reactions $^{6}Li(p, p'')^{6}Li^{**}$ and $^{12}C(p, p')^{12}C^{*}$ (4.433 MeV) were unresolved. Since the two γ rays were also unresolved, coincidence measurements at these angles were not possible.

The normalization of the angular distribution was determined from an angular distribution obtained later at the same energy by the direct measurement technique. This distribution in turn was normalized to the $^{6}Li(p, p)^{6}Li$ cross section.

(3) Results

The results, expressed in terms of center-of-momentum differential cross section, are given in Table 5 and plotted in Figure 18b. The greater part of the standard error given for each point was estimated from the statistics of the number of coincidences obtained, and the smaller part from the uncertainty in the correction for random coincidences. The error in the normalization relative to the correct ^{6}Li(p, p)^{6}Li cross section was estimated to be about 3 1/2%.

PARTICLE MEASUREMENTS

(1) Apparatus and Procedure

The differential cross section for the ^{6}Li(p, p'')^{6}Li** reaction was measured by direct observation of the proton group with the same apparatus and procedure used in the study of the ^{6}Li(p, p')^{6}Li* reaction. The results were comparable to those obtained with the slower and more complicated p-γ coincidence technique. Angular distributions over a range of lab angles between about 20^{o} and 165^{o} were taken at 12 values of incident proton lab energy between 5.0 and 9.4 MeV.

The lithium target thickness traversed by the beam ranged from about 30 to 130 μgm/cm^{2} for the various targets that were used. Targets were kept thin to prevent broadening of the ^{6}Li(p, p'')^{6}Li** proton group. This was crucial because of the large many-body reaction background to be subtracted. For example, at 6.55 MeV the background counts were from 2 1/2 to 10 times as numerous as the counts in this proton group. The background was strongest at forward angles.

At some energies and angles proton groups from the reactions $^{6}Li(p, p'')^{6}Li^{**}$ and $^{12}C(p, p')^{12}C^{*}$ were unresolved. Then the sum of the counts in the two groups was obtained, together with the number of counts in the group from the reaction $^{12}C(p, p)^{12}C$. The relative yields of the reactions $^{12}C(p, p)^{12}C$ and $^{12}C(p, p')^{12}C^{*}$ were determined at these energies and angles by using a carbon foil target. The number of counts from the $^{12}C(p, p')^{12}C^{*}$ reaction in the unresolved groups could then be calculated and subtracted.

(2) Results

The results, expressed in terms of center-of-momentum differential cross section, are given in Table 5. The angular distributions are plotted in Figures 17 to 22.

The discussion of errors is similar to that given in connection with the results from the $^{6}Li(p, p')^{6}Li^{*}$ reaction. The systematic errors were estimated to be considerably smaller than the background subtraction errors, and in most cases, to be negligible. However, in a few cases the $^{6}Li(p, p'')^{6}Li^{**}$ proton group may not have been resolved from small contaminant groups. This effect, enhanced by the thin targets used and the low reaction yield, would tend to make the measured differential cross section systematically high at a few energies and angles.

(3) Legendre Polynomial Fit

A Legendre polynomial series was fitted to each angular distribution by the same method used for the $^{6}Li(p, p')^{6}Li^{*}$

reaction. At 5.80-MeV incident proton lab energy both the direct measurement and the coincidence data were used.

The angular distributions from 5.00 to 7.00 MeV can be fitted with polynomial series containing terms up to P_3. All the fits are good except for the angular distribution at 5.20 MeV, which probably suffers from systematic errors. The angular distributions from 7.80 to 9.40 MeV may contain contributions from higher order polynomials, but these are very small.

The calculated angular distributions are plotted in Figures 17 to 22. Two angular distributions for 7.80 MeV are plotted in Figure 21b; one with the P_4 term and one without. The coefficients of the Legendre polynomials and their calculated standard errors are given in Table 6, and plotted in Figure 23.

D. THE REACTION $^4He(^3He, p'')^6Li^{**}$

(1) Apparatus

Negatively charged ^3He ions were injected into the tandem and the doubly charged component of the accelerated beam was used to bombard ^4He gas.

A de-excitation γ-ray yield was measured rather than a particle yield, and it was therefore possible to use the gas target chamber shown in Figure 24. After passing through a collimator and an anti-scattering baffle, the beam entered the ^4He target gas through a 6250 Å nickel foil and passed through a tantalum target tube, outside of which the detector was placed. A liquid-nitrogen cooled charcoal cold trap was used to help remove any traces of unwanted gases from the target volume.

The chamber was designed so that the usual sources of background radiation, foils containing the gas and the beam stopper, were well separated from the detector. Thus only an entrance foil was used, and the target gas filled the entire volume between the foil and the beam stopper. The foil was about 15 cm from the detector; the beam stopper, about 75 cm.

Tantalum was used for the target tube in order to reduce background radiation produced by particles striking its walls. The multiple scattering of beam into the walls was considered in choosing the tube diameter of 1.9 cm. The diameter was kept reasonably small so that experiments requiring a large detector solid angle could be performed.

The 7.62-cm γ-ray detector used in the study of the $^{6}Li(p, p'')^{6}Li^{**}$ reaction was placed with its face about 9.3 cm from the center of the target tube. The face of the detector was covered with a 2.105 gm/cm^2 graphite shield, and the sides with a lead shield about 10.8-cm thick. Additional lead was used to improve the detector shielding from the foil, from the beam stopper, and from the portion of the beam path not immediately in front of the detector.

The shielding gave an effective target length of 9 or 10 cm. The distance between the foil and the center of the detector face was about 15 cm. The gas pressure, 8 cm of mercury, was chosen so that the beam energy loss in the gas along the target length was about the same as the beam energy straggling in the foil and in the gas between the foil and the center of the detector. The three effects combined gave an incident ^{3}He lab energy distribution with a standard deviation of about 22 keV.

Average energy losses in the foil and in the gas between the foil and the center of the detector face were about 100 keV and 70 keV respectively. These were taken into consideration in the determination of the center of the beam-energy distribution. The energy loss of the beam and the standard deviation of its energy distribution changed only slightly over the ^{3}He energy range studied.

(2) Procedure

The total cross section for the ^{4}Hc(^{3}Hc, p'')^{6}Li** reaction was determined over a range of incident ^{3}He lab energy between 13.81 and 16.45 MeV. The technique, used also in the study of the ^{6}Li(p, p'')^{6}Li** reaction, was to measure the yield of the 3.56-MeV de-excitation γ rays.

The average beam current was about 7 10^{-9} A with 5 μC collected at each energy. The spectra were free from the 4.433-MeV contaminant γ ray present in the spectra from the ^{6}Li(p, p'')^{6}Li** reaction, but were otherwise similar. At 1.0-MeV energy intervals the ^{4}He target gas was removed from the chamber and a background spectrum taken.

The background, most of it due to the presence of neutrons, was smoothly varying under the photo- and first escape peaks of the 3.56-MeV γ ray. It changed only slightly with ^{3}He energy. Background subtraction was done by the CIT IBM 7094 computer with the help of a Fortran code. The procedure consisted of normalizing the appropriate background spectrum to the portion of each complete spectrum above the 3.56-MeV γ ray, and performing a channel-by-channel subtraction. A small correction for

analyzer dead time was made, and the counts in the photo- and first escape peaks summed. Over the upper 2/3 of the energy range studied, the background was typically about 15% of the number of counts in the peaks.

In order to determine the absolute normalization of the total cross section, it was necessary to know the detector photopeak efficiency for a line source perpendicular to its axis. This was found by determining the off-axis point source efficiency, from which the line-source efficiency was found by integration.

The point source efficiency E(x) was determined at a number of values of x, the source distance perpendicular to the detector axis. For this purpose a Th C'' 2.615-MeV γ-ray source was used, and the relative number of photopeak counts found at each value of its position x. The geometry and detector shielding were the same as used with the line source formed by the ^{4}He target.

The quantity E(0) for a 3.56-MeV point source was then calculated. First the total efficiency at x = 0 was calculated by the CIT IBM 7094 computer with the help of a Fortran code prepared by Goosman (1965). The calculation took into account the carbon absorber in front of the detector. Then the photopeak to total efficiency ratio r was found by extrapolation from curves by Heath (1957). Finally, these two quantities were multiplied to give E(0), to which the measured E(x) was normalized. E(x) for a 3.56-MeV source was calculated in a similar fashion for two values of $x \neq 0$, and agreement with the measured E(x) was reasonable.

It was necessary to make two approximations in the determination of E(x). The first was that r was independent of x; the second, that the functional form of E(x) was the same for 3.56-MeV and 2.615-MeV γ rays. It was possible to make an approximate

correction for the second assumption, because of the small change of γ-ray attenuation in lead and carbon shielding between these energies.

The efficiency F for the line source target was calculated from E(x):

$$F = \int_{\text{along source}} E(x)dx$$

The relation between N, the number of events occurring per unit length of the target, and n, the number of counts recorded in the photopeak, was thus obtained:

$$N = \frac{n}{F}$$

The total cross section was then calculated at 15.83-MeV ^{3}He lab energy from the photopeak counts, the target pressure and temperature, and the amount of integrated beam. This permitted normalization of the γ-ray yield data.

The total normalization standard error was estimated to be about 20%, dominated by contributions from an estimated geometrical error of about 15%, and from an estimated error in r of about 10%. Most of the geometrical error was due to the fact that the normalization measurements were made after the equipment had been dismantled, and it was therefore necessary to reproduce the relative geometry of the detector, the shielding, and the beam-axis location used when taking the γ-ray yield data.

(3) Results

The results, expressed in terms of center-of-momentum total cross section divided by 4π, are given in Table 7 and plotted in Figure 25. The energy scale given was corrected for losses in the foil and in the target gas.

An error of about 1 1/2% was estimated to be due to gain shift and uncertainty in pressure measurement and in beam integration. The individual contributions were about 1/2%, 1% and 1% respectively. The rest of the standard error given for each point was estimated from a combined statistical and background error varying from 1% to 4%. The normalization standard error was estimated to be about 20%. Although the ratio V/c is somewhat larger than at corresponding excitation energies in the $^{6}Li(p, p'')^{6}Li^{**}$ reaction, the error caused by measuring the reaction cross section by the γ-ray yield was estimated to be negligible.

The standard deviation of the beam energy distribution in the lab system was about 22 keV; in the center-of-momentum system, about 13 keV. The error in the energy scale caused by uncertainty in the location of the center of the energy distribution was estimated to be about 20 keV in the lab system, or about 11 keV in the center-of-momentum system.

E. NORMALIZATION

Several reactions forming ^{7}Be as the compound nucleus have been studied by different investigators, and in most cases a different normalization of the data has been used. The problem can be considered in two parts: the determination of a consistent

relative normalization for the different experiments, and the determination of the overall absolute normalization.

There are two facts important to the discussion. The first is that the determination of the relative normalization of reactions induced through the same entrance channel is straightforward if a thin target is used, because the groups corresponding to all the reaction products occur in any given spectrum of particles emitted from the target. The second fact is that the differential cross sections for the reactions ^{6}Li(p, ^{3}He)^{4}He and ^{4}He(^{3}He, p)^{6}Li are related by reciprocity when the incident particle energies correspond to the same excitation energy in ^{7}Be. Because of these facts, the relative normalization of any two reactions can be established.

An effort was made to find a consistent normalization for the already-existing data of several experiments, and these will be discussed in turn. The normalization of McCray (1962) was taken as unity, since this was the procedure followed in the study of the ^{6}Li(p, p)^{6}Li, ^{6}Li(p, p')^{6}Li*, and ^{6}Li(p, p'')^{6}Li** reactions.

The ^{6}Li(p, p)^{6}Li data of Fasoli et al. (1964a), originally normalized to the ^{4}He(^{3}He, p)^{6}Li data of Tombrello and Parker (1963), were renormalized to the ^{6}Li(p, p)^{6}Li data of McCray with the same procedure used in the normalization of the present ^{6}Li(p, p)^{6}Li data. The results are shown in Figure 4. A factor of 0.867 $\pm$ 1% is required for consistency with McCray's normalization.

Both the ^{6}Li(p, ^{3}He)^{4}He data of Fasoli et al. (1964b) and that of Jeronmyo et al. (1963) were also originally normalized to the ^{4}He(^{3}He, p)^{6}Li data of Tombrello and Parker. Therefore, the factor 0.87 is again required for consistency with McCray's normalization. These two sets of ^{6}Li(p, ^{3}He)^{4}He data have a discrepancy of about 3% in their relative normalization.

Angular distributions for the reaction $^{6}Li(p, ^{3}He)^{4}He$ were taken at 2.60- and at 2.89-MeV incident proton lab energy. The technique was similar to that used in the study of the $^{6}Li(p,p')^{6}Li^{*}$ reaction. The results, given in Table 8, were used to obtain a renormalization of $^{6}Li(p, ^{3}He)^{4}He$ data obtained by Marion (1956). A factor of $0.675 \pm 3\%$ is required for consistency with McCray's normalization. This disagrees somewhat with the result of a similar measurement made by McCray, which yielded a factor of about 0.55. Data of Heydenburg and Han (1962), which were originally normalized to Marion's data, require the same factor of 0.675.

The $^{4}He(^{3}He, p)^{6}Li$ reaction was studied in collaboration with Professor Tombrello. The absolute differential cross section was found for two angles at an incident ^{3}He lab energy of 10.97 MeV. This energy corresponds closely to a proton energy of 2.6 MeV in the inverse reaction. The gas scattering chamber was similar to that described by Tombrello and Senhouse (1963). The possibility of error introduced by scattering from rather thick (1.02 mm) slits defining the detector solid angle was taken into account in the estimation of the accuracy of the results. Using reciprocity, the results for the inverse reaction were calculated and compared with a smooth curve drawn through the 2.60-MeV $^{6}Li(p, ^{3}He)^{4}He$ data. It was found that the $^{4}He(^{3}He, p)^{6}Li$ results required the factor $0.850 \pm 2\%$ for consistency with McCray's normalization. The results are shown in Figure 26.

Preliminary results obtained by Spiger and Tombrello (1964) for the $^{4}He(^{3}He, p)^{6}Li$ reaction at 10.94-MeV energy were compared with the $^{6}Li(p, ^{3}He)^{4}He$ angular distribution at 2.60-MeV proton energy. The energies correspond exactly to the same ^{7}Be excitation energy. The factor $0.795 \pm 2\%$ was found to be required by these $^{4}He(^{3}He, p)^{6}Li$ data for consistency with McCray's normalization. The results are shown in Figure 26.

The $^{4}He(^{3}He, ^{3}He)^{4}He$ reaction was studied by Tombrello and Parker simultaneously with the $^{4}He(^{3}He, p)^{6}Li$ reaction, and the data therefore require the same normalization factor, 0.867. Similarly, data from the reactions $^{4}He(^{3}He, ^{3}He)^{4}He$, $^{4}He(^{3}He, p')^{6}Li^{*}$, and $^{4}He(^{3}He, p)^{6}Li$ studied by Spiger and Tombrello all require the same factor, 0.795.

The relative normalization of the experiments discussed was fairly well determined. More uncertainty exists in the answer to the second part of the problem, the determination of the correct overall normalization. It is emphasized that the absolute normalization taken as unity, that of McCray, is not necessarily the best one. In fact, the absolute normalization obtained from the studies of reactions induced through the $^{4}He + ^{3}He$ channel is probably the most dependable. The results for the relative normalization are summarized in Table 9; those for the absolute normalization, in Table 10. The magnitude factors of Table 10 are the reciprocals of the relative normalization factors of Table 9 and are proportional to the magnitude of ^{7}Be cross sections with the absolute normalization found by each investigator.

III. THEORETICAL INTERPRETATION OF THE DATA

A. OUTLINE OF THE ANALYSIS

The reactions were analyzed with the objective of obtaining information about the structure of the compound nucleus, ^{7}Be. For the reactions amenable to a detailed analysis, a two step procedure was followed. First, the maximum possible amount of information about the scattering matrix was extracted from the cross sections. Second, this information was connected with properties of states of the compound nucleus using resonance theory. This step requires the assumption that the compound nuclear part of the reaction mechanism is dominant.

Most of the resonant states encountered were broad and had many open decay channels involving particles with spin. The analysis of such states is difficult, because the simple formulas of resonance theory tend to break down, or to involve more parameters than can be evaluated, or both. Therefore, the emphasis of the analysis was on the determination of resonant ℓ-values in as many channels as possible, rather than on the extraction of parameters such as partial widths. This was done by using resonance theory to fit the energy dependence of the scattering matrix in the vicinity of the resonant states. The information obtained from the analysis permitted spin and parity assignments to be made.

Some results of scattering and resonance theories will be discussed before they are applied to the analysis of the data.

B. RESULTS OF SCATTERING AND RESONANCE THEORIES

(1) Scattering Theory

The quantum mechanical description of the scattering and reaction processes in terms of a scattering matrix $\underset{\approx}{U}$ is well known (Lane and Thomas 1958). If a channel is specified by the quantum numbers of a pair of nuclei that can initiate, or result from, a reaction, then the elements $U_{cc'}$ relate the amplitude of the outgoing wave in channel c' to those of the incoming waves in channels c. The index c stands for the quantum numbers of the pair, which in one commonly used representation are α, s, ℓ, J, and M. All the internal quantum numbers of the pair are designated by α. The remaining quantum numbers, defining the relative motion of the pair, refer respectively to the channel spin, the relative orbital angular momentum, the total angular momentum, and the total angular momentum projection. Angular momenta are coupled in the following fashion:

$$\vec{s} = \vec{I}_1 + \vec{I}_2$$

$$\vec{J} = \vec{s} + \vec{\ell}$$

where I_1 and I_2 are the spins of the members of the pair. Because

$$U^{JJ'} = U^{J}\delta_{J'J}$$

and $\underset{\approx}{U}$ is independent of M, an element can be written

$$U_{c'c} = U^{J}_{\alpha' s' \ell', \alpha s \ell}$$

$\underset{\approx}{U}$ is symmetric, and the sub-matrix referring to the open channels is unitary.

When the separation r_c of the pair of nuclei in channel c is greater than some channel radius a_c, there is assumed to be no nuclear interaction. Then the relative motion is described by the Schrödinger equation for a Coulomb field. The Coulomb field parameter η_c can be written in terms of the charge numbers of the pair, Z_1 and Z_2, their reduced mass μ_c, and their wave number k_c:

$$\eta_c = \frac{Z_1 Z_2 e^2 \mu_c}{\hbar^2} \frac{1}{k_c} \qquad (1)$$

The quantities μ_c and k_c can be written in terms of the masses of the pair, M_1 and M_2, and their center-of-momentum kinetic energy E_c:

$$\mu_c = \frac{M_1 M_2}{M_1 + M_2}$$

$$k_c = \left(\frac{2\mu_c |E_c|}{\hbar^2}\right)^{\frac{1}{2}}$$

For positive E_c (channel c open) the Schrödinger equation has the solutions $F_c(k_c r_c)$ and $G_c(k_c r_c)$, the regular and irregular Coulomb functions. For negative E_c (channel c closed) the solution is $W_c(-\eta_c, \ell + \frac{1}{2}, 2k_c r_c)$, the exponentially decaying Whittaker function. Other relevant quantities are the phase ω_c,

$$\omega_c = \sum_{n=1}^{\ell} \tan^{-1} \frac{\eta_c}{n}$$

and the amplitude for Rutherford scattering C_c:

$$C_c(\theta) = \frac{1}{\sqrt{4\pi}}\,\eta_c(\mathrm{cosec}^2\,\tfrac{\theta}{2})\exp(-2i\eta_c \log\,\sin\,\tfrac{\theta}{2})$$

where θ is the center-of-momentum angle between the beam axis and the direction of the observed particle.

If the particles which initiate the reaction are unpolarized and the detectors are spin-insensitive, the differential center-of-momentum cross section $\frac{d\sigma}{d\Omega}$ for the reaction $\alpha \to \alpha'$ is given by

$$k_\alpha^2 \frac{d\sigma}{d\Omega} = \pi |C_\alpha(\theta)|^2 \delta_{\alpha'\alpha}$$

$$+ \frac{1}{(2I_1+1)(2I_2+1)}\sqrt{\pi}\sum_{J\ell s}(2J+1)\ \mathrm{Re}\left\{-iT^J_{\alpha s\ell,\,\alpha s\ell}C^*_\alpha(\theta)\right\}P_\ell(\cos\theta)\delta_{\alpha'\alpha}$$

$$+\frac{1}{(2I_1+1)(2I_2+1)}\sum_{\substack{L\\ss'}} B_L(\alpha's',\alpha s)P_L(\cos\theta)$$

where

$$T^J_{\alpha's'\ell',\,\alpha s\ell} = e^{2i\omega_{\alpha'\ell'}}\delta_{\alpha's'\ell',\,\alpha s\ell} - U^J_{\alpha's'\ell',\,\alpha s\ell}$$

$$B_L(\alpha's',\alpha s) = \frac{1}{4}(-)^{s-s'}\sum_{J_1J_2\ell_1\ell_2\ell_1'\ell_2'} \bar{Z}(\ell_1J_1\ell_2J_2sL)\bar{Z}(\ell_1'J_1\ell_2'J_2,\,s'L) \tag{2}$$

$$\times\, T^{J_1}_{\alpha's'\ell_1'\,\alpha s\ell_1}\, T^{J_2\,*}_{\alpha's'\ell_2',\,\alpha s\ell_2}$$

The $\bar{Z}$ coefficients can be written in terms of Clebsch-Gordan and Racah coefficients:

$$\bar{Z}(\ell_1 J_1 \ell_2 J_2, sL) = \sqrt{(2\ell_1+1)(2\ell_2+1)(2J_1+1)(2J_2+1)}\ c(\ell_1 \ell_2\ L,00)W(\ell_1 J_1 \ell_2 J_2, sL)$$

When there is no danger of confusion the labels α and c are sometimes interchanged.

For $\alpha = \alpha'$ (elastic scattering) the first part of equation (2) can be identified with Rutherford scattering, the third with nuclear scattering, and the second with the interference between the two. For $\alpha \neq \alpha'$, the total cross section σ is given by

$$\sigma = \frac{\pi}{k_\alpha^2} \frac{1}{(2I_1+1)(2I_2+1)} \left\{ \sum_{J\ell\ell' ss'} (2J+1) \left| U^J_{\alpha' s' \ell', \alpha s \ell} \right|^2 \right\}$$

which is the coefficient of the Legendre polynomial P_0 multiplied by 4π.

The elements of $\underset{\approx}{U}$ present in any term of the third part of equation (2) can be written down immediately from the triangle conditions for the Racah coefficients and the conservation of parity. This provides an easy way of determining which elements of $\underset{\approx}{U}$, and hence which compound states, can contribute to the coefficient of a given Legendre polynomial P_L. The triangle conditions are

$$\begin{gathered} \Delta(J_1 J_2 L),\ \Delta(\ell_1 J_1 s),\ \Delta(\ell_1 L \ell_2),\ \Delta(J_2 s \ell_2) \\ \Delta(\ell_1' J_1 s'),\ \Delta(\ell_1' L \ell_2'),\ \Delta(J_2 s' \ell_2') \end{gathered} \tag{3}$$

The conservation of parity is contained in the Clebsch-Gordan coefficients $c(\ell_1 \ell_2 L, 00)$ and $c(\ell_1' \ell_2' L, 00)$. The parity π of an element of $\underset{\approx}{U}$ is given by

$$\pi = (-)^{\ell} \pi_1 \pi_2 = (-)^{\ell'} \pi_1' \pi_2' \tag{4}$$

where π_1 and π_2 are the intrinsic parities of the members of the pair that initiate the reaction, and the primed quantities refer to the pair that results from the reaction. The coefficients of the even order polynomials contain the elements of the scattering matrix in the forms $T_{c'c}(\pi = +)T^*_{c'''c''}(+)$ and $T_{c'c}(-)T^*_{c'''c''}(-)$. The coefficients of the odd order polynomials contain the elements in the form $T_{c'c}(+)T^*_{c'''c''}(-)$. The spin and parity assignment of a compound state, denoted J^{π}, is the same as that of the elements of $\underset{\approx}{U}$ through which it is formed and decays.

(2) Resonance Theories

In order to describe reactions that proceed via the formation of a compound nucleus, it is desirable to have an expansion of the scattering matrix in terms of the parameters of some set of states that can be associated with those of the compound nucleus. Such expansions are given by complex eigenvalue theory or by R-matrix theory.

In complex eigenvalue theory the resonant states of the Hamiltonian which describes the system are defined to be those that have purely outgoing waves in all channels. The eigenvalues are complex and correspond to the locations of poles of the analytically continued scattering matrix.

Several expansions of the scattering matrix have been given by the complex eigenvalue theory of Humblet and Rosenfeld (Humblet and Rosenfeld 1961), (Rosenfeld 1961), (Humblet 1962), (Humblet 1964a), (Jeukenne 1964), (Humblet 1964b), (Mahaux 1965a), (Rosenfeld 1965), (Mahaux 1965b). These have been altered slightly here to be consistent with the definition of the scattering matrix given by Lane and Thomas (1958). It is possible to write an expansion with all terms independent of the channel radii:

$$e^{-i(\omega_{c'} + \omega_c)} U_{c'c} - \delta_{c'c}$$

$$= P_{c'}^{\frac{1}{2}}(0) P_c^{\frac{1}{2}}(0) Q_{c'c} - i \sum_n \frac{e^{i(\bar{\xi}_{c'n} + \bar{\xi}_{cn})}}{\sqrt{\kappa_{c'n} \kappa_{cn}} \left| \frac{P_{c'n}(0)\ P_{cn}(0)}{k_{c'n} k_{cn}} \right|^{\frac{1}{2}}} q_n \Gamma_{c'n}^{\frac{1}{2}} \Gamma_{cn}^{\frac{1}{2}} \frac{P_{c'}^{\frac{1}{2}}(0) P_c^{\frac{1}{2}}(0)}{E - E_n + \frac{i\Gamma_n}{2}} \tag{5}$$

The center-of-momentum energy of the system is E, and the energy eigenvalue of the state n is $E_n - \frac{i\Gamma_n}{2}$, with E_n interpreted as the energy of the state, and Γ_n as its width. The radius-independent penetration factors $P_c(0)$ are defined by

$$P_c(0) = k_c^{(2\ell + 1)} \frac{1}{(\ell!)^2} \left\{ (\ell^2 + \eta_c^2) \cdots (1 + \eta_c^2) \right\} \frac{2\pi\eta_c}{e^{2\pi\eta_c} - 1} \tag{6}$$

$Q_{c'c}$ is an unknown, complex, energy-dependent "background" term. The quantities q_n are unknown real constants, but are approximately unity for a sufficiently narrow state (Humblet 1964b). The quantities κ_{cn} are defined by

$$\kappa_{cn} = \mathrm{Re}(k_{cn})$$

The k_{cn} and P_{cn} quantities are the energy-dependent k_c and $P_c(0)$ quantities evaluated at the complex energy eigenvalue n. The phases $\bar{\xi}_{cn}$ are unknown real constants. The quantities Γ_{cn} are positive real constants interpreted as the partial widths of state n for channels c. The relation

$$\Gamma_n = \sum_{c(\text{open})} \Gamma_{cn} \tag{7}$$

is valid.

Other expansions are possible, including one that does not have the property of term-by-term independence of channel radii that was emphasized by Humblet (1964a):

$$e^{-i(\omega_{c'} + \omega_c)} e^{i(\varphi_{c'} + \varphi_c)} U_{c'c} - \delta_{c'c}$$

$$= P_{c'}^{\frac{1}{2}}(a) P_c^{\frac{1}{2}}(a) \bar{Q}_{c',c} - i \sum_n \frac{e^{i(\bar{\xi}_{c'n} + \bar{\xi}_{cn})} O_{c'n} O_{cn}}{\sqrt{\kappa_{c'n} a_{c'} \kappa_{cn} a_c}} q_n \Gamma_{c'n}^{\frac{1}{2}} \Gamma_{cn}^{\frac{1}{2}} \frac{P_c^{\frac{1}{2}}(a) P_{c'}^{\frac{1}{2}}(a)}{E - E_n + \frac{i\Gamma_n}{2}} \tag{8}$$

The phases φ_c are given by

$$\varphi_c = \tan^{-1} \frac{F_c(k_c a_c)}{G_c(k_c a_c)}$$

and the radius-dependent penetration factors $P_c(a)$ by

$$P_c(a) = \left(\frac{k_c r_c}{F_c^2 + G_c^2} \right)_{r_c = a_c} \tag{9}$$

These are the well known penetration factors of R-matrix theory. Usually a_c is chosen according to the relation

$$a_c = R_o(A_1^{\frac{1}{3}} + A_2^{\frac{1}{3}}) \tag{10}$$

where R_o is approximately $1.45\ 10^{-13}$ cm and A_1 and A_2 are the mass numbers of the pair of nuclei in channel c. The quantities O_{cn} are given by

$$O_{cn} = (G_{cn} + iF_{cn})_{r_c = a_c} \tag{11}$$

where G_c and F_c are evaluated at the complex energy eigenvalue n.

For $c' \neq c$, the single-level approximation without background for equation (5) yields

$$|U_{c'c}|^2 = C_{c'c1}(0) \frac{P_{c'}(0)P_c(0)}{(E - E_1)^2 + \frac{\Gamma^2}{4}} \tag{12}$$

where the resonant state has been given the label 1 and the constant $C_{c'c1}$ is essentially the product of the partial widths for channels c' and c:

$$C_{c'c1}(0) = \frac{1}{\kappa_{c'1}\kappa_{c1}\left|\frac{P_{c'1}(0)P_{c1}(0)}{k_{c'n}k_{cn}}\right|} q_n^2 \Gamma_{c'1}\Gamma_{c1} \tag{13}$$

The same approximation for equation (8) yields

$$|U_{c'c}|^2 = C_{c'c1}(a) \frac{P_{c'}(a)P_c(a)}{(E - E_1)^2 + \frac{\Gamma_1^2}{4}} \tag{14}$$

where

$$C_{c'c1}(a) = \frac{|O_{c'1}O_{c1}|^2}{\kappa_{c'1}a_{c'}\kappa_{c1}a_c} q_n^2 \Gamma_{c'1}\Gamma_{c1} \tag{15}$$

The single-level formulas (12) and (14) are the Breit-Wigner formulas of complex eigenvalue theory.

For $c' \neq c$, the two-level approximation without background for equation (5) yields

$$|U_{c'c}|^2 = P_{c'}(0)P_c(0) \left| \frac{C_{c'c1}^{\frac{1}{2}}(0)}{E - E_1 + \frac{i\Gamma_1}{2}} + \frac{C_{c'c2}^{\frac{1}{2}}(0)e^{i\zeta_{c'c}(0)}}{E - E_2 + \frac{i\Gamma_2}{2}} \right|^2$$

where the relative phase $\zeta_{c'c}(0)$ is given by

$$\zeta_{c'c}(0) = \bar{\xi}_{c'2} + \bar{\xi}_{c2} - \bar{\xi}_{c'1} - \bar{\xi}_{c1} \tag{16}$$

The same approximation for equation (8) yields an expression the same as (16) with the label (0) replaced by (a) and the relative phase given by

$$\zeta_{c'c}(a) = \zeta_{c'c}(0) + \arg(O_{c'2}O_{c2}) - \arg(O_{c'1}O_{c1}) \tag{17}$$

The two-level formulas can be written as two single-level terms plus an interference term:

$$|U_{c'c}|^2 = P_{c'}P_c \left[\frac{C_{c'c1}}{(E-E_1)^2+\frac{\Gamma_1^2}{4}} + \frac{C_{c'c2}}{(E-E_2)^2+\frac{\Gamma_2^2}{4}} \right. \tag{18}$$

$$\left. + 2C_{c'c1}^{\frac{1}{2}}C_{c'c2}^{\frac{1}{2}} \frac{\left\{(E-E_1)(E-E_2)+\frac{\Gamma_1\Gamma_2}{4}\right\}\cos\zeta_{c'c}+\left\{(E-E_1)\frac{\Gamma_2}{2}-(E-E_2)\frac{\Gamma_1}{2}\right\}\sin\zeta_{c'c}}{\left\{(E-E_1)^2+\frac{\Gamma_1^2}{4}\right\}\left\{(E-E_2)^2+\frac{\Gamma_2^2}{4}\right\}} \right]$$

The parameters ($C_{c'c1}$, $C_{c'c2}$, $\zeta_{c'c}$) can be replaced by other parameters (α, β, γ) to obtain a form of equation (18) suitable for fitting to experimental data:

$$|U_{c'c}|^2 = P_{c'}P_c \frac{\alpha E^2 + \beta E + \gamma}{\left\{(E-E_1)^2+\frac{\Gamma_1^2}{4}\right\}\left\{(E-E_2)^2+\frac{\Gamma_2^2}{4}\right\}} \tag{19}$$

The parameters (α, β, γ) and (E_1, Γ_1, E_2, Γ_2) can be obtained from an analysis of the data and the parameters ($C_{c'c1}$, $C_{c'c2}$, $\zeta_{c'c}$), which are directly related to resonance theory, calculated from the relations

$$C_{c'c1} = \frac{(E_1^2+\frac{\Gamma_1^2}{4})\alpha + E_1\beta + \gamma \pm \frac{\Gamma_1}{2}\sqrt{-\beta^2+4\alpha\gamma}}{(E_1-E_2)^2+\frac{1}{4}(\Gamma_1-\Gamma_2)^2}$$

$$C_{c'c2} = \frac{(E_2^2+\frac{\Gamma_2^2}{4}) + E_2\beta + \gamma \pm \frac{\Gamma_2}{2}\sqrt{-\beta^2+4\alpha\gamma}}{(E_1-E_2)^2+\frac{1}{4}(\Gamma_1-\Gamma_2)^2}$$

$$2C^{\frac{1}{2}}_{c'c1}C^{\frac{1}{2}}_{c'c2}\cos\zeta_{c'c} = \frac{-2(E_1E_2 + \frac{\Gamma_1\Gamma_2}{4})\alpha - (E_1+E_2)\beta - 2\gamma \mp (\frac{\Gamma_1+\Gamma_2}{2})\sqrt{-\beta^2 + 4\alpha\gamma}}{(E_1 - E_2)^2 + \frac{1}{4}(\Gamma_1 - \Gamma_2)^2}$$

$$2C^{\frac{1}{2}}_{c'c1}C^{\frac{1}{2}}_{c'c2}\sin\zeta_{c'c} = \frac{(E_1\Gamma_2 - E_2\Gamma_1)\alpha - (\frac{\Gamma_1 - \Gamma_2}{2})\beta \pm (E_1 - E_2)\sqrt{-\beta^2 + 4\alpha\gamma}}{(E_1 - E_2)^2 + \frac{1}{4}(\Gamma_1 - \Gamma_2)^2} \qquad (20)$$

The last two relations immediately give $\tan\zeta_{c'c}$, and since $C^{\frac{1}{2}}_{c'c1}$ and $C^{\frac{1}{2}}_{c'c2}$ are positive, $\zeta_{c'c}$ is determined. The equations (20) were obtained by comparing equations (18) and (19) and performing straightforward but tedious algebra.

Two solutions for the set of parameters $(C_{c'c1}, C_{c'c2}, \zeta_{c'c})$ will exist if several obviously necessary conditions such as

$$-\beta^2 + 4\alpha\gamma \geq 0$$

are satisfied by the parameters (α, β, γ) and $(E_1, \Gamma_1, E_2, \Gamma_2)$. The two solutions give the same energy dependence for $|U_{c'c}|^2$, and further information is necessary to distinguish between them. Equation (7) may be helpful in some cases.

The energy dependence of a sum of the form

$$a|U_{c'c}|^2 + b|U_{c'''c''}|^2 + \text{---} \qquad (21)$$

where a, b, --- are known constants, is often of interest when several elements of the scattering matrix are dominated by the same resonant state (or states of the same J^{π}). This can happen when several channel spins contribute to a reaction. In the single-

level approximation the energy dependence of equations (12) and (14) is correct for the sum, although the multiplying constant changes its meaning:

$$C_{c'c1} \rightarrow aC_{c'c1} + bC_{c'''c''1} + \text{---} \tag{22}$$

In the two-level approximation the same holds true for the energy dependence of equation (19), although the meaning of the parameters (α, β, γ) is changed. Although there are now too many unknowns to obtain all the parameters $(C_{c'c1}, C_{c'c2}, \zeta_{c'c})(C_{c'''c''1}, C_{c'''c''2}, \zeta_{c'''c''})$, ---, the phases can be eliminated and D, a simple function of the parameters C, obtained:

$$D \equiv \Gamma_2(aC_{c'c1} + bC_{c'''c''1} + \text{---}) - \Gamma_1(aC_{c'c2} + bC_{c'''c''2} + \text{---}) \tag{23}$$

$$= \frac{\left\{\Gamma_2(E_1^2 - \frac{\Gamma_1\Gamma_2}{4}) - \Gamma_1(E_2^2 - \frac{\Gamma_1\Gamma_2}{4})\right\}\alpha + (E_1\Gamma_2 - E_2\Gamma_1)\beta + (\Gamma_2 - \Gamma_1)\gamma}{(E_1 - E_2)^2 + \frac{1}{4}(\Gamma_1 - \Gamma_2)^2} \tag{24}$$

In the expansion of the differential cross section given by equation (2), the coefficients of several polynomials may be dominated by a sum of the form (21), with the set of constants (a, b, ---) different for each polynomial. In favorable cases it may be possible to separate the contributions of several channel spins if experimental information about several polynomials is available.

Alternatives to the complex eigenvalue expansions of the scattering matrix are provided by R-matrix theory (Lane and Thomas 1958). In this theory, eigenfunctions of the Hamiltonian

are obtained for real energy eigenvalues E_λ by imposing real boundary conditions B_c on the logarithmic derivative of the wave function at the channel radii a_c. These radii, usually chosen in accordance with equation (10), define the channel surfaces. The projection of an eigenfunction λ on a channel surface c is called a reduced width amplitude, denoted by $\gamma_{\lambda c}$, and is real. In the interaction region (all $r_c < a_c$) the eigenfunctions are complete, and the actual scattering wave function can be expanded in terms of them. Moreover, the scattering matrix can be written, at least formally, in terms of Coulomb wave functions, known phases, and the quantities a_c, B_c, E_λ, and $\gamma_{\lambda c}$.

The general expression for the scattering matrix is extremely cumbersome. However, if the B_c are properly chosen, then at certain values of the energy of the system only one term in the expansion of the scattering wave function may be large. This is the condition for the extreme single-level approximation, and the scattering matrix then becomes

$$e^{-i(\omega_{c'} + \omega_c)} e^{i(\varphi_{c'} + \varphi_c)} U_{c'c} - \delta_{c'c} = -i2\gamma_{\lambda c'}\gamma_{\lambda c} \frac{P_{c'}^{\frac{1}{2}}(a)\, P_c^{\frac{1}{2}}(a)}{E - (E_\lambda + \Delta_\lambda) + \frac{i\Gamma_\lambda}{2}} \tag{25}$$

$P_c(a)$ is the radius-dependent penetration factor for channel c defined by equation (9). The energy-dependent total width Γ_λ is given by

$$\Gamma_\lambda = \sum_{c(\text{open})} \Gamma_{\lambda c} \tag{26}$$

with the partial widths $\Gamma_{\lambda c}$ defined by

$$\Gamma_{\lambda c} = 2P_c(a)\gamma_{\lambda c}^2 \tag{27}$$

The level shift Δ_λ, also energy dependent, is given by

$$\Delta_\lambda = \sum_{\text{all } c} \Delta_{\lambda c} \tag{28}$$

where

$$\Delta_{\lambda c} = -(S_c - B_c)\gamma_{\lambda c}^2 \tag{29}$$

and the shift factors S_c are given by

$$S_{c(\text{open})} = \left(k_c r_c \frac{F_c F_c' + G_c G_c'}{F_c^2 + G_c^2}\right)_{r_c=a_c} \tag{30}$$

$$S_{c(\text{closed})} = \left(k_c r_c \frac{W_c'}{W_c}\right)_{r_c=a_c} \tag{31}$$

where the prime denotes differentiation with respect to $k_c r_c$. Usually the B_c are chosen so that the level shift vanishes at the peak of a resonance.

For $c' \neq c$, the extreme single-level approximation (25) yields the single-level formula

$$|U_{c'c}|^2 = 4\gamma^2_{\lambda c'}\gamma^2_{\lambda c} \frac{P_{c'}(a)P_c(a)}{\left\{E - (E_\lambda + \Delta_\lambda)\right\}^2 + \frac{\Gamma^2_\lambda}{4}} \tag{32}$$

which is the Breit-Wigner formula of R-matrix theory.

The energy dependence of a sum of the form (21) was discussed in connection with the complex eigenvalue single-level and two-level formulas. The same discussion also applies to the R-matrix formula (32), and the multiplying constant changes its meaning as follows:

$$4\gamma^2_{\lambda c'}\gamma^2_{\lambda c} \rightarrow 4a\gamma^2_{\lambda c'}\gamma^2_{\lambda c} + 4b\gamma^2_{\lambda c'''}\gamma^2_{\lambda c''} + \text{---}$$

The problem of separating the contributions from several channel spins is the same in the two theories.

Although for a narrow resonant state the Humblet-Rosenfeld single-level formulas and the corresponding R-matrix formula all have essentially the same energy dependence, for a broad state this is no longer true. The most obvious difference is in the penetration factors $P_c(0)$ and $P_c(a)$, the former tending to be more rapidly varying with energy, as shown in Figure 27. If the formulas are used to analyze a broad state when several channels are open, a crucial difference is the energy dependence of the R-matrix quantities $(E_\lambda + \Delta_\lambda)$ and Γ_λ, while the corresponding Humblet-Rosenfeld quantities E_1 and Γ_1 are constants. In fact, the energy dependence of the R-matrix formula is unknown unless

the reduced widths $\gamma^2_{\lambda c}$ for all channels are known, although often only the $\gamma^2_{\lambda c}$ for the open channels are important. Similar remarks apply to the two-level formulas of the two theories.

Although the Humblet-Rosenfeld formulas tend to be simpler than the R-matrix ones, they do not necessarily provide the more accurate approximation to the energy dependence of the scattering matrix. For example, the correct cusp behavior of $|U_{c'c}|^2$ at the threshold for a channel $c''(c'' \neq c', c)$ is contained in the R-matrix single-level formula, but not in the corresponding Humblet-Rosenfeld formulas. Moreover, the Humblet-Rosenfeld formulas are not unitary. Nevertheless, good fits to experimental data have been achieved with the Humblet-Rosenfeld theory by Jeukenne (1964) and Mahuax (1965b), using the radius-independent penetration factors.

Although a more detailed comparison of the two theories is not relevant to the applications to be discussed, it should be noted that up to the present (1966) it has been within the framework of R-matrix theory that most data have been analyzed and most nuclear model calculations performed. Therefore, a comparison of the results to be discussed with previous work and with theoretical predictions would be more straightforward within the framework of an R-matrix analysis. A complete R-matrix analysis has not been possible, however, because of the large width of one of the resonant states involved, and the large number of open channels. Although a knowledge of the form of the R-matrix single-level formula has been useful, the simplicity of the Humblet-Rosenfeld formulas has been decisive, and they have been used in most of the following analysis.

C. THE ELASTIC SCATTERING $^{6}Li(p, p)^{6}Li$

The behavior of the excitation functions in Figure 7 suggests the existence of a broad state in ^{7}Be at about 10-MeV excitation energy. The reacting particles have the following properties:

	p	^{6}Li
J^{π}	$\frac{1}{2}^{+}$	1^{+}

and hence the channel spins are

s	s'
$\frac{1}{2}, \frac{3}{2}$	$\frac{1}{2}, \frac{3}{2}$

The expansion (2) can be evaluated and, at least in principle, compared with the data to give information about the scattering matrix, and hence, about the properties of such a state. The expansion is seriously complicated by the Rutherford scattering amplitude $C_{\alpha}(\theta)$, even though the $|C_{\alpha}(\theta)|^{2}$ term can be removed because the absolute normalization of the data is known. If ℓ is the highest relative orbital angular momentum to contribute appreciably to the elastic scattering, there are $4\ell + 3$ terms of different angular dependence in expansion (2), and hence the same number of parameters to be determined from each angular distribution. In some cases, these parameters completely determine (or over-determine) the scattering matrix, but in the present case, because the particles have spin and reaction channels are open, they do not. A detailed study of polarization and of the reaction channels is, in principle, required to determine even the part of

the scattering matrix describing the elastic scattering. This is equivalent to saying that the $4\ell + 3$ parameters are independent even though they are all functions of this matrix, because the number of unknown quantities in the matrix exceeds $4\ell + 3$.

Because of the rather high energy, several ℓ-values must be considered, and the data are not nearly accurate enough for the $4\ell + 3$ independent parameters to be extracted. Consequently, attempts were made to guess the appropriate resonant and non-resonant elements of the scattering matrix with the hope that the procedure would suggest which elements are resonant. The cross section corresponding to each guess was calculated and compared with experiment. The results were inconclusive because of the large number of unknown quantities, and the large width of the ^{7}Be structure.

It is interesting that the angular distributions in the vicinity of the 10-MeV peak are somewhat similar to those in the vicinity of the 7.18-MeV state obtained by McCray (1962). Possibly this is due to the dominance of the same ℓ-value, $\ell = 1$ according to McCray's analysis. If this is the case, and if the 10-MeV peak is predominantly due to a single ^{7}Be resonant state, some limits are set on its J^{π}:

Channel Spins	$s = \frac{1}{2}, \frac{3}{2}$
Orbital Angular Momentum	$\ell = (1)$
Possible Spin and Parity	$J^{\pi} = (\frac{1}{2}^{-}, \frac{3}{2}^{-}, \text{or } \frac{5}{2}^{-})$

Moreover, because of the isotopic spins assignments

	p	^{6}Li
T	$\frac{1}{2}$	0

the state should have the isotopic spin assignment $T = \frac{1}{2}$. Both the formation and the decay of states of any other isotopic spin are forbidden in this reaction. The possibility of obtaining information about the partial widths of the state is discussed in Appendix A.

In addition to the broad ^{7}Be structure at 10-MeV excitation energy, there is possible evidence for additional very broad structure at roughly 13 MeV (Figure 7).

D. THE INELASTIC SCATTERING ^{6}Li(p, p')^{6}Li*

In several ways the analysis of inelastic scattering is simpler than that of elastic scattering. A simple Legendre polynomial expansion of the cross section is possible, and fewer values of the outgoing relative orbital angular momentum need be considered because of the decreased energy available for the penetration of the Coulomb-centrifugal barrier. Moreover, the expansions of the scattering matrix given by resonance theory are simpler, although usually only the product $\Gamma_{c'n}\Gamma_{cn}$ can be determined from inelastic scattering alone, and not the individual partial widths.

The behavior of the coefficients of the first few Legendre polynomials, Figure 15, strongly supports the existence of a broad state in ^{7}Be at about 10-MeV excitation energy. Information about the properties of such a state can be obtained from a knowledge of which elements of the scattering matrix are present in each coefficient. These are determined by the triangle conditions (3), the conservation of parity, and the properties,

	p	^{6}Li	^{6}Li*
J^π	$\frac{1}{2}^+$	0^+	3^+

which determine the channel spins,

s	s'
$\frac{1}{2}, \frac{3}{2}$	$\frac{5}{2}, \frac{7}{2}$

According to equation (4), the parity of an element of the scattering matrix is given by

$$(-)^{\ell} \text{ or } (-)^{\ell'}$$

If the contributions from the s, p, and d incoming ℓ-values, and from the s and p outgoing ℓ-values are included, the polynomial expansion given by equation (2) is

$$k^2 \frac{d\sigma}{d\Omega} = \left\{ \frac{1}{3} \left| U^{\frac{7}{2}}_{\frac{7}{2}\ 0,\frac{3}{2}\ 2} \right|^2 + \frac{1}{4} \left| U^{\frac{5}{2}}_{\frac{5}{2}\ 0,\frac{3}{2}\ 2} \right|^2 + \frac{1}{4} \left| U^{\frac{5}{2}}_{\frac{5}{2}\ 0,\frac{1}{2}\ 2} \right|^2 \right.$$

$$\left. + \frac{1}{4} \left| U^{\frac{5}{2}}_{\frac{7}{2}\ 1,\frac{3}{2}\ 1} \right|^2 + \frac{1}{4} \left| U^{\frac{5}{2}}_{\frac{5}{2}\ 1,\frac{3}{2}\ 1} \right|^2 + \frac{1}{6} \left| U^{\frac{3}{2}}_{\frac{5}{2}\ 1,\frac{3}{2}\ 1} \right|^2 + \frac{1}{6} \left| U^{\frac{3}{2}}_{\frac{5}{2}\ 1,\frac{1}{2}\ 1} \right|^2 \right\} P_0(\cos\theta)$$

$$+ 2\mathrm{Re}\left\{-\frac{1}{\sqrt{10}}\, U^{\frac{7}{2}\,*}_{\frac{7}{2}\,0,\frac{3}{2}\,2}\, U^{\frac{5}{2}}_{\frac{7}{2}\,1,\frac{3}{2}\,1} + \frac{3}{20}\, U^{\frac{5}{2}\,*}_{\frac{5}{2}\,0,\frac{3}{2}\,2}\, U^{\frac{5}{2}}_{\frac{5}{2}\,1,\frac{3}{2}\,1}\right.$$

$$\left. -\sqrt{\frac{7}{200}}\, U^{\frac{5}{2}\,*}_{\frac{5}{2}\,0,\frac{3}{2}\,2}\, U^{\frac{3}{2}}_{\frac{5}{2}\,1,\frac{3}{2}\,1} - \frac{1}{\sqrt{20}}\, U^{\frac{5}{2}\,*}_{\frac{5}{2}\,0,\frac{1}{2}\,2}\, U^{\frac{3}{2}}_{\frac{5}{2}\,1,\frac{1}{2}\,1}\right\} P_1(\cos\theta)$$

$$+ \left\{\frac{1}{20}\left|U^{\frac{5}{2}}_{\frac{7}{2}\,1,\frac{3}{2}\,1}\right|^2 - \frac{4}{25}\left|U^{\frac{5}{2}}_{\frac{5}{2}\,1,\frac{3}{2}\,1}\right|^2 - \sqrt{\frac{63}{1250}}\,\mathrm{Re}\left(U^{\frac{5}{2}\,*}_{\frac{5}{2}\,1,\frac{3}{2}\,1}\, U^{\frac{3}{2}}_{\frac{5}{2}\,1,\frac{3}{2}\,1}\right)\right.$$

$$\left. - \frac{2}{75}\left|U^{\frac{3}{2}}_{\frac{5}{2}\,1,\frac{3}{2}\,1}\right|^2 + \frac{1}{30}\left|U^{\frac{3}{2}}_{\frac{5}{2}\,1,\frac{1}{2}\,1}\right|^2\right\} P_2(\cos\theta) \qquad (33)$$

If the most significant ℓ-values have been included in equation (33), it is clear from the form of the P_2 coefficient that both the formation and the decay of the state are predominantly p-wave. The identity of the predominant ℓ-values could in principle be tested by fitting the ℓ-dependent single-level formulas (12), (14) or (32) to the coefficients of P_0 or of P_2, if the coefficients are dominated by a sum of the form (21), in which a single resonant state is significant. Certainly this condition can be only approximately satisfied. The coefficient of P_0 contains contributions from many states, and the coefficient of P_2, while simpler in this respect, contains terms such as $\mathrm{Re}(U^{5/2\,*}\, U^{3/2})$, this particular term having a relatively large numerical factor.

With these complications in mind, attempts were made to fit the coefficients of P_0 and of P_2 in the vicinity of the resonant state with formulas (12) and (14), using the different possible combinations of ℓ-values. The procedure is described in Appendix B. A fit to the coefficient of P_0 was not possible, suggesting that several states contribute significantly to the reaction. Good fits to the coefficient of P_2 were possible, but only for p-wave decay of the state. The fits were considerably better for p-wave formation of the state than for f-wave formation. The fits with the radius-dependent and radius-independent penetration factors are shown in Figures 28a and b respectively, the former being superior. The parameters of the fits are summarized in Table 11, and the most important are

E_1	Γ_1	ℓ	ℓ'
10.0	1.8	(1)	1

where the first two quantities are in terms of MeV ^{7}Be excitation energy.

The encouraging success of the fits, suggesting that the ℓ-values are correctly determined, permits negative parity to be assigned to the state and limits to be set on its spin assignment:

	Formation	Decay
Channel Spins	$s = \frac{1}{2}, \frac{3}{2}$	$s = \frac{5}{2}, \frac{7}{2}$
Orbital Angular Momentum	$\ell = (1)$	$\ell' = 1$
Possible Spin and Parity	$J^\pi = (\frac{1}{2}^-, \frac{3}{2}^-, \text{ or } \frac{5}{2}^-)$	$J^\pi = \frac{3}{2}^-, \frac{5}{2}^-, \frac{7}{2}^-, \text{or } \frac{9}{2}^-$

Therefore

$$J^{\pi} = \frac{3}{2}^{-} \text{ or } \frac{5}{2}^{-} \text{ or possibly } \left(\frac{7}{2}^{-} \text{ or } \frac{9}{2}^{-}\right)$$

Moreover, because of the isotopic spin assignments

	p	^{6}Li	^{6}Li*
T	$\frac{1}{2}$	0	0

the state should have isotopic spin $T = \frac{1}{2}$. Both the formation and the decay of states of any other isotopic spin are forbidden in this reaction.

It will be apparent later that the state has $J^{\pi} = \frac{3}{2}^{-}$.

Therefore, only the $s' = \frac{5}{2}$ partial width for the decay of the state is significant, because the decay is predominantly p-wave. Since the experimental value of the P_2 coefficient is negative, equation (33) implies that the $s = \frac{3}{2}$ partial width for the formation of the state is non-zero. The possibility of obtaining qualitative information about the partial widths is considered in Appendix B.

Little can be said about the coefficients of polynomials other than P_0 and P_2, except that many states of both parities, some with appreciable widths for high ℓ-values, contribute to the reaction, or direct interactions are playing an appreciable role.

E. THE INELASTIC SCATTERING ^{6}Li(p, p'')^{6}Li**

The behavior of the coefficients of the first few polynomials, Figure 23, supports the existence of a broad state in ^{7}Be at about 10-MeV excitation energy, but the anomalous behavior at about

11 MeV is a different feature, and not apparent in the $^6Li(p, p)^6Li$ and $^6Li(p, p')^6Li^*$ reactions. The elements of the scattering matrix present in each coefficient are determined by the following properties of the initial and final products:

	p	^{6}Li	^{6}Li**
J^π	$\frac{1}{2}^+$	1^+	0^+

Hence the channel spins are

s	s'
$\frac{1}{2}, \frac{3}{2}$	$\frac{1}{2}$

and the parity of a scattering matrix element is

$$(-)^{\ell} = (-)^{\ell'}$$

If the contributions from the s, p, and d incoming ℓ-values, and from the s and p outgoing ℓ-values are included, the polynomial expansion given by equation (2) is

$$k^2 \frac{d\sigma}{d\Omega} = \left\{ \frac{1}{12} \left| U^{\frac{1}{2}}_{\frac{1}{2}\,0,\frac{1}{2}\,0} \right|^2 + \frac{1}{12} \left| U^{\frac{1}{2}}_{\frac{1}{2}\,0,\frac{3}{2}\,2} \right|^2 \right.$$

$$\left. + \frac{1}{12} \left| U^{\frac{1}{2}}_{\frac{1}{2}\,1,\frac{1}{2}\,1} \right|^2 + \frac{1}{12} \left| U^{\frac{1}{2}}_{\frac{1}{2}\,1,\frac{3}{2}\,1} \right|^2 \right.$$

$$+\frac{1}{6}\left|U^{\frac{3}{2}}_{\frac{1}{2}\,1,\frac{1}{2}\,1}\right|^2+\frac{1}{6}\left|U^{\frac{3}{2}}_{\frac{1}{2}\,1,\frac{3}{2}\,1}\right|^2\Big\}P_0(\cos\theta)$$

$$+\{\text{coef.}\}P_1(\cos\theta)$$

$$+\Big\{\frac{1}{6}\left|U^{\frac{3}{2}}_{\frac{1}{2}\,1,\frac{1}{2}\,1}\right|^2-\frac{2}{15}\left|U^{\frac{3}{2}}_{\frac{1}{2}\,1,\frac{3}{2}\,1}\right|^2 \tag{34}$$

$$+\frac{1}{3}\mathrm{Re}\left(U^{\frac{1}{2}*}_{\frac{1}{2}\,1,\frac{1}{2}\,1}U^{\frac{3}{2}}_{\frac{1}{2}\,1,\frac{1}{2}\,1}\right)-\frac{\sqrt{10}}{30}\mathrm{Re}\left(U^{\frac{1}{2}}_{\frac{1}{2}\,1,\frac{3}{2}\,1}U^{\frac{3}{2}}_{\frac{1}{2}\,1,\frac{3}{2}\,1}\right)\Big\}P_2(\cos\theta)$$

The coefficient of P_1 was not worked out because it was not possible to make use of it.

If the most significant ℓ-values have been included in equation (34), it is clear from the form of the P_2 coefficient that both the formation and the decay of the broad state are predominantly p-wave. This cannot be tested by the fitting of single-level formulas (12) and (14), as was done in the analysis of the ^{6}Li(p, p')^{6}Li* reaction, because of the presence of the 11-MeV anomaly.

It is important to decide if the anomaly could be a cusp associated with a nearby neutron threshold. The ^{6}Be + n threshold, located at 10.68 MeV and about 100 keV broad, is fairly well separated in energy from the anomaly. In addition, according to the R-matrix single-level formula, if the reactions ^{6}Li(p, p)^{6}Li, ^{6}Li(p, p')^{6}Li* and ^{6}Li(p, p'')^{6}Li** proceed through the same

compound state, then the same cusp should appear in all of them. That it does not appear in the first two reactions is evident from Figures 5 and 15. Moreover, because the anomaly seems to appear in the negative parity scattering matrix elements, it would have to be associated with the p-wave part of the ^{6}Be + n channel (since both these particles have positive parity), while large cusps are generally associated with the s-wave part of the neutron channel.

Therefore, it seems probable that the anomaly is caused by the interference between the broad 10 MeV state and a narrower one at about 11 MeV with the same J^π. The states must be of the same J^π to interfere in the coefficient of P_0. The behavior of this coefficient cannot be explained in terms of non-interfering states. This two-level hypothesis, and the identity of the dominant ℓ-values, could in principle be tested by fitting the two-level formula (19) to the coefficients of P_0 or of P_2, if the same conditions discussed in connection with the ^{6}Li(p, p')^{6}Li* analysis are satisfied. The difficulties are similar; the coefficient of P_0 contains contributions from many states, and the coefficient of P_2, although simpler in this respect, contains terms such as $\mathrm{Re}(U^{1/2*} U^{3/2})$.

With these complications in mind, attempts were made to fit the two-level formula (19) to the coefficients of P_0 and of P_2 over a range of excitation energy containing the interesting features of the data. The procedure is described in Appendix C. Fits to the coefficient of P_0 were possible using essentially the same position and width for the broad 10-MeV state that were obtained from the ^{6}Li(p, p')^{6}Li* analysis. The quality of the fits was not changed appreciably by the inclusion of a smoothly varying, non-interfering background from other states. Fits were only possible for p-wave decay of the resonant states, and were superior for the radius-

dependent penetration factors. The fits are plotted in Figures 29, 30, and 31a, in which p-wave formation of the resonant states has been assumed. The parameters of the fits are summarized in Table 12 and the most important are

E_1	Γ_1	E_2	Γ_2	ℓ	ℓ'
10.0	1.8	11.0	0.4	(1)	1

where the first four quantities are in terms of MeV ^{7}Be excitation energy, and the indices 1 and 2 refer to the broad and to the narrower states respectively.

Similar fits to the coefficient of P_2 were also possible, but the position and width obtained for the broad state were somewhat different from those obtained from the ^{6}Li(p, p')^{6}Li* analysis. It is quite possible that this is due to the $\mathrm{Re}(U^{1/2*} U^{3/2})$ terms in the coefficient. A sample fit is shown in Figure 31b.

The encouraging success of the fits, suggesting that the two-level hypothesis is correct and that the ℓ-values are correctly determined, permits negative parity to be assigned to the states and limits to be set on their spin assignment:

	Decay
Channel Spin	$s' = \frac{1}{2}$
Orbital Angular Momentum	$\ell' = 1$
Possible Spin and Parity	$J^\pi = \frac{1}{2}^-, \frac{3}{2}^-$

No further restriction is obtained from the consideration of the probable $\ell = 1$ formation of the states. These restrictions on J^{π} can be combined with those obtained for the broad state from the $^{6}Li(p, p')^{6}Li^{*}$ analysis, to yield the unique assignment $J^{\pi} = \frac{3}{2}^{-}$ for both states.

Returning to the $^{6}Li(p, p'')^{6}Li^{**}$ reaction, it can be seen in Figure 23 that the coefficient of P_2 has roughly the same energy dependence as that of P_0, and is at least as large at about 10.5 MeV. Such a large P_2 coefficient can be accounted for within the framework of equation (34) only if terms of the form $Re(U^{1/2*} U^{3/2})$ are significant; this was also suggested by the two-level fit to the P_2 coefficient. An appreciable contribution to the reaction from a $J^{\pi} = \frac{1}{2}^{-}$ state is therefore suggested. This state is apparently very broad, because it did not have to be taken into consideration to obtain good fits to the P_0 coefficient.

The narrower $J^{\pi} = \frac{3}{2}^{-}$ state seems to be weakly excited and to be observed only through its interference with the broad $J^{\pi} = \frac{3}{2}^{-}$ state. Because the channel spin of the initial products is not unique, it is not possible to decompose the two-level fit into terms of the form contained in equation (18). However, under the assumption that the second term in equation (23) is much less than the first, the contribution to the fit from the broad state alone can be approximately separated, and is plotted for a particular case in Figure 29d. The difference between the fitted curve and this curve is approximately the interference contribution to the reaction.

Because of the isotopic spin assignments

	p	^{6}Li	$^{6}Li^{*}$	$^{6}Li^{**}$
T	$\frac{1}{2}$	0	0	1

both the formation and the decay of $T = \frac{3}{2}$ compound states is forbidden in the $^6Li(p, p)^6Li$ and $^6Li(p, p')^6Li^*$ reactions, but only the formation is forbidden in the $^6Li(p, p'')^6Li^{**}$ reaction. The narrower $J^\pi = \frac{3}{2}^-$ state is not observed in the first two of these reactions (Figures 5 and 15), but is observed to contribute weakly to the third. These facts imply that its isotopic spin assignment should be $T = \frac{3}{2}$.

The possibility of obtaining information about partial widths is considered in Appendix C. The discussion of the coefficients of polynomials other than P_0 and P_2 is the same as that given in the discussion of the $^6Li(p, p')^6Li^*$ reaction.

F. THE REACTION $^4He(^3He, p'')^6Li^{**}$

The general features of the coefficient of the Legendre polynomial P_0, Figure 25, are quite similar to those observed in the $^6Li(p, p'')^6Li^{**}$ reaction: a broad peak supporting the existence of a broad ^7Be state at about 10 MeV, and an anomaly supporting the existence of a narrower state at about 11 MeV. The elements of the scattering matrix present in the coefficient are determined by the following properties of the initial and final products:

	^3He	^4He	p	$^6Li^{**}$
J^π	$\frac{1}{2}^+$	0^+	$\frac{1}{2}^+$	0^+

Hence the channel spins are

$$s = \frac{1}{2}, \quad s' = \frac{1}{2}$$

and the parity of a scattering matrix element is

$$(-)^{\ell} = (-)^{\ell'}$$

If the contributions from the s, p, and d incoming ℓ-values, and from the s and p outgoing ℓ-values are included, the polynomial expansion given by equation (2) is

$$k^2 \frac{d\sigma}{d\Omega} = \left\{ \frac{1}{4} \left| U^{\frac{1}{2}}_{\frac{1}{2}\,0,\frac{1}{2}\,0} \right|^2 + \frac{1}{4} \left| U^{\frac{1}{2}}_{\frac{1}{2}\,1,\frac{1}{2}\,1} \right|^2 + \frac{1}{2} \left| U^{\frac{3}{2}}_{\frac{1}{2}\,1,\frac{1}{2}\,1} \right|^2 \right\} P_0(\cos\theta)$$

$$+ \left\{\text{coef.}\right\} P_1(\cos\theta) + \left\{\text{coef.}\right\} P_2(\cos\theta) \qquad (35)$$

where the coefficients of P_1 and of P_2 have not been worked out.

The two-level formula (19) was fitted to the coefficient of P_0 over the same range of excitation energy used in the ^{6}Li(p, p")^{6}Li** analysis. The procedure is described in Appendix D. Good fits were obtained for p-wave formation and decay of the states and for positions and widths essentially the same as those obtained from the ^{6}Li(p, p')^{6}Li* and ^{6}Li(p, p'')^{6}Li** analyses. The fits are plotted in Figures 25, 32, and 33. It can be seen that the quality of the fits is not changed appreciably by the inclusion of a smoothly varying, non-interfering background from other states, but is influenced by the range of data fitted. The success of the fits is further evidence that the two-level hypothesis is correct and that the ℓ-values are correctly determined. The J^{π} restrictions on the states are the same as those obtained from the ^{6}Li(p, p'')^{6}Li** reaction.

Since the channel spins of both the initial and the final products are unique in the $^{4}He(^{3}He, p'')^{6}Li^{**}$ reaction, the two-level fit can be decomposed into two single-level contributions plus an interference contribution, as in equation (18). This is shown in Figure 34, in which, although not necessary, a non-interfering background has been assumed. The narrower state is very weakly excited. Strictly speaking, as discussed in connection with equations (20), there are two possible decompositions. The other one consists of an extremely large contribution from the narrower level almost cancelling an extremely large interference contribution. The first decomposition is probably the more plausible one.

Because of the isotopic spin assignments

	^{4}He	^{3}He	p	$^{6}Li^{**}$
T	0	$\frac{1}{2}$	$\frac{1}{2}$	1

and the fact that the narrower state seems to be weakly excited, the isotopic spin assignment $T = \frac{3}{2}$ is implied for this state, in agreement with the $^{6}Li(p, p'')^{6}Li^{**}$ analysis.

The possibility of obtaining information about partial widths is considered in Appendix D.

G. REACTIONS STUDIED BY OTHER INVESTIGATORS

The $^4He(^3He, ^3He)^4He$, $^4He(^3He, p)^6Li$, and $^4He(^3He, p')^6Li^*$ reactions have been studied by Spiger and Tombrello (1964). In the first and third of these reactions another broad ^7Be state was observed at about 9.2-MeV excitation energy having the following properties: $J^\pi = (\frac{7}{2}^-)$, large partial widths for $^4He + ^3He$ and for $^6Li^* + p$, and small partial width for $^6Li + p$. The $^4He(^3He, p)^6Li$ reaction and its inverse, the $^6Li(p, ^4He)^3He$ reaction (Heydenburg and Han 1962), do not seem to be dominated either by the 9.2-MeV state or by the 10-MeV ($J^\pi = \frac{3}{2}$, $T = \frac{1}{2}$) state. Some direct interaction contribution to the reaction mechanism seems to be present.

The information from all reactions studied is consistent with a small $^6Li + p$ partial width for the 9.2-MeV state, and a small $^4He + ^3He$ partial width and a large $^6Li + p$ partial width for the 10-MeV state. However, the $^4He + ^3He$ partial width of the 10-MeV state must be non-zero, since it has a strong, probably dominant, influence on the $^4He(^3He, p'')^6Li^{**}$ reaction. The reason for this may be the attenuation of the influence of the 9.2-MeV state because of its location near threshold, and its high spin, which requires f-wave decay.

A $T = \frac{3}{2}$ state, presumably the same state as reported here, has recently been observed in the $^9Be(p, t)^7Be$ reaction by Détraz et al. (1965) who assign to it the following properties:

Resonant Energy	Width	J^π	T
10.79 ± 0.04	0.298 ± 0.025	$\frac{3}{2}^-$	$\frac{3}{2}$

where the first two quantities are in terms of MeV ^7Be excitation energy.

IV. SUMMARY

Two states in ^{7}Be with the following properties were identified:

Resonant Energy	Width	J^{π}	T
10.0	1.8	$\frac{3}{2}^{-}$	$\frac{1}{2}$
11.0 ± 0.05	0.4 ± 0.05	$\frac{3}{2}^{-}$	$\frac{3}{2}$

where the quantities in the first two columns are in terms of MeV ^{7}Be excitation energy.

From the interference of the two states in the total cross sections for the reactions ^{6}Li(p, p'')^{6}Li** and ^{4}He(^{3}He, p'')^{6}Li** it was inferred that they have the same J^{π}. In both of the channels

$$^{6}\text{Li}^{*}(3^{+},\ T = 0) + p'$$

$$^{6}\text{Li}^{**}(0^{+},\ T = 1) + p''$$

the ℓ-value of the decay of the first state was found to be one, permitting the J^{π} assignment to be made from the conservation of angular momentum and parity. The basic reason that a unique assignment is possible is the large difference in the spins of the first and second excited states of ^{6}Li.

The T assignment of the first state was made from the fact that it is observed in all of the reactions ^{6}Li(p, p)^{6}Li, ^{6}Li(p, p')^{6}Li*, ^{6}Li(p, p'')^{6}Li** and ^{4}He(^{3}He, p'')^{6}Li**, in which both the formation and the decay of $T = \frac{1}{2}$ states is allowed. The T assignment of the

second state was made from two facts: that it is observed in only the last two reactions, which are the ones in which the decay of $T = \frac{3}{2}$ states is allowed, and that it is weakly excited, which is consistent with its forbidden formation. Probably the $T = \frac{3}{2}$ state is observed because of a small amount of mixing with the $T = \frac{1}{2}$ state.

The data were fitted with formulas from complex eigenvalue resonance theory, and the ℓ-values determined through the ℓ-dependence of the penetration factors in these formulas. The ℓ-values crucial to the J^{π} assignment were well determined; fits using the allowed ℓ-values were impossible. To achieve good fits, it was necessary to use radius-dependent penetration factors. Although the fits with the radius-independent penetration factors were poorer, the ℓ-values given by the fits, and hence the J^{π} assignments, were the same.

The value obtained for the resonant incoming and outgoing ℓ-values ($\ell = \ell' = 1$) in the $^{6}Li(p, p')^{6}Li^{*}$ and $^{6}Li(p, p'')^{6}Li^{**}$ reactions is consistent with the resonant behavior of the P_2 coefficients and the lack of resonant behavior of coefficients of polynomials higher than P_3. This is because of the form of the expansion of the cross section in terms of the scattering matrix.

Although the identification of the two states in ^{7}Be and their assignments seem to be independent on the resonance theory used, the same is not necessarily true for their detailed properties. This is particularly the case for the $T = \frac{1}{2}$ state, because of its large width. To a lesser extent, it may also be the case for the $T = \frac{3}{2}$ state. This state, and the one observed in the $^{9}Be(p, t)^{7}Be$ reaction (Détraz et al. 1965), are presumably the same, and it is possible that at least some of the discrepancy in energy and in width is due to the resonance theory used.

The estimates of partial widths (Appendices A to D) depend not only on the resonance theory used, but also on strong assumptions about the importance of other states. The situation is further complicated by the spins of the particles involved. It can be said, however, that the $T = \frac{1}{2}$ state seems to have a large width for $^6Li + p$, and for $^6Li^* + p'$, a considerably smaller width for $^6Li^{**} + p''$, and a small (but by no means zero) width for $^4He + ^3He$. Moreover, the $T = \frac{3}{2}$ state seems to have very small widths for the isotopic-spin forbidden channels, $^6Li + p$, $^6Li^* + p'$, and $^4He + ^3He$, although the widths for the first and third of these channels, at least, are non-zero. It seems to have an appreciable width for the isotopic-spin allowed channel $^6Li^{**} + p''$.

Some evidence was found for extremely broad $J^\pi = \frac{1}{2}^-$ structure in ^7Be at an excitation energy of roughly 10 MeV or greater, and possibly for other broad structure at roughly 13 MeV.

All the information obtained seems to be at least approximately consistent with the calculations of Barker (1966). The parameters of these calculations were constrained to give reasonable agreement with the locations of the first five states and the $T = \frac{3}{2}$ state in the mirror nucleus, ^7Li. Considering this, and the large widths involved, the 9.2-MeV ($J^\pi = \frac{7}{2}^-$) state of Spiger and Tombrello (1964), the 10-MeV ($J^\pi = \frac{3}{2}^-$, $T = \frac{1}{2}$) state, and the 11-MeV ($J^\pi = \frac{3}{2}^-$, $T = \frac{3}{2}$) state occur at roughly the energies predicted, although the ordering of the first two states differs from the prediction. The existence of a broad $J^\pi = \frac{1}{2}^-$ state at roughly 10 MeV is consistent with prediction, as are the qualitative properties of the partial widths of the 10-MeV ($J^\pi = \frac{3}{2}^-$, $T = \frac{1}{2}$) state.

The analysis carried out suggests that the version of complex eigenvalue theory using radius-dependent penetration factors leads to better approximations than the version using radius-independent factors, although the situation is too complicated to provide an unambiguous test of different versions of resonance theory. The conclusion about penetration factors is just the opposite of that drawn by Jeukenne (1964) from an analysis of other reactions. The disagreement may be related to the fact that the ideal situation for an unambiguous test is not easy to find. The simple formulas of any version of resonance theory are only approximations, and in most cases, at least, it is difficult to know if the approximations are good enough to distinguish between different versions of the theory.

APPENDIX A - $^{6}Li(p, p)^{6}Li$ REACTION

With the assumptions that the 10-MeV peak is predominantly due to a single ^{7}Be resonant state, and that a large part of its width is for the emission of p-wave protons to the ground state of ^{6}Li, a sum of R-matrix reduced widths can be estimated using equations (26) and (27):

$$\Gamma_1 = 2P_{p1}(a_p)\left\{\gamma^2_{1(p\frac{3}{2})} + \gamma^2_{1(p\frac{1}{2})}\right\}, \quad a_p = 4.08\ 10^{-13}\text{cm} \quad .$$

The subscript 1 labels the state, the subscript p labels the particles and their relative orbital angular momentum, and the other subscript labels the channel spin. For example, the subscript $(p\frac{3}{2})$ means

$$^{6}\text{Li} + p, \quad \ell = 1, \quad s = \frac{3}{2}$$

and the subscript $(p\frac{1}{2})$,

$$^{6}\text{Li} + p, \quad \ell = 1, \quad s = \frac{1}{2} \quad .$$

The total width Γ_1 was estimated from the 180° excitation function in Figure 7, and the penetration factor calculated with the CIT IBM 7090 computer using a Fortran code prepared by Tombrello (1963). The following result was obtained:

$$\left\{\gamma^2_{1(p\frac{3}{2})} + \gamma^2_{1(p\frac{1}{2})}\right\} \simeq 0.75 \pm 0.5 \text{ MeV}$$

which is roughly similar to the value of about 1.2 MeV for $\gamma^2_{(p\frac{3}{2})}$ found by McCray (1962) for the 7.18-MeV state.

APPENDIX B - $^{6}Li(p, p')^{6}Li^{*}$ REACTION

The problem of fitting the single level formulas (12) or (14) to an experimentally determined polynomial coefficient is that of determining the parameters (C_1', E_1, Γ_1) in the expression

$$(\text{poly. coef.}) = \frac{1}{k^2} \frac{C_1' P_\ell P_{\ell'}}{(E - E_1)^2 + \frac{\Gamma_1^2}{4}} .$$

This amounts to the determination of the parameters (α, β, γ) in the expression

$$\frac{P_\ell P_{\ell'}}{k^2(\text{poly. coef.})} = \alpha E^2 + \beta E + \gamma \qquad \text{(B1)}$$

where

$$\begin{aligned} C_1' &= \frac{1}{\alpha} \\ E_1 &= -\frac{\beta}{2\alpha} \\ \Gamma_1 &= \sqrt{\frac{4\gamma}{\alpha} - \frac{\beta^2}{\alpha^2}} \end{aligned} \qquad \text{(B2)}$$

The parameters (α, β, γ) were determined by the method of least squares using the CIT IBM 7094 computer with a Fortran code. At each energy, using the value of the polynomial coefficient and its error given in Table 3, the quantity on the left hand side of equation (B1) and its error were calculated, and a weighting factor assigned

equal to the square of the reciprocal of this error. The parameters (C_1', E_1, Γ_1) were calculated from equations (B2). The errors of E_1 and Γ_1 were determined by rewriting equations (B2) in terms of the independent variables; the polynomial coefficients at each energy and their errors. Fits to only the P_2 coefficient were possible and, for convenience, the parameter C_1' was replaced by another parameter C_1:

$$C_1 = -\frac{75}{2} C_1' \quad .$$

The factor $-\frac{75}{2}$ is the reciprocal of one of the numerical factors occurring in the expansion of the P_2 coefficient given by equation (33).

The results are summarized in Table 11, in which only the fit with $\ell = \ell' = 1$ and radius-dependent penetration factors has a reasonable χ^2. The corresponding values of (E_1, Γ_1, C_1) given in the first row, are assumed to be the best choices.

Quantitative information about the partial widths is contained in the quantity C_1, if the $J^\pi = \frac{3}{2}^-$ state completely dominates the expansion of the P_2 coefficient in equation (33), although, as has already been discussed, this can be only approximately true at best. Under this restriction, C_1 has the meaning of equation (22) (but includes the factor $-\frac{75}{2}$):

$$C_1 = F_1 q_1^2 \Gamma_{(p'\frac{5}{2})1} \left\{ \Gamma_{(p\frac{3}{2})1} - \frac{5}{4} \Gamma_{(p\frac{1}{2})1} \right\} \qquad \text{(B3)}$$

and the numerical factor F_1, which can be calculated, is given by

$$F_1(a) = \frac{|O_{p'1} O_{p1}|^2}{\kappa_{p'1} \kappa_{p1} a_p^2}, \quad a_p = 4.08 \ \ 10^{-13} \text{cm}$$

for radius-dependent penetration factors, and by

$$F_1(0) = \frac{1}{\kappa_{p'1} \kappa_{p1} \left| \frac{P_{p'1}(0) P_{p1}(0)}{k_{p'1} k_{p1}} \right|}$$

for radius-independent penetration factors. The subscript 1 labels the state, the subscripts p and p' label the particles and their relative orbital angular momentum, which is equal to 1 in all cases, and the other subscript labels the channel spin. For example, the subscript $(p' \frac{5}{2})$ means

$$^6\text{Li}^* + p', \quad \ell' = 1, \quad s' = \frac{5}{2} .$$

No uncertainty is given for C_1 in Table 11, because this is probably dominated by the assumptions leading to its interpretation by equation (B3).

APPENDIX C - $^{6}Li(p, p'')^{6}Li^{**}$ REACTION

The problem of fitting the two-level formula (19) to an experimentally determined polynomial coefficient is that of determining the two sets of parameters (α, β, γ) and $(E_1, \Gamma_1, E_2, \Gamma_2)$ in the expression

$$(\text{poly. coef.}) = \frac{P_{\ell'} P_{\ell}}{k^2} \frac{\alpha E^2 + \beta E + \gamma}{\left\{(E - E_1)^2 + \frac{\Gamma_1^2}{4}\right\}\left\{(E - E_2)^2 + \frac{\Gamma_2^2}{4}\right\}} .$$

If the parameters $(E_1, \Gamma_1, E_2, \Gamma_2)$ are known, this reduces to the linear problem of the determination of the parameters (α, β, γ) in the expression

$$\left\{(E - E_1)^2 + \frac{\Gamma_1^2}{4}\right\}\left\{(E - E_2)^2 + \frac{\Gamma_2^2}{4}\right\} \frac{k^2}{P_{\ell} P_{\ell'}} (\text{poly. coef.}) = \alpha E^2 + \beta E + \gamma .$$

Parameters (α, β, γ) were determined for a large number of values of parameters $(E_1, \Gamma_1, E_2, \Gamma_2)$, using a method identical to that described in Appendix B, and the polynomial coefficients and their errors given in Tables 4 and 6.

The final values of the resonant parameters were obtained from fits to the P_0 coefficient over a somewhat restricted range of ^{7}Be excitation energy. This was felt to be a more reliable procedure than using a range including lower energies, in which the p-wave elements of interest are attenuated by the proximity of the reaction threshold, and may be masked by s-wave background effects. Some features of the dependence of the fits on the set of parameters $(E_1, \Gamma_1, E_2, \Gamma_2)$ can be seen in Figures 29 and 30. The quality of the fits is somewhat insensitive to the precise values of

these parameters and to the presence of a reasonable non-interfering background, which has been plotted for the cases in which it was subtracted. Good fits can be obtained with $E_1 = 10.0$ MeV, $\Gamma_1 = 1.8$ MeV, which are the values obtained from the $^6Li(p, p')^6Li^*$ reaction. The results for the other parameters are given in Table 12, in which rough estimates of the uncertainties have been made.

As in the $^6Li(p, p')^6Li^*$ reaction, quantitative information about partial widths can be obtained only if certain conditions are fulfilled. No information was obtained from the P_2 coefficient because of the possible appreciable contribution from a broad $J^\pi = \frac{1}{2}^-$ state. This problem is not as serious with the P_0 coefficient, both because of the numerical factors involved, and the fact that the contribution from states with $J^\pi \neq \frac{3}{2}^-$ can be included as a non-interfering background. If the P_0 coefficient is dominated by the $J^\pi = \frac{3}{2}^-$ states, the quantity D, having the meaning of equation (23) can be estimated from the fits:

$$D = \Gamma_2 F_1 q_1 \Gamma_{(p'' \frac{1}{2})1} \left\{ \Gamma_{(p\frac{3}{2})1} + \Gamma_{(p\frac{1}{2})1} \right\} - \Gamma_1 F_2 q_2 \Gamma_{(p'' \frac{1}{2})2} \left\{ \Gamma_{(p\frac{3}{2})2} + \Gamma_{(p\frac{1}{2})2} \right\}. \quad (C1)$$

The factors a and b in equation (23) are both equal to $\frac{1}{6}$ by equation (34). The factor of 6 has been absorbed in the definition of D, equation (C1). The numerical factors F and the subscripts are defined as in Appendix B; for example, the subscript $(p'' \frac{1}{2})$ means

$$^6Li^{**} + p'', \quad \ell' = 1, \quad s' = \frac{1}{2} .$$

The subscripts 1 and 2 label the broad and the narrower states respectively.

As should be expected, D, unlike the parameters $(E_1, \Gamma_1, E_2, \Gamma_2)$, depends on the background assumed. It depends on these parameters also, as can be seen in Figures 29 and 30. Values of D are given in Table 12, in which rough estimates of the uncertainty due to causes other than background have been made.

APPENDIX D - $^4He(^3He, p'')^6Li^{**}$ REACTION

By fitting the two-level formula (19) to the P_0 coefficient with a method identical to that described in Appendix C, the parameters (α, β, γ) were determined for a large number of values of the parameters $(E_1, \Gamma_1, E_2, \Gamma_2)$. The values of the polynomial coefficients and their errors given in Table 7 were used. Some features of the dependence of the fits on the latter parameters can be seen in Figures 32 and 33, and the discussion is the same as that given in Appendix C for the $^6Li(p, p'')^6Li^{**}$ reaction.

The condition for obtaining information about partial widths is also the same as discussed in Appendix C: the P_0 coefficient must be dominated by the $J^{\pi} = \frac{3}{2}^-$ states. If this is the case, the quantities (C_1, C_2, ζ), defined by equations (13), (15), (16) and (17), can be obtained from the fits, because the channel spins of the initial and final products are unique. Using the notation of Appendix B,

$$C_1 = F_1 q_1^2 \Gamma_{(p'' \frac{1}{2})1} \Gamma_{(He \frac{1}{2})1}$$

$$C_2 = F_2 q_2^2 \Gamma_{(p'' \frac{1}{2})2} \Gamma_{(He \frac{1}{2})2}$$

where the subscripts 1 and 2 label the broad and the narrower states respectively, and the numerical factor F_1, for example, is given by

$$F_1(a) = \frac{|O_{p''1} O_{He1}|^2}{\kappa_{p''1}{}^a{}_{p''} \kappa_{He1}{}^a{}_{He}}$$

where $a_{p''} = 4.08\ 10^{-13}$cm, $a_{He} = 4.39\ 10^{-13}$cm.

The parameters (C_1, C_2, ς) were found from the parameters (α, β, γ) and $(E_1, \Gamma_1, E_2, \Gamma_2)$ by solving equations (20) (making allowance for the factor of $\frac{1}{2}$ occurring in the P_0 coefficient, equation (35)), and retaining the solution discussed in connection with the decomposition of the fit in Figure 34. As can be seen in Figures 32 and 33, the values obtained for (C_1, C_2, ς) depend both on the parameters $(E_1, \Gamma_1, E_2, \Gamma_2)$ and on the background assumed. Values of (C_1, C_2, ς), obtained using radius-dependent penetration factors, are given in Table 13, in which rough estimates of uncertainty due to causes other than background have been made.

REFERENCES

1. F. Ajzenberg-Selove and T. Lauritsen, Nucl. Phys. 11, 1 (1959), and Nucl. Phys. to be published.
2. F. C. Barker, Nucl. Phys. to be published (1966).
3. Y. R. Cusson and M. E. Nordberg, private communication (1961).
4. G. Dearnaley and A. B. Whitehead, Nucl. Instr. Methods 12, 205 (1961).
5. C. Détraz, J. Cerny, R. H. Pehl, Phys. Rev. Letters 14, 708 (1965).
6. U. Fasoli, E. A. Silverstein, D. Toniolo, and G. Zago, Nuovo Cimento 34, 1832 (1964a).
7. U. Fasoli, D. Toniolo, and G. Zago, Phys. Letters 8, 127 (1964b).
8. R. L. Heath, "Scintillation Spectrometry: Gamma-Ray Spectrum Catalogue", Phillips Petroleum Report IDO-16408 (1957).
9. D. Goosman, private communication (1965).
10. W. D. Harrison and A. B. Whitehead, Phys. Rev. 132, 2607 (1963).
11. N. P. Heydenburg and I. G. Han, Bull. Am. Phys. Soc. 7, 58 (1962), and private communication.
12. J. Humblet and L. Rosenfeld, Nucl. Phys. 26, 529 (1961).
13. J. Humblet, Nucl. Phys. 31, 544 (1962).

14. J. Humblet, Nucl. Phys. 50, 1 (1964a).

15. J. Humblet, Nucl. Phys. 57, 386 (1964b).

16. J. P. Jeukenne, Nucl. Phys. 58, 1 (1964).

17. J. M. F. Jeronymo, G. S. Mani, and A. Sadeghi, Nucl. Phys. 43, 424 (1963).

18. A. M. Lane and R. G. Thomas, Rev. Mod. Phys. 30, 257 (1958).

19. C. Mahaux, Nucl. Phys. 68, 481 (1965a).

20. C. Mahaux, Nucl. Phys. 71, 241 (1965b).

21. J. B. Marion, G. Weber, and F. S. Mozer, Phys. Rev. 104, 1402 (1956).

22. J. A. McCray, Ph. D. thesis, California Institute of Technology (1962), and Phys. Rev. 130, 2034 (1963).

23. J. D. Pearson, Ph. D. thesis, California Institute of Technology (1963).

24. L. Rosenfeld, Nucl. Phys. 26, 594 (1961).

25. L. Rosenfeld, Nucl. Phys. 70, 1 (1965).

26. R. J. Spiger and T. A. Tombrello, Bull. Am. Phys. Soc. 9, 703 (1964), and private communication.

27. T. A. Tombrello, private communication (1963).

28. T. A. Tombrello, and P. D. Parker, Phys. Rev. 130, 1112 (1963).

29. T. A. Tombrello and L. S. Senhouse, Phys. Rev. 129, 2252 (1963), and L. S. Senhouse, Ph. D. thesis, California Institute of Technology (1964).

TABLE 1

$^{6}Li(p, p)^{6}Li$ Differential Cross Section

The center-of-momentum differential cross section and its estimated standard error are given for each incident proton laboratory energy as a function of laboratory angle. The corresponding center-of-momentum angle and its cosine are also given. Millibarn per steradian units are used. (Page 9)

TABLE 1

$^{6}Li(p, p)^{6}Li$ Differential Cross Section

Lab Angle	CM Angle	Cosine CM Angle	2.40 MeV $\frac{d\sigma}{d\Omega}$	2.40 MeV Estimated % Error	2.60 MeV $\frac{d\sigma}{d\Omega}$	2.60 MeV Estimated % Error	2.80 MeV $\frac{d\sigma}{d\Omega}$	2.80 MeV Estimated % Error	3.00 MeV $\frac{d\sigma}{d\Omega}$	3.00 MeV Estimated % Error
33.8°	39.1°	0.775								
47.6	54.8	0.576	198	2	169	2			141	3
55.5	63.4	0.449	153	1	133	2	121	2		
65.0	73.7	0.281	117	1	103.0	1	96.5	2	91.0	1
71.3	80.4	0.167	96.8	2	88.7	1	84.0	2	81.0	1
80.5	90.0	0.000	79.2	2	72.2	2	69.5	2	66.0	2
90.0	99.6	-0.167	65.0	2	60.0	3	58.0	3	58.4	2
100.0	109.4	-0.331	55.3	2	49.6	4			48.0	3
107.4	116.5	-0.446	49.7	2	45.0	4	44.5	3	43.0	5
116.7	125.3	-0.578	47.2	5	41.3	5	38.8	4	38.9	5
125.0	132.7	-0.678	46.2	5	38.8	5	36.8	4	38.0	2
133.8	140.7	-0.774	46.0	5	38.2	5	37.1	3	35.1	5
145.0	150.5	-0.870	47.1	5	38.8	5	35.5	3	34.1	2
160.0	163.3	-0.958	48.4	5	40.8	4	35.2	4	33.3	3

TABLE 1 (cont.)

$^{6}Li(p, p)^{6}Li$ Differential Cross Section

Lab Angle	CM Angle	Cosine CM Angle	3.20 MeV $\frac{d\sigma}{d\Omega}$	3.20 MeV Estimated % Error	3.40 MeV $\frac{d\sigma}{d\Omega}$	3.40 MeV Estimated % Error	3.60 MeV $\frac{d\sigma}{d\Omega}$	3.60 MeV Estimated % Error	3.80 MeV $\frac{d\sigma}{d\Omega}$	3.80 MeV Estimated % Error
33.8°	39.1°	0.775	243	3	230	3				
47.6	54.8	0.576	129	1	122.8	1				
55.5	63.4	0.449	105.5	1	101.5	1	102	15	97	15
65.0	73.7	0.281	86.9	1	83.8	2				
71.3	80.4	0.167	77	6	74.8	2	72	5	72	5
80.5	90.0	0.000	64.2	2	64.7	3	63	5	67	5
90.0	99.6	-0.167	58	7	56.7	3	58	7	58.1	2
100.0	109.4	-0.331	48.1	5	52.0	3			52.3	2
107.4	116.5	-0.446	43	10	47.7	2	44	7	48.3	2
116.7	125.3	-0.578	39	10	41.6	2	40	7	42	7
125.0	132.7	-0.678	37.4	2	37.8	2			43.3	2
133.8	140.7	-0.774	34.1	3	37.0	3	37	5	42	5
145.0	150.5	-0.870	33.8	2	35.6	3			41.1	2
160.0	163.3	-0.958	33.4	2	34.9	2	37	6	42	6

TABLE 1 (cont.)

$^{6}Li(p, p)^{6}Li$ Differential Cross Section

Lab Angle	CM Angle	Cosine CM Angle	4.00 MeV $\frac{d\sigma}{d\Omega}$	4.00 MeV Estimated % Error	4.20 MeV $\frac{d\sigma}{d\Omega}$	4.20 MeV Estimated % Error	4.40 MeV $\frac{d\sigma}{d\Omega}$	4.40 MeV Estimated % Error	4.60 MeV $\frac{d\sigma}{d\Omega}$	4.60 MeV Estimated % Error
33.8°	39.1°	0.775								
47.6	54.8	0.576							127	15
55.5	63.4	0.449	99	5	108	15	118	15	105	15
65.0	73.7	0.281								
71.3	80.4	0.167	70	5	64	6	63	5	61	7
80.5	90.0	0.000	61	5	58	10	54	10	53	10
90.0	99.6	-0.167	58	5	55	10	52	10	49	6
100.0	109.4	-0.331								
107.4	116.5	-0.446	50	5	48	6	45	6	45	6
116.7	125.3	-0.578	48	5	45	7	45	7	42	7
125.0	132.7	-0.678								
133.8	140.7	-0.774	45	5	45	6	47	7	45	7
145.0	150.5	-0.870								
160.0	163.3	-0.958	45	5	48	6	50	7	54	10

TABLE 1 (cont.)

$^{6}Li(p, p)^{6}Li$ Differential Cross Section

Lab Angle	CM Angle	Cosine CM Angle	4.80 MeV $\frac{d\sigma}{d\Omega}$	4.80 MeV Estimated % Error	5.00 MeV $\frac{d\sigma}{d\Omega}$	5.00 MeV Estimated % Error	5.20 MeV $\frac{d\sigma}{d\Omega}$	5.20 MeV Estimated % Error	5.40 MeV $\frac{d\sigma}{d\Omega}$	5.40 MeV Estimated % Error
33.8°	39.1°	0.775					211	3	263	5
47.6	54.8	0.576	119	15	121	15	118.0	2	132	3
55.5	63.4	0.449	100	7	100	7	90.8	2	89.0	3
65.0	73.7	0.281					63.6	2		
71.3	80.4	0.167	58	7	61	7	56.8	5	52.7	3
80.5	90.0	0.000	54	7	47	7	45.4	1	43.2	3
90.0	99.6	-0.167	49	6	46	6	39.5	6	38.5	3
100.0	109.4	-0.331					38.9	2	36	5
107.4	116.5	-0.446	46	5	41.5	5	38	8	37.0	3
116.7	125.3	-0.578	42	5	41.1	5	35	7	37.5	3
125.0	132.7	-0.678								
133.8	140.7	-0.774	45	5	43.4	5	42	8	41.0	3
145.0	150.5	-0.870					47.6	1	48.0	3
160.0	163.3	-0.958	56	5	55.0	5	52.8	2	54	4

TABLE 1 (cont.)

$^{6}Li(p, p)^{6}Li$ Differential Cross Section

Lab Angle	CM Angle	Cosine CM Angle	5.50 MeV $\frac{d\sigma}{d\Omega}$	5.50 MeV Estimated % Error	5.60 MeV $\frac{d\sigma}{d\Omega}$	5.60 MeV Estimated % Error	5.80 MeV $\frac{d\sigma}{d\Omega}$	5.80 MeV Estimated % Error	6.00 MeV $\frac{d\sigma}{d\Omega}$	6.00 MeV Estimated % Error
33.8°	39.1°	0.775					229	3	222	3
47.6	54.8	0.576			133	8	135	8	119.7	1
55.5	63.4	0.449			95	8	91	8	90	5
65.0	73.7	0.281					56.6	1	51.4	1
71.3	80.4	0.167			49	7	46.5	5	44.5	5
80.5	90.0	0.000	39.5	3	38.5	5	35.9	2	33.0	1
90.0	99.6	-0.167			36	7	30.9	2	28.5	5
100.0	109.4	-0.331					29.0	5	27.0	5
107.4	116.5	-0.446			34	6	29.5	6	27.0	5
116.7	125.3	-0.578	32.5	3	33	6	30	10	26.9	2
125.0	132.7	-0.678								
133.8	140.7	-0.774			36	7	32	12	29.5	5
145.0	150.5	-0.870					37.3	2	34.5	5
160.0	163.3	-0.958			48	8	44	8	42.0	5

TABLE 1 (cont.)

$^{6}Li(p, p)^{6}Li$ Differential Cross Section

Lab Angle	CM Angle	Cosine CM Angle	6.50MeV $\frac{d\sigma}{d\Omega}$	6.50MeV Estimated % Error	7.00MeV $\frac{d\sigma}{d\Omega}$	7.00MeV Estimated % Error	7.50MeV $\frac{d\sigma}{d\Omega}$	7.50MeV Estimated % Error	8.00MeV $\frac{d\sigma}{d\Omega}$	8.00MeV Estimated % Error
33.8°	39.1°	0.775							237	3
47.6	54.8	0.576			143	10			116	3
55.5	63.4	0.449			71	10			64.3	3
65.0	73.7	0.281							34.4	3
71.3	80.4	0.167			33	7			25.3	3
80.5	90.0	0.000	29.9	2	25.6	5	22.5	3	20.1	3
90.0	99.6	-0.167			24	7			19.5	3
100.0	109.4	-0.331							20.2	2
107.4	116.5	-0.446			23	7			19.9	2
116.7	125.3	-0.578	24.0	4	22.0	3	19.9	2	19.0	2
125.0	132.7	-0.678							18.8	2
133.8	140.7	-0.774			24	7			18.7	2
145.0	150.5	-0.870							21.0	2
160.0	163.3	-0.958			30	7			23.9	3

TABLE 1 (cont.)

$^{6}Li(p, p)^{6}Li$ Differential Cross Section

Lab Angle	CM Angle	Cosine CM Angle	8.50 MeV $\frac{d\sigma}{d\Omega}$	8.50 MeV Estimated % Error	9.00 MeV $\frac{d\sigma}{d\Omega}$	9.00 MeV Estimated % Error	9.50 MeV $\frac{d\sigma}{d\Omega}$	9.50 MeV Estimated % Error	10.00 MeV $\frac{d\sigma}{d\Omega}$	10.00 MeV Estimated % Error
33.8°	39.1°	0.775								
47.6	54.8	0.576								
55.5	63.4	0.449			56.5	5			47.8	5
65.0	73.7	0.281							23.6	4
71.3	80.4	0.167			22.0	5			16.3	4
80.5	90.0	0.000	17.7	3	16.4	3	15.0	3	13.5	3
90.0	99.6	-0.167			17.0	2			14.6	3
100.0	109.4	-0.331							15.2	4
107.4	116.5	-0.446	17.3	2	17.3	2			15.0	3
116.7	125.3	-0.578			16.2	2	15.0	2	13.6	3
125.0	132.7	-0.678								
133.8	140.7	-0.774			14.7	2			11.2	3
145.0	150.5	-0.870							12.5	4
160.0	163.3	-0.958			18.7	2			14.5	3

TABLE 1 (cont.)

$^{6}Li(p, p)^{6}Li$ Differential Cross Section

Lab Angle	CM Angle	Cosine CM Angle	10.50 MeV $\frac{d\sigma}{d\Omega}$	10.50 MeV Estimated % Error	11.00 MeV $\frac{d\sigma}{d\Omega}$	11.00 MeV Estimated % Error	11.50 MeV $\frac{d\sigma}{d\Omega}$	11.50 MeV Estimated % Error	12.00 MeV $\frac{d\sigma}{d\Omega}$	12.00 MeV Estimated % Error
33.8°	39.1°	0.775			228	3			204	3
47.6	54.8	0.576			97.2	3			82.6	3
55.5	63.4	0.449			48.3	3			40.3	3
65.0	73.7	0.281		69° lab	15.3	3			17.3	3
71.3	80.4	0.167							11.5	3
80.5	90.0	0.000	12.5	3	11.8	3	10.9	3	10.3	3
90.0	99.6	-0.167			13.4	3			11.2	3
100.0	109.4	-0.331			13.8	3			12.4	3
107.4	116.5	-0.446			13.4	3			11.8	3
116.7	125.3	-0.578	12.6	3	12.0	2	11.15	2	10.6	2
125.0	132.7	-0.678			10.3	3			8.62	3
133.8	140.7	-0.774			9.83	3			7.45	3
145.0	150.5	-0.870			9.19	3			7.17	3
160.0	163.3	-0.958			10.4	3			7.98	3

TABLE 2

$^{6}Li(p, p')^{6}Li^{*}$ Differential Cross Section

The center-of-momentum differential cross section and its estimated standard error are given for each incident proton laboratory energy as a function of laboratory angle and of cosine of center-of-momentum angle. Millibarn per steradian units are used. The estimated normalization standard error is also given. (Pages 14 and 15)

TABLE 2

$^{6}Li(p, p')^{6}Li^{*}$ Differential Cross Section

Lab Energy = 3.60 MeV				Lab Energy = 4.20 MeV			
Lab Angle	Cosine CM Angle	$\frac{d\sigma}{d\Omega}$	Estimated Error	Lab Angle	Cosine CM Angle	$\frac{d\sigma}{d\Omega}$	Estimated Error
				20.5°	0.900	2.58	0.12
				29.4	0.800	2.77	0.08
35.3°	0.700	1.64	0.49	36.5	0.700	3.28	0.13
41.4	0.600	1.66	0.25	42.7	0.600	3.66	0.13
47.0	0.500	1.69	0.25	48.5	0.500	4.34	0.17
52.3	0.400	2.61	0.16				
				59.3	0.300	4.86	0.17
62.7	0.200	2.23	0.27	64.6	0.200	5.10	0.14
67.4	0.106	2.94	0.21	69.8	0.100	5.45	0.15
72.9	0.000	2.90	0.12	75.1	0.000	5.87	0.15
78.2	-0.100	3.01	0.12	80.5	-0.100	5.69	0.16
				86.2	-0.200	5.98	0.18
89.5	-0.300	3.19	0.16	92.1	-0.300	6.24	0.16
95.6	-0.400	3.66	0.18	98.3	-0.400	6.46	0.16
102.5	-0.500	3.36	0.20	105.1	-0.500	6.35	0.19
110.0	-0.600	3.62	0.22	112.7	-0.600	6.54	0.20
118.7	-0.700	3.67	0.22	121.3	-0.700	6.70	0.23
129.3	-0.800	3.68	0.22	131.7	-0.800	7.11	0.32
143.6	-0.900	3.92	0.23	145.5	-0.900	7.24	0.25
				160.0	-0.956	7.52	0.23
165.0	-0.983	4.22	0.21	165.0	-0.981	7.75	0.23
Normalization Error 2%				Normalization Error 2%			

TABLE 2 (cont.)

Lab Energy = 4.60 MeV				Lab Energy = 5.00 MeV			
Lab Angle	Cosine CM Angle	$\frac{d\sigma}{d\Omega}$	Estimated Error	Lab Angle	Cosine CM Angle	$\frac{d\sigma}{d\Omega}$	Estimated Error
20.8°	0.900	4.40	0.20	21.0°	0.900	6.67	0.17
29.8	0.800	4.65	0.12	30.0	0.800	7.47	0.22
36.9	0.700	5.15	0.11	37.3	0.700	7.93	0.28
43.3	0.600	5.70	0.12	43.7	0.600	8.15	0.24
				49.6	0.500	8.38	0.42
54.7	0.400	6.62	0.33	55.2	0.400	9.05	0.23
60.1	0.300	6.78	0.24	60.6	0.300	9.68	0.22
65.4	0.200	7.22	0.25	65.9	0.200	9.83	0.22
70.6	0.100	7.65	0.27	71.2	0.100	9.83	0.22
76.0	0.000	7.56	0.26	76.6	0.000	10.13	0.23
80.5	-0.082	7.25	0.25	80.5	-0.071	9.63	0.16
81.5	-0.100	7.65	0.27	82.1	-0.100	10.21	0.21
87.1	-0.200	7.76	0.31	87.8	-0.200	9.51	0.29
93.0	-0.300	7.86	0.31	93.7	-0.300	9.61	0.25
99.3	-0.400	7.46	0.37	100.0	-0.400	9.59	0.24
106.1	-0.500	8.00	0.32	106.8	-0.500	9.60	0.23
113.7	-0.600	7.99	0.32	114.3	-0.600	9.13	0.25
122.2	-0.700	8.25	0.33	122.9	-0.700	9.16	0.24
132.5	-0.800	8.38	0.34	133.1	-0.800	9.20	0.26
146.2	-0.900	8.15	0.33	146.6	-0.900	9.05	0.28
160.0	-0.958	8.61	0.30	160.0	-0.958	9.70	0.39
165.0	-0.981	8.38	0.34	165.0	-0.980	9.32	0.22
Normalization Error 2%				Normalization Error 1 1/2%			

TABLE 2 (cont.)

Lab Energy = 5.40 MeV				Lab Energy = 5.80 MeV			
Lab Angle	Cosine CM Angle	$\frac{d\sigma}{d\Omega}$	Estimated Error	Lab Angle	Cosine CM Angle	$\frac{d\sigma}{d\Omega}$	Estimated Error
21.1°	0.900	10.16	0.18	21.2°	0.900	12.60	0.26
30.2	0.800	11.25	0.20	30.4	0.800	12.84	0.26
37.5	0.700	11.71	0.19	37.7	0.700	13.15	0.26
				44.2	0.600	13.98	0.42
49.9	0.500	12.22	0.24	50.2	0.500	13.12	0.25
55.5	0.400	12.22	0.22	55.8	0.400	13.07	0.21
61.0	0.300	12.38	0.25	61.3	0.300	13.10	0.18
66.3	0.200	12.61	0.25	66.7	0.200	12.90	0.19
71.7	0.100	12.56	0.25	72.0	0.100	12.60	0.25
77.1	0.000	12.18	0.24	77.5	0.000	12.29	0.17
				80.5	-0.055	12.22	0.17
82.6	-0.100	11.96	0.24	83.0	-0.100	12.01	0.24
88.3	-0.200	11.63	0.17	88.6	-0.200	11.63	0.17
94.2	-0.300	11.27	0.25	94.6	-0.300	10.98	0.16
100.5	-0.400	11.04	0.17	101.0	-0.400	10.53	0.16
107.4	-0.500	10.46	0.21	107.8	-0.500	10.12	0.18
114.9	-0.600	10.28	0.23	115.3	-0.600	9.52	0.19
123.4	-0.700	9.78	0.15	123.8	-0.700	9.03	0.18
133.6	-0.800	9.50	0.17	133.9	-0.800	8.66	0.17
147.0	-0.900	9.50	0.24	147.2	-0.900	8.10	0.16
165.0	-0.980	9.39	0.24	165.0	-0.979	8.24	0.16
Normalization Error 3%				Normalization Error 1 1/2%			

TABLE 2 (cont.)

Lab Energy = 6.20 MeV				Lab Energy = 6.60 MeV			
Lab Angle	Cosine CM Angle	$\frac{d\sigma}{d\Omega}$	Estimated Error	Lab Angle	Cosine CM Angle	$\frac{d\sigma}{d\Omega}$	Estimated Error
21.3°	0.900	13.12	0.29	21.4°	0.900	13.83	0.22
30.5	0.800	13.15	0.17	30.6	0.800	13.30	0.21
37.9	0.700	13.30	0.29				
44.4	0.600	13.53	0.34	44.5	0.600	13.23	0.18
50.4	0.500	13.25	0.16	50.5	0.500	13.05	0.17
				56.2	0.400	13.01	0.17
61.5	0.300	13.01	0.17	61.7	0.300	12.95	0.19
66.9	0.200	12.37	0.37	67.2	0.200	12.29	0.10
72.3	0.100	12.34	0.15	72.6	0.100	11.90	0.14
77.7	0.000	11.78	0.24	78.0	0.000	11.80	0.18
80.5	-0.050	11.55	0.23	80.5	-0.045	11.65	0.23
83.3	-0.100	11.40	0.28	83.5	-0.100	11.32	0.23
89.0	-0.200	10.95	0.27	89.2	-0.200	10.85	0.22
95.0	-0.300	10.69	0.11	95.2	-0.300	10.75	0.21
101.3	-0.400	10.00	0.20	101.5	-0.400	9.83	0.29
108.1	-0.500	9.30	0.23	108.4	-0.500	9.30	0.23
115.6	-0.600	8.72	0.22	115.8	-0.600	8.50	0.13
124.1	-0.700	8.65	0.13	124.3	-0.700	8.10	0.16
134.2	-0.800	8.15	0.12	134.4	-0.800	7.72	0.12
147.4	-0.900	7.84	0.12	147.6	-0.900	7.60	0.19
165.0	-0.979	7.90	0.31	165.0	-0.979	6.94	0.42
Normalization Error 1 1/2%				Normalization Error 3%			

TABLE 2 (cont.)

Lab Energy = 7.00 MeV				Lab Energy = 7.80 MeV			
Lab Angle	Cosine CM Angle	$\frac{d\sigma}{d\Omega}$	Estimated Error	Lab Angle	Cosine CM Angle	$\frac{d\sigma}{d\Omega}$	Estimated Error
21.5°	0.900	13.51	0.31	21.6°	0.900	12.22	0.19
30.7	0.800	13.07	0.18	30.9	0.800	11.70	0.29
				38.3	0.700	11.46	0.26
44.7	0.600	12.72	0.20	44.9	0.600	11.60	0.23
50.7	0.500	12.70	0.18	50.9	0.500	11.55	0.12
56.4	0.400	12.40	0.15	56.7	0.400	11.60	0.14
61.9	0.300	12.05	0.17	62.2	0.300	11.28	0.16
67.3	0.200	11.83	0.18	67.6	0.200	10.50	0.21
72.7	0.100	11.47	0.14	73.1	0.100	10.46	0.16
78.2	0.000	11.16	0.13	78.5	0.000	10.00	0.15
				80.5	-0.036	9.90	0.15
83.7	-0.100	10.82	0.15	84.1	-0.100	9.37	0.19
89.5	-0.200	9.94	0.14	89.8	-0.200	8.70	0.13
95.4	-0.300	9.66	0.17	95.8	-0.300	8.13	0.16
101.8	-0.400	8.75	0.12	102.1	-0.400	7.62	0.11
108.6	-0.500	8.63	0.13	108.8	-0.500	7.42	0.11
116.0	-0.600	8.02	0.12	116.4	-0.600	7.14	0.11
124.5	-0.700	7.65	0.15	124.8	-0.700	6.66	0.13
134.6	-0.800	7.34	0.21	134.9	-0.800	6.55	0.13
145.7	-0.880	7.37	0.22	148.0	-0.900	6.42	0.13
147.8	-0.900	7.25	0.18	160.0	-0.955	6.62	0.13
165.0	-0.979	7.09	0.14	165.0	-0.978	6.50	0.12
Normalization Error 1 1/2%				Normalization Error 2%			

TABLE 2 (cont.)

Lab Energy = 8.60 MeV				Lab Energy = 9.40 MeV			
Lab Angle	Cosine CM Angle	$\frac{d\sigma}{d\Omega}$	Estimated Error	Lab Angle	Cosine CM Angle	$\frac{d\sigma}{d\Omega}$	Estimated Error
21.6°	0.900	11.85	0.21	21.7°	0.900	11.21	0.22
38.5	0.700	11.70	0.18	38.6	0.700	10.88	0.22
45.0	0.600	11.83	0.11	45.2	0.600	11.05	0.12
51.1	0.500	11.61	0.29	51.2	0.500	11.14	0.09
56.8	0.400	11.24	0.17	57.0	0.400	10.67	0.09
62.4	0.300	10.85	0.13	62.6	0.300	10.35	0.09
67.9	0.200	10.50	0.11	68.0	0.200	10.00	0.15
73.3	0.100	10.26	0.16				
78.8	0.000	9.55	0.16	79.0	0.000	9.10	0.25
84.3	-0.100	9.10	0.14	84.5	-0.100	8.60	0.25
90.1	-0.200	8.50	0.17	90.3	-0.200	7.86	0.16
96.1	-0.300	8.15	0.16	96.3	-0.300	7.36	0.18
102.4	-0.400	7.50	0.07	102.6	-0.400	6.57	0.08
109.2	-0.500	6.95	0.17	109.4	-0.500	6.36	0.13
116.6	-0.600	6.48	0.11	116.8	-0.600	6.05	0.15
125.1	-0.700	6.22	0.12	125.3	-0.700	5.20	0.21
135.1	-0.800	6.07	0.10	135.2	-0.800	5.34	0.21
148.1	-0.900	5.92	0.15	148.3	-0.900	5.31	0.21
160.0	-0.955	5.92	0.18	160.0	-0.955	5.24	0.26
165.0	-0.978	5.89	0.08	165.0	-0.978	5.15	0.17
Normalization Error 2%				Normalization Error 1 1/2%			

TABLE 3

$^{6}Li(p, p')^{6}Li^{*}$ Polynomial Coefficients

The Legendre polynomial coefficients and standard errors obtained from the angular distributions are given as a function of incident proton laboratory energy and of corresponding ^{7}Be excitation energy. The coefficients and errors are in units of millibarns per steradian; energies are in MeV.
(Pages 16 and 73)

TABLE 3

$^{6}Li(p, p')^{6}Li^{*}$ Polynomial Coefficients

Lab Energy	^{7}Be Excitation Energy	P_0 Coef.	Error	P_1 Coef.	Error	P_2 Coef.	Error	P_3 Coef.	Error	P_4 Coef.	Error	P_5 Coef.	Error
3.60	8.70	2.78	0.08	-1.46	0.14	-0.23	0.15						
4.20	9.21	5.27	0.11	-2.55	0.09	-0.62	0.08	-0.25	0.10	0.33	0.12		
4.60	9.55	6.94	0.15	-2.11	0.11	-0.99	0.12	-0.33	0.15	0.23	0.17		
5.00	9.90	9.00	0.14	-1.09	0.09	-1.55	0.11	-0.56	0.14	0.34	0.16		
5.40	10.24	11.21	0.34	0.98	0.09	-1.91	0.11	-0.88	0.14	0.12	0.16		
5.80	10.58	11.51	0.18	2.72	0.10	-1.51	0.12	-0.54	0.14	0.25	0.15		
6.20	10.92	11.28	0.18	3.21	0.09	-1.19	0.12	-0.62	0.14	0.19	0.16		
6.60	11.27	11.13	0.33	3.63	0.13	-0.90	0.11	-0.22	0.13	0.43	0.15		
7.00	11.61	10.62	0.17	3.71	0.10	-0.52	0.13	-0.39	0.15	0.56	0.16	0.22	0.16
7.80	12.30	9.54	0.19	3.53	0.10	-0.42	0.09	-0.75	0.11	0.55	0.13	0.44	0.13
8.60	12.98	9.25	0.18	3.77	0.11	-0.58	0.10	-0.88	0.11	0.16	0.12	0.00	0.11
9.40	13.67	8.58	0.19	3.83	0.11	-0.61	0.12	-1.00	0.11	0.22	0.14	0.19	0.14

TABLE 4

$^{6}Li(p, p'')^{6}Li^{**}$ Data from Gamma Ray Measurements

The data obtained from the γ-ray measurements are given as a function of incident proton laboratory energy and of corresponding ^{7}Be center-of-momentum energy. The data and estimated standard errors are expressed in terms of the coefficient of Legendre polynomial P_0, which is the total cross section divided by 4π. The energies are in MeV; the coefficients and errors in millibarns per steradian. There is a systematic uncertainty in the incident proton laboratory energy scale of about 0.01 MeV, and a distribution with a standard deviation of about 30 keV associated with each laboratory energy value given. The estimated normalization standard errors are those associated with the normalization of these data to the angular distribution data at 5.80 MeV obtained from particle measurements.
(Pages 20 and 76)

TABLE 4

$^{6}Li(p, p'')^{6}Li^{**}$ Data from Gamma-Ray Measurements

3.08- by 3.08-cm Detector				7.62- by 7.62-cm Detector			
Lab Energy	^{7}Be Excitation Energy	P_0 Coef.	Estimated Error	Lab Energy	^{7}Be Excitation Energy	P_0 Coef.	Estimated Error
4.26	9.26	0.0042	0.0007	4.80	9.72	0.303	0.011
4.31	9.31	0.0069	0.0007	5.00	9.90	0.538	0.016
4.36	9.35	0.0165	0.0012	5.20	10.07	0.767	0.027
4.41	9.39	0.0342	0.0014	5.30	10.15	0.890	0.034
4.46	9.43	0.0569	0.0020	5.40	10.24	0.985	0.042
4.51	9.48	0.0842	0.0029	5.60	10.41	1.197	0.042
4.56	9.52	0.1143	0.0040	5.70	10.50	1.282	0.045
4.77	9.69	0.278	0.009	5.80	10.58	1.310	0.046
4.97	9.87	0.491	0.015	6.00	10.75	1.342	0.047
5.17	10.04	0.732	0.022	6.10	10.84	1.295	0.045
5.37	10.21	0.901	0.027	6.20	10.92	1.207	0.042
5.57	10.38	1.166	0.035	6.30	11.01	0.939	0.033
5.77	10.55	1.290	0.039	6.40	11.09	0.815	0.029
5.97	10.72	1.278	0.038	6.50	11.18	0.760	0.027
6.18	10.90	1.142	0.034	6.60	11.27	0.758	0.028
6.38	11.07	0.765	0.038	6.80	11.44	0.736	0.027
6.58	11.25	0.801	0.040	7.00	11.61	0.704	0.027
6.78	11.42	0.775	0.039	7.20	11.78	0.675	0.028
6.98	11.59	0.785	0.047	7.40	11.96	0.653	0.038
				7.60	11.13	0.650	0.030
				7.80	12.30	0.648	0.037
Normalization Error 3 1/2%				Normalization Error 3 1/2%			

TABLE 5

$^{6}Li(p, p'')^{6}Li^{**}$ Differential Cross Section

The center-of-momentum differential cross section and its estimated standard error are given for each incident proton laboratory energy as a function of laboratory angle and of cosine of center-of-momentum angle. Millibarn per steradian units are used. The estimated normalization standard error is also given. At 5.80 MeV the data from the coincidence measurements and from the direct measurements are given separately. (Pages 24 and 25)

TABLE 5

$^{6}Li(p, p'')^{6}Li^{**}$ Differential Cross Section

Lab Energy = 5.00 MeV				Lab Energy = 5.20 MeV			
Lab Angle	Cosine CM Angle	$\frac{d\sigma}{d\Omega}$	Estimated Error	Lab Angle	Cosine CM Angle	$\frac{d\sigma}{d\Omega}$	Estimated Error
				18.9°	0.900	0.75	0.06
26.5°	0.800	0.38	0.03	27.1	0.800	0.45	0.05
32.9	0.700	0.30	0.03	33.7	0.700	0.53	0.05
43.7	0.500	0.31	0.03	44.8	0.500	0.24	0.02
58.3	0.200	0.30	0.04	59.7	0.200	0.40	0.04
73.0	-0.100	0.40	0.04	74.7	-0.100	0.67	0.07
83.7	-0.300	0.45	0.05				
				91.8	-0.400	1.00	0.07
96.3	-0.500	0.62	0.07				
103.7	-0.600	0.81	0.07	105.9	-0.600	1.32	0.10
123.4	-0.800	0.75	0.06				
Normalization Error 2%				Normalization Error 1 1/2%			

TABLE 5 (cont.)

Lab Energy = 5.40 MeV

Lab Angle	Cosine CM Angle	$\frac{d\sigma}{d\Omega}$	Estimated Error
19.3°	0.900	1.00	0.10
27.6	0.800	0.82	0.08
40.2	0.600	0.50	0.05
55.9	0.300	0.34	0.06
70.9	0.000	0.54	0.06
81.5	-0.200	0.75	0.07
107.6	-0.600	1.33	0.19
127.1	-0.800	1.71	0.12
165.0	-0.985	2.26	0.16

Normalization Error 2%

TABLE 5 (cont.)

Lab Energy = 5.80 MeV

Lab Angle	Cosine CM Angle	Coincidence $\frac{d\sigma}{d\Omega}$	Coincidence Estimated Error	Direct $\frac{d\sigma}{d\Omega}$	Direct Estimated Error
19.8°	0.900	1.631	0.054	1.76	0.17
28.3	0.800	1.340	0.047	1.12	0.08
35.2	0.700	0.916	0.045	0.96	0.10
41.2	0.6	0.735	0.035	0.93	0.13
46.8	0.5	0.537	0.038	0.55	0.06
52.1	0.4	0.464	0.029	0.31	0.05
62.4	0.2	0.396	0.028	0.39	0.04
67.5	0.1	0.476	0.035	0.45	0.03
72.6	0.0			0.68	0.06
83.4	-0.2	1.064	0.052	1.03	0.08
89.2	-0.3	1.250	0.056	1.28	0.06
95.4	-0.4	1.465	0.064	1.47	0.10
109.7	-0.6	2.03	0.09	2.07	0.07
118.5	-0.7	2.19	0.09	2.30	0.10
129.1	-0.8	2.47	0.12	2.75	0.10

Normalization Error 2%

TABLE 5 (cont.)

Lab Energy = 6.05 MeV				Lab Energy = 6.30 MeV			
Lab Angle	Cosine CM Angle	$\frac{d\sigma}{d\Omega}$	Estimated Error	Lab Angle	Cosine CM Angle	$\frac{d\sigma}{d\Omega}$	Estimated Error
20.0°	0.900	1.84	0.18	20.2°	0.900	1.04	0.10
28.7	0.800	1.26	0.13	28.9	0.800	0.84	0.08
41.7	0.600	0.67	0.07				
				47.8	0.500	0.43	0.06
52.7	0.400	0.42	0.04				
				63.6	0.200	0.38	0.04
68.2	0.100	0.54	0.06				
				79.4	-0.100	0.67	0.07
84.3	-0.200	1.03	0.11				
96.4	-0.400	1.68	0.12	97.1	-0.400	1.21	0.10
110.7	-0.600	2.08	0.12				
				120.1	-0.700	1.77	0.11
130.0	-0.800	2.71	0.16				
165.0	-0.983	3.37	0.18	165.0	-0.982	2.54	0.15
Normalization Error 1 1/2%				Normalization Error 1 1/2%			

TABLE 5 (cont.)

Lab Energy = 6.55 MeV				Lab Energy = 6.80 MeV			
Lab Angle	Cosine CM Angle	$\frac{d\sigma}{d\Omega}$	Estimated Error	Lab Angle	Cosine CM Angle	$\frac{d\sigma}{d\Omega}$	Estimated Error
20.3°	0.900	0.94	0.09	20.5°	0.900	0.97	0.06
29.2	0.800	0.59	0.06				
36.2	0.700	0.55	0.06	36.4	0.700	0.53	0.04
48.1	0.500	0.29	0.03	48.5	0.500	0.33	0.03
				64.5	0.200	0.31	0.05
69.3	0.100	0.40	0.05				
				75.0	0.000	0.44	0.03
85.6	-0.200	0.71	0.07				
				92.0	-0.300	0.90	0.06
104.5	-0.500	0.96	0.08	105.0	-0.500	1.09	0.07
120.7	-0.700	1.36	0.10				
				131.6	-0.800	1.49	0.10
145.1	-0.900	1.73	0.12				
165.0	-0.982	1.86	0.11	165.0	-0.982	1.81	0.12
Normalization Error 2%				Normalization Error 2%			

TABLE 5 (cont.)

Lab Energy = 7.20 MeV				Lab Energy = 7.80 MeV			
Lab Angle	Cosine CM Angle	$\frac{d\sigma}{d\Omega}$	Estimated Error	Lab Angle	Cosine CM Angle	$\frac{d\sigma}{d\Omega}$	Estimated Error
20.7°	0.900	0.88	0.08	20.9°	0.900	0.60	0.07
29.6	0.800	0.70	0.06	29.9	0.800	0.52	0.06
43.1	0.600	0.39	0.04	43.5	0.600	0.38	0.05
				54.9	0.400	0.27	0.03
59.8	0.300	0.30	0.04				
				70.9	0.100	0.34	0.06
				76.3	0.000	0.28	0.04
81.1	-0.100	0.56	0.05				
				93.4	-0.300	0.69	0.08
98.9	-0.400	0.89	0.08				
				114.0	-0.600	0.94	0.09
121.9	-0.700	1.34	0.12				
				132.8	-0.800	1.10	0.11
145.9	-0.900	1.52	0.10				
165.0	-0.981	1.71	0.12	165.0	-0.980	1.39	0.11
Normalization Error 2%				Normalization Error 1 1/2%			

TABLE 5 (cont.)

Lab Energy = 8.60 MeV				Lab Energy = 9.40 MeV			
Lab Angle	Cosine CM Angle	$\frac{d\sigma}{d\Omega}$	Estimated Error	Lab Angle	Cosine CM Angle	$\frac{d\sigma}{d\Omega}$	Estimated Error
21.1°	0.900	0.47	0.05	21.2°	0.900	0.35	0.05
				30.4	0.800	0.32	0.05
37.5	0.700	0.38	0.06				
49.8	0.500	0.27	0.06	50.1	0.500	0.08	0.04
55.4	0.400	0.18	0.03	55.8	0.400	0.15	0.02
				61.3	0.300	0.20	0.02
66.2	0.200	0.23	0.03				
				72.0	0.100	0.30	0.04
80.5	-0.064	0.37	0.07				
				88.7	-0.200	0.68	0.05
100.4	-0.400	0.72	0.06				
				107.7	-0.500	0.78	0.05
123.3	-0.700	0.94	0.06	123.7	-0.700	0.84	0.05
146.9	-0.900	1.02	0.07	147.2	-0.900	0.85	0.05
165.0	-0.980	1.10	0.07	165.0	-0.979	0.84	0.05
Normalization Error 1 1/2%				Normalization Error 2 1/2%			

TABLE 6

$^{6}Li(p, p'')^{6}Li^{**}$ Polynomial Coefficients

The Legendre polynomial coefficients and standard errors obtained from the angular distributions are given as a function of incident proton laboratory energy and of corresponding ^{7}Be excitation energy. The coefficients and standard errors are in units of millibarns per steradian; energies are in MeV. (Pages 26 and 76)

TABLE 6

$^{6}Li(p,p'')^{6}Li^{**}$ Polynomial Coefficients

Lab Energy	^{7}Be Excitation Energy	P_0 Coef.	Error	P_1 Coef.	Error	P_2 Coef.	Error	P_3 Coef.	Error	P_4 Coef.	Error
5.00	9.90	0.478	0.018	-0.27	0.04	0.23	0.04	0.06	0.06		
5.20	10.07	0.764	0.043	-0.58	0.12	0.41	0.15	0.38	0.12		
5.40	10.24	0.919	0.036	-0.64	0.06	0.81	0.06	0.18	0.08		
5.80	10.58	1.310	0.030	-0.88	0.04	1.38	0.05	0.40	0.04		
6.05	10.80	1.373	0.040	-0.97	0.07	1.42	0.08	0.44	0.09		
6.30	11.01	1.012	0.033	-0.79	0.06	0.94	0.06	0.18	0.08		
6.55	11.22	0.780	0.034	-0.58	0.04	0.69	0.05	0.21	0.06		
6.80	11.44	0.811	0.026	-0.55	0.04	0.71	0.05	0.29	0.05		
7.20	11.78	0.771	0.029	-0.51	0.04	0.64	0.05	0.24	0.06		
7.80	12.30	0.606	0.025	-0.43	0.04	0.50	0.05	0.10	0.06	-0.08	0.06
8.60	12.98	0.531	0.020	-0.41	0.03	0.36	0.04	0.17	0.04	-0.07	0.05
9.40	13.67	0.494	0.019	-0.42	0.03	0.16	0.03	0.31	0.03	0.06	0.05

TABLE 7

$^{4}He(^{3}He, p'')^{6}Li^{**}$ Data

The data are expressed in terms of the coefficient of the Legendre polynomial P_0, which is the total center-of-momentum cross section divided by 4π, and given as a function of the incident ^{3}He energy and corresponding ^{7}Be excitation energy. The coefficients and estimated standard errors are in millibarns per steradian, the energies in MeV. There is a systematic uncertainty in the incident ^{3}He laboratory energy scale of about 20 keV, and a distribution with a standard deviation of about 22 keV associated with each laboratory energy value given. (Pages 31 and 79)

TABLE 7

$^{4}He(^{3}He, p'')^{6}Li^{**}$ Data

Lab Energy	^{7}Be Excitation Energy	P_0 Coef.	Estimated Error
13.81	9.48	0.049	0.002
14.01	9.59	0.095	0.003
14.21	9.71	0.152	0.005
14.42	9.83	0.218	0.006
14.62	9.95	0.264	0.005
14.82	10.06	0.311	0.006
15.02	10.17	0.356	0.007
15.22	10.28	0.404	0.008
15.43	10.40	0.443	0.009
15.63	10.52	0.479	0.009
15.73	10.58	0.492	0.009
15.83	10.63	0.511	0.009
15.93	10.69	0.492	0.009
16.03	10.75	0.485	0.009
16.13	10.80	0.470	0.008
16.23	10.86	0.465	0.008
16.33	10.92	0.445	0.009
16.44	10.98	0.435	0.009
16.54	11.04	0.411	0.008
16.64	11.10	0.419	0.008
16.74	11.15	0.409	0.008
16.84	11.21	0.422	0.008
16.94	11.27	0.419	0.008
17.04	11.32	0.415	0.008
17.24	11.44	0.410	0.008

TABLE 7 (cont.)

Lab Energy	^{7}Be Excitation Energy	P_0 Coef.	Estimated Error
17.44	11.55	0.384	0.008
17.64	11.67	0.380	0.007
17.84	11.78	0.368	0.007
18.05	11.90	0.369	0.007
18.25	12.02	0.370	0.007
18.45	12.13	0.362	0.007

Absolute Normalization Error 20%

TABLE 8

$^{6}Li(p, ^{3}He)^{4}He$ Angular Distributions

The center-of-momentum differential cross section and its estimated % standard error are given for each incident proton laboratory energy as a function of ^{3}He laboratory angle and of cosine of center-of-momentum angle. Millibarn per steradian units are used. The normalization error is also given. There is an uncertainty of +0.03 and -0.02 MeV in the 2.88 MeV laboratory energy. (Page 33)

TABLE 8

$^{6}Li(p, ^{3}He)^{4}He$ Angular Distributions

Lab Energy = 2.60 MeV				Lab Energy = 2.88 MeV			
Lab Angle	Cosine CM Angle	$\frac{d\sigma}{d\Omega}$	Estimated % Error	Lab Angle	Cosine CM Angle	$\frac{d\sigma}{d\Omega}$	Estimated % Error
7.7°	0.982	12.28	4	10.6°	0.970	10.38	6
11.0	0.970	12.53	4	19.0	0.919	10.05	6
19.3	0.917	10.58	4	21.4	0.900	8.31	10
28.2	0.829	10.27	4	27.8	0.832	9.44	5
30.7	0.800	9.75	3 1/2	30.7	0.798	9.05	4
38.1	0.700	10.22	1 3/4	34.6	0.745	9.64	5
44.6	0.600	10.32	1 3/4	38.1	0.697	9.42	2
50.6	0.500	10.46	1 3/4	44.6	0.597	10.10	2
56.3	0.400	10.29	1 3/4	50.6	0.497	10.40	2
61.8	0.300	10.26	1 3/4	56.3	0.395	10.40	2
67.2	0.200	10.10	1 3/4	61.8	0.295	10.39	2
72.6	0.100	10.00	1 3/4	67.2	0.195	10.04	2
78.1	0.000	9.86	1 3/4	72.6	0.094	9.76	2
80.1	-0.034	9.54	1 3/4	78.1	-0.005	9.65	2
83.6	-0.100	9.19	1 3/4	83.6	-0.106	9.10	2
85.7	-0.137	9.34	1 3/4	84.7	-0.126	9.09	2
89.4	-0.200	9.19	1 3/4	89.3	-0.207	9.01	2
91.2	-0.235	8.99	1 3/4	90.9	-0.235	8.60	2
95.3	-0.300	8.70	1 3/4	95.3	-0.306	8.75	2
97.8	-0.341	8.64	1 3/4	97.4	-0.342	8.55	2
101.6	-0.400	8.65	1 3/4	101.6	-0.404	8.42	2
105.0	-0.451	8.60	1 3/4	104.2	-0.445	8.35	2
108.4	-0.500	8.68	1 3/4	108.4	-0.505	8.25	2
112.6	-0.559	8.79	1 3/4	112.1	-0.553	8.16	2

TABLE 8 (cont.)

Lab Energy = 2.60 MeV				Lab Energy = 2.88 MeV			
Lab Angle	Cosine CM Angle	$\frac{d\sigma}{d\Omega}$	Estimated % Error	Lab Angle	Cosine CM Angle	$\frac{d\sigma}{d\Omega}$	Estimated % Error
115.9°	-0.600	8.72	1 3/4	120.4°	-0.660	8.40	2
121.1	-0.665	8.50	2	131.1	-0.775	8.35	2
131.7	-0.774	8.84	2 1/2	145.1	-0.886	8.15	2
145.5	-0.888	8.53	3	147.7	-0.902	8.70	6
Normalization Error 1.8%				Normalization Error 1.8%			

TABLE 9

Relative Normalization Factors

The relative normalization factors and their estimated standard errors are given for a number of experiments forming ^{7}Be as the compound nucleus. The data from each experiment should be multiplied by the factor given to obtain a consistent relative normalization. (Page 34)

TABLE 9

Relative Normalization

Reaction	Reference	Relative Normalization Factor	Estimated % Standard Error
$^{6}Li(p, p)^{6}Li$	McCray (1962)	1.000	
	Harrison (present work)	1.000	1
	Fasoli et al. (1964a)	0.867	1
$^{6}Li(p, p')^{6}Li^{*}$	Harrison (present work)	1.000	1
$^{6}Li(p, p'')^{6}Li^{**}$	Harrison (present work)	1.000	1
$^{6}Li(p,{}^{3}He)^{4}He$	Fasoli et al. (1964b)	0.867	3
	Jeronymo et al. (1963)	0.867	3
	Marion (1956)	0.675	3
	Heydenburg (1962)	0.675	~4
$^{4}He({}^{3}He,p)^{6}Li$	Tombrello and Parker (1963)	0.867	~4
	Harrison (present work)	0.850	2
	Spiger and Tombrello (1964)	0.795	2
$^{4}He({}^{3}He,p')^{6}Li^{*}$	Spiger and Tombrello (1964)	0.795	2
$^{4}He({}^{3}He,p'')^{6}Li^{**}$	Harrison (present work)	1.0	20
$^{4}He({}^{3}He,{}^{3}He)^{4}He$	Tombrello and Parker (1963)	0.867	~4
	Spiger and Tombrello (1964)	0.795	2

TABLE 10
Absolute Normalization

Reference	Magnitude Factor	Estimated % Standard Error
McCray (1962)	1.000	7 or 8
Marion (1956)	1.483	15
Tombrello and Parker (1963)	1.153	4 or 5
Harrison (present work)	1.176	+4, -7
Spiger and Tombrello (1964)	1.258	4 or 5

The magnitude factors given are the reciprocals of the normalization factors given in Table 9 and are proportional to the magnitude of ^{7}Be cross sections with the absolute normalization found by each investigator. For example, the absolute normalization of Spiger and Tombrello implies that cross sections are 1.258 as large as implied by the absolute normalization of McCray. The estimated percent standard error for each absolute normalization determination is given. (Page 34)

TABLE 11

Parameters from the $^{6}Li(p, p')^{6}Li^{*}$ Fits

Penetration Factor	^{7}Be Excitation Energy Range Fitted (MeV)	χ^2 ÷(degrees of freedom)	ℓ	ℓ'	E_1 (MeV ^{7}Be excitation energy)	ΔE_1	Γ_1 (same units as E_1)	$\Delta\Gamma_1$	C_1 (MeV^2)
Radius-Dependent	8.70 to 11.61	0.79	1	1	9.96	0.05	1.8	0.1	16.7
Radius-Dependent	8.70 to 11.61	3.8	3	1	9.63	0.05	1.6	0.1	240
Radius-Independent	8.70 to 11.61	4.3	1	1	9.62	0.05	1.5	0.1	22,000
Radius-Independent	8.70 to 11.61	9.9	3	1	9.38	0.05	1.3	0.1	660,000

The results of the single-level fits to the coefficient of P_2 are summarized. The resonant parameters on the first line correspond to the fit with the most reasonable χ^2, and are assumed to be the best choices. The resonant energy is denoted by E_1, its calculated standard error by ΔE_1, the total width by Γ_1, and its calculated standard error by $\Delta\Gamma_1$. The meaning of the parameter C_1 is discussed in Appendix B. (Pages 57, 74, and 75)

TABLE 12

Parameters from the $^{6}Li(p, p'')^{6}Li^{**}$ Fits

	E_2 (MeV ^{7}Be excitation energy)	ΔE_2	Γ_2 (same units as E_1)	$\Delta\Gamma_2$	D (MeV^3)	ΔD
No background subtracted	11.0	0.05	0.4	0.05	1.9	0.3
Background subtracted	11.0	0.05	0.4	0.05	1.5	0.3

The results of the two-level fits to the coefficient of P_0 are summarized. The resonant parameters for the state labelled by 2 are given, and the notation is the same as used in Table 11 for state 1. The parameters obtained for state 1 from these fits are the same as in Table 11. Radius-dependent penetration factors for $\ell = \ell' = 1$ were used, and the range of data fitted was from 10.4- to 11.6-MeV ^{7}Be excitation energy. The dependence of quantity D, defined in Appendix C, on the arbitrary background plotted in Figures 29 and 30 can be seen. The estimated uncertainty ΔD does not include the uncertainty due to the unknown background. (Pages 62, 77 and 78)

TABLE 13

Parameters from the $^{4}He(^{3}He, p'')^{6}Li^{**}$ Fits

	C_1 (MeV^2)	ΔC_1	C_2 (MeV^2)	ΔC_2	ζ	$\Delta\zeta$
No background subtracted	1.38	0.06	0.0130	0.0040	259^{o}	large
Background subtracted	1.24	0.06	0.0156	0.0040	207^{o}	large

The results of the two-level fits to the coefficient of P_0 are summarized. The values of the parameters (C_1, C_2, ζ), defined in Appendix D and by equation (17), correspond to values of the parameters ($E_1, \Gamma_1, E_2, \Gamma_2$) approximately the same as in Tables 11 and 12. They were obtained for radius-dependent penetration factors with $\ell = \ell' = 1$, and the range of data fitted was from 10.4- to 11.6-MeV ^{7}Be excitation energy. The dependence of the parameters (C_1, C_2, ζ) on the arbitrary background plotted in Figures 32 and 33 can be seen. The uncertainties ($\Delta C_1, \Delta C_2, \Delta\zeta$) do not include the uncertainty due to the unknown background. There is an additional uncertainty in C_1 and C_2 due to the 20% uncertainty in the normalization of the data. (Page 80)

Figure 1
Energy Level Diagram of ^{7}Be

The two regions of very broad cross hatching represent ^{7}Be structure for which the evidence is uncertain. (Page 1)

FIGURE 1 126

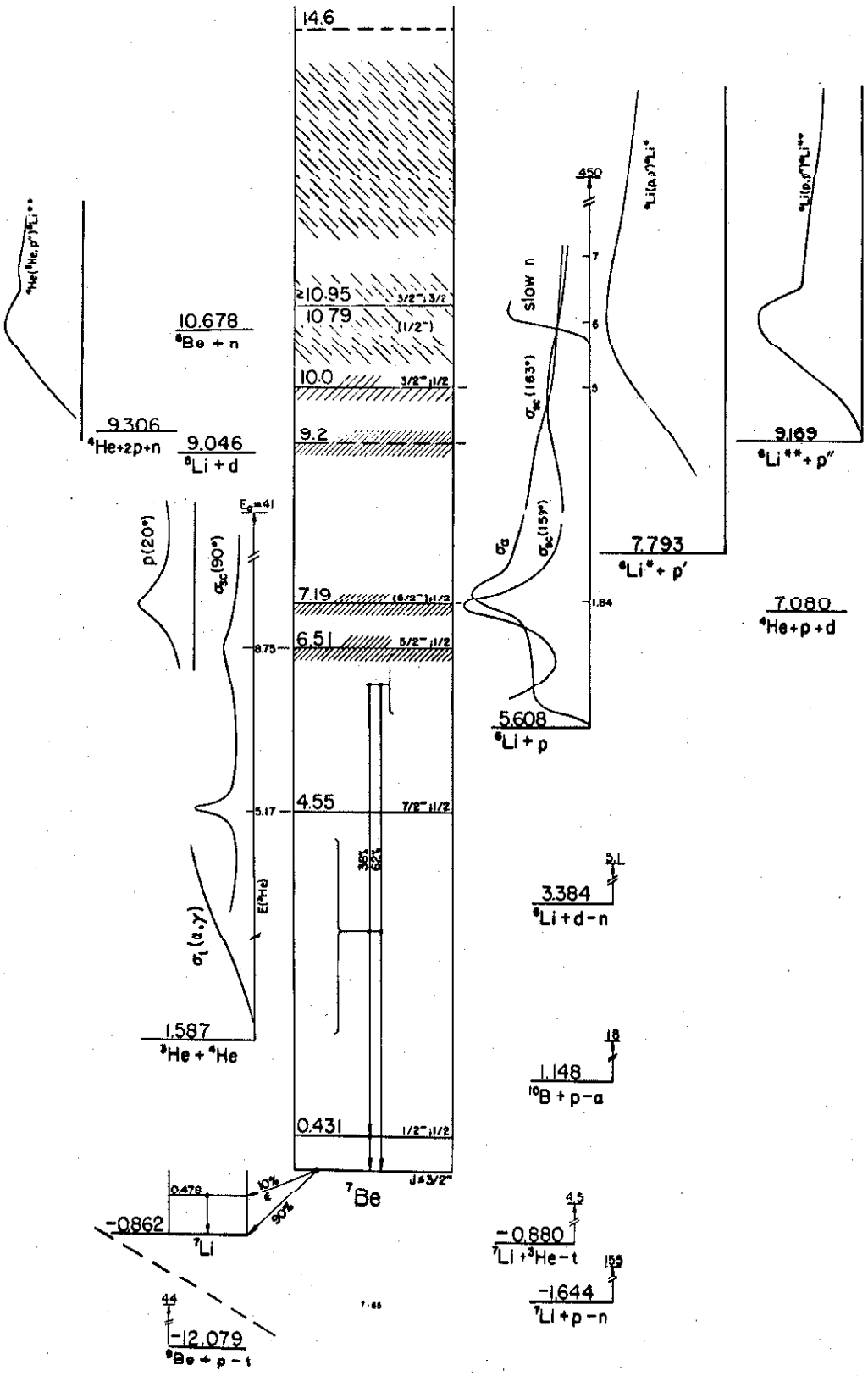
14.6
≥10.95
10.79
10.0
9.2
7.19
6.51
4.55
0.431
J=3/2⁻
⁷Be
10.678
⁶Be + n
9.306
⁴He+2p+n
9.046
⁵Li + d
1.587
³He + ⁴He
-0.862
⁷Li
-12.079
⁹Be + p - t
slow n
5.608
⁶Li + p
7.793
⁶Li* + p'
9.169
⁶Li** + p''
7.080
⁴He+p+d
3.384
⁶Li+d-n
1.148
¹⁰B + p-α
-0.880
⁷Li +³He-t
-1.644
⁷Li + p-n

Figure 2
Top and Side Views of the Scattering Chamber

The diameter of the chamber is about 25 cm.
(Pages 4, 8, 10 and 11)

FIGURE 2 128

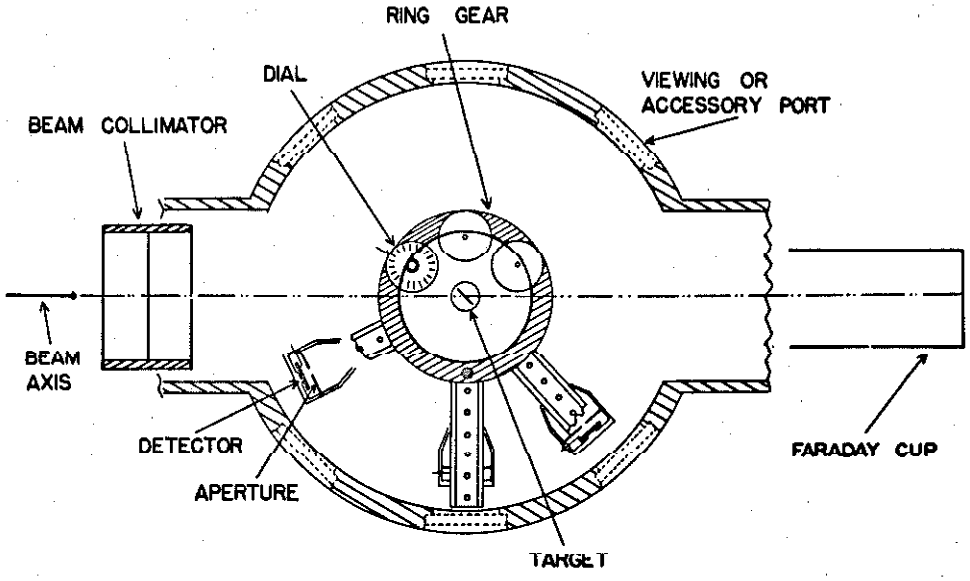

TOP VIEW

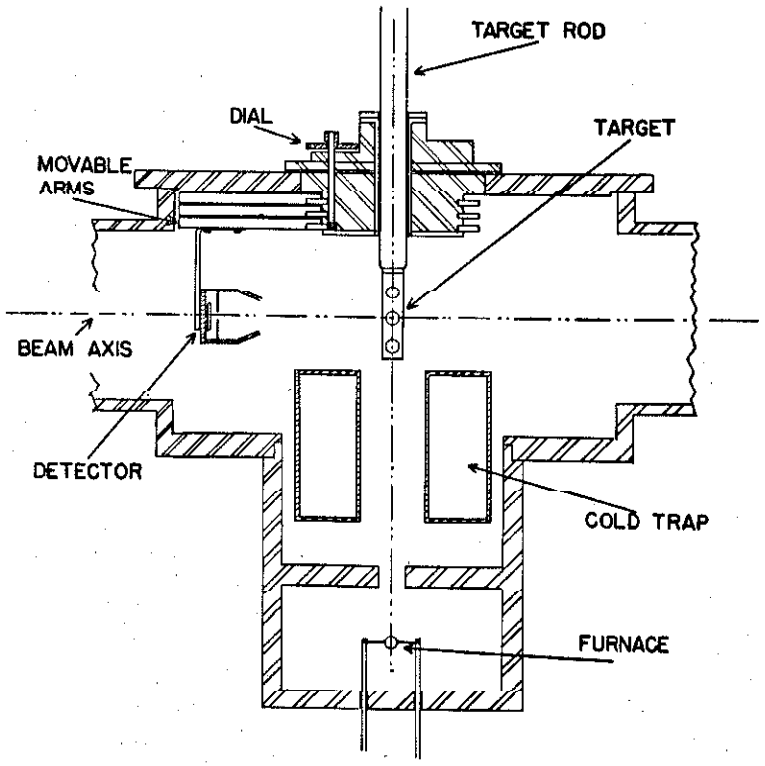

SIDE VIEW

Figure 3

Particle Spectrum Obtained with Lithium Drifted Detector

The spectrum was obtained from the bombardment of a ^{6}Li target with 12.00-MeV protons. The detector was at a laboratory angle of 55.5° with a 0.008-mm thick aluminum foil over the entrance aperture. (Pages 8 and 9)

FIGURE 3

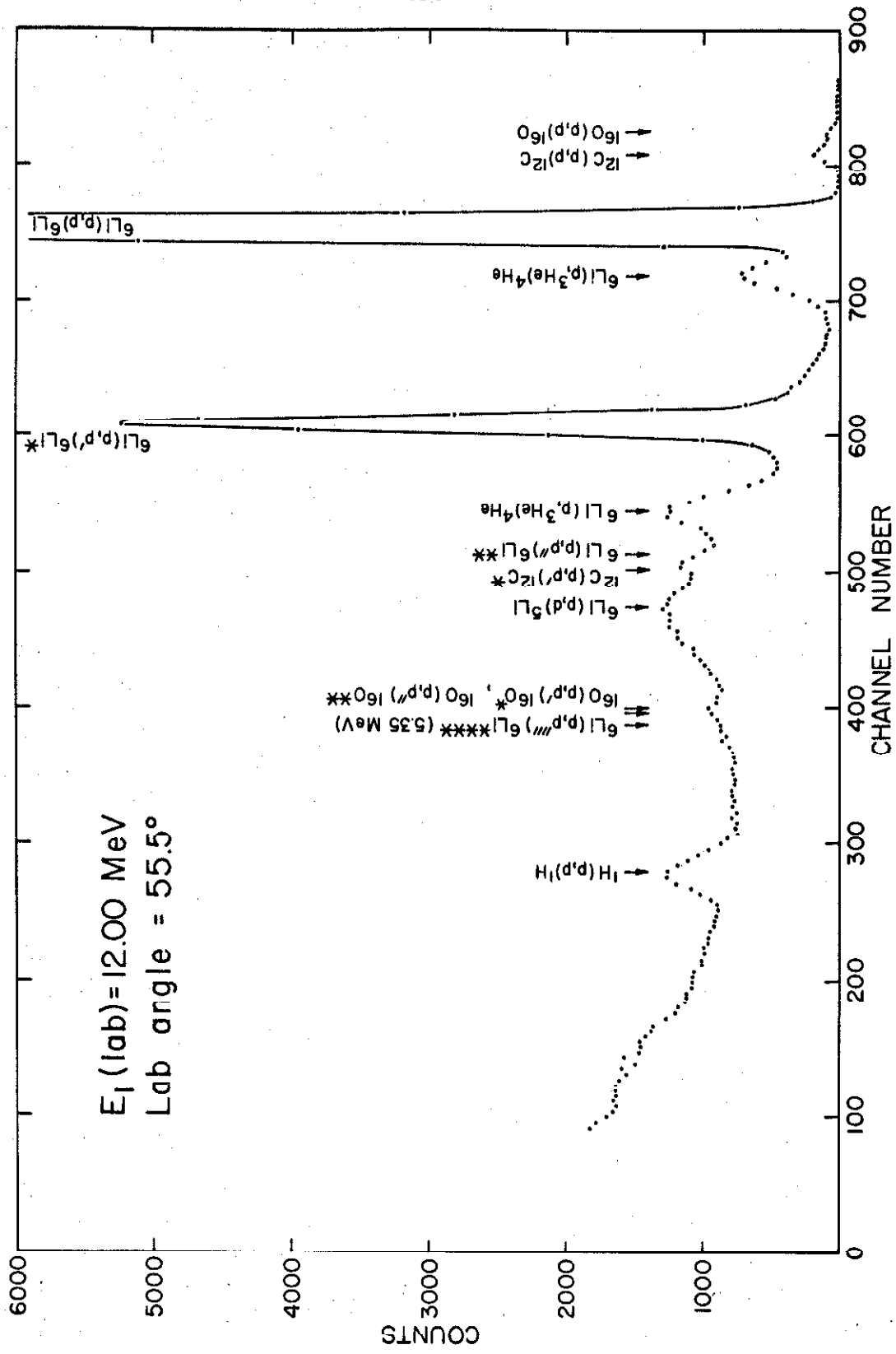
E_I (lab) = 12.00 MeV
Lab angle = 55.5°
$^1H(p,p)^1H$
$^6Li(p,p''')^6Li^{****}$ (5.35 MeV)
$^{16}O(p,p')^{16}O^*$, $^{16}O(p,p'')^{16}O^{**}$
$^6Li(p,d)^5Li$
$^{12}C(p,p')^{12}C^*$
$^6Li(p,p'')^6Li^{**}$
$^6Li(p,^3He)^4He$
$^6Li(p,p')^6Li^*$
$^6Li(p,^3He)^4He$
$^6Li(p,p)^6Li$
$^{12}C(p,p)^{12}C$
$^{16}O(p,p)^{16}O$
COUNTS
CHANNEL NUMBER
0
100
200
300
400
500
600
700
800
900
1000
2000
3000
4000
5000
6000

Figure 4

^{6}Li(p, p)^{6}Li Relative Normalization

The results of the normalization of the present data (Harrison and Whitehead 1963) and that of Fasoli et al. (1964a) to the data of McCray (1962) are shown. The incident proton laboratory energies are given. (Pages 8 and 32)

FIGURE 4 132

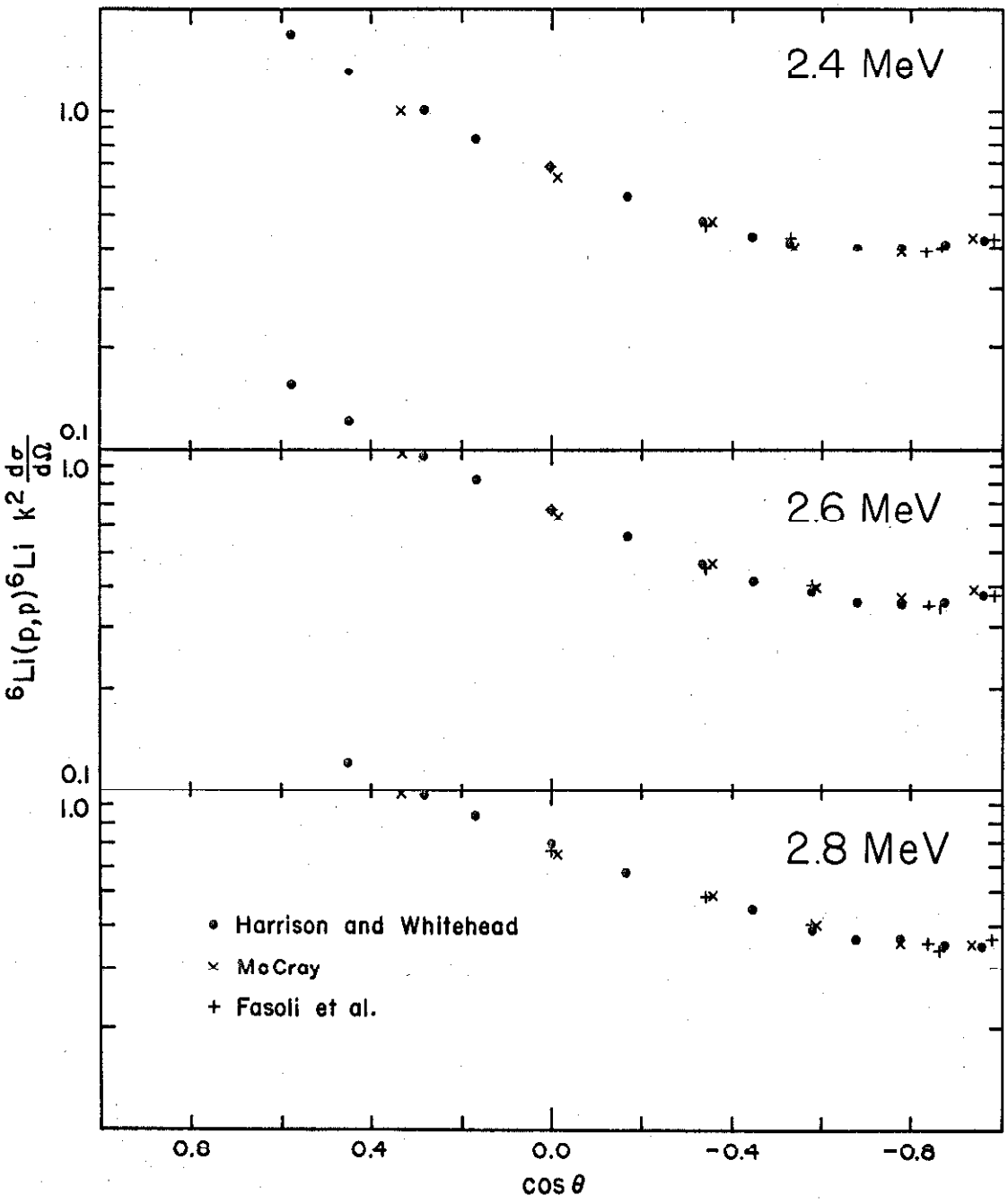
2.4 MeV
2.6 MeV
2.8 MeV
1.0
0.1
1.0
0.1
1.0
$^6Li(p,p)^6Li\ k^2 \frac{d\sigma}{d\Omega}$
Harrison and Whitehead
McCray
Fasoli et al.
0.8
0.4
0.0
-0.4
-0.8
cos θ

Figure 5
Preliminary $^{6}Li(p, p)^{6}Li$ Data

Three excitation functions with an approximate normalization are plotted. The center-of-momentum angles are given. (Pages 9, 61, and 64)

FIGURE 5 134

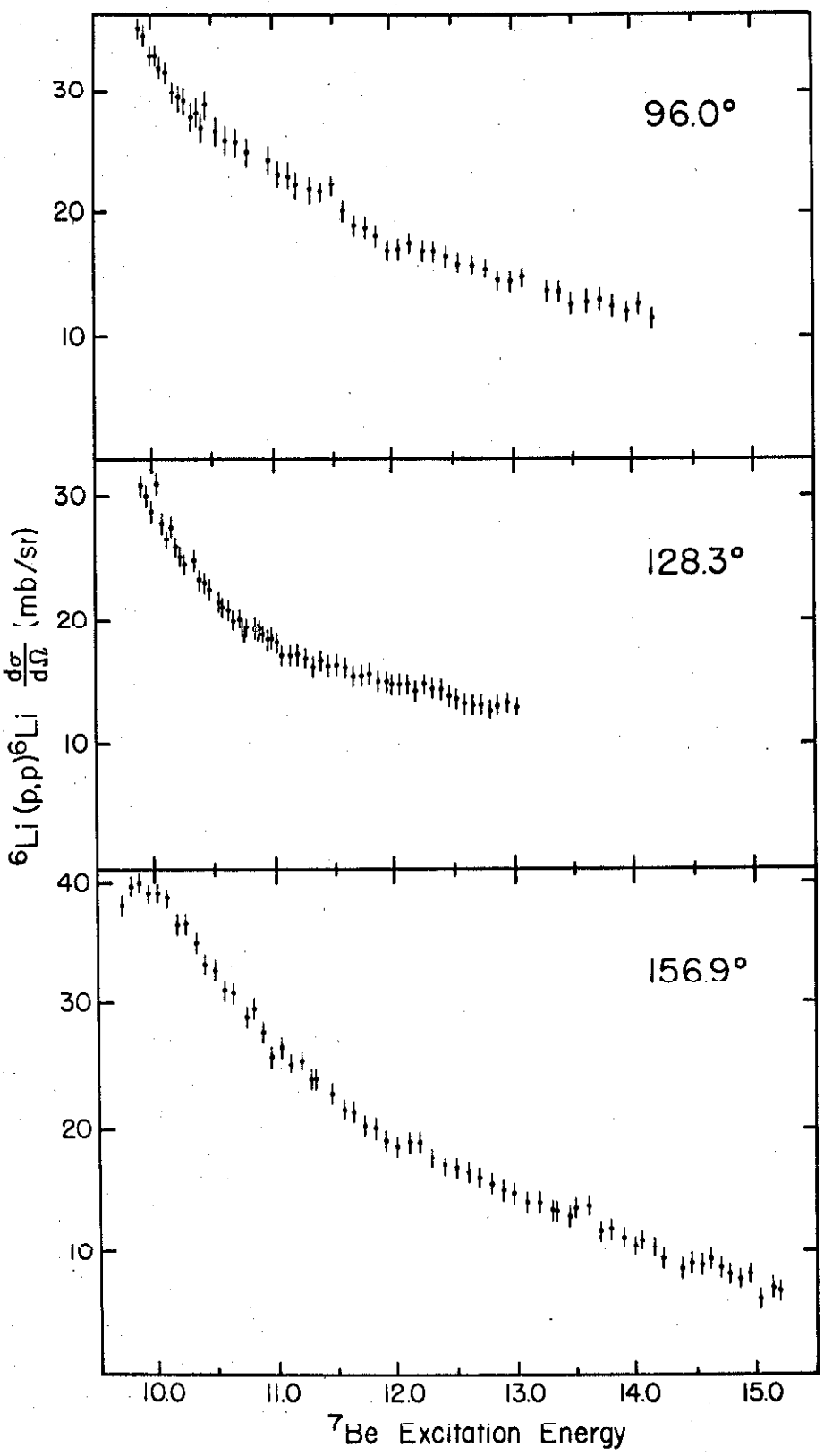
96.0°
128.3°
156.9°
30
20
10
40
10.0
11.0
12.0
13.0
14.0
15.0
^{6}Li (p,p)^{6}Li $\frac{d\sigma}{d\Omega}$ (mb/sr)
^{7}Be Excitation Energy

Figure 6
$^{6}Li(p, p)^{6}Li$ Angular Distributions

Smooth curves have been drawn through the data, with arrows to indicate the ordinate scale to be associated with each curve. The curves are labelled with two numbers. The first denotes the incident proton laboratory energy, and the second the corresponding ^{7}Be excitation energy. Both are in MeV. The center-of-momentum angle is denoted by θ. (Page 9)

FIGURE 6 136

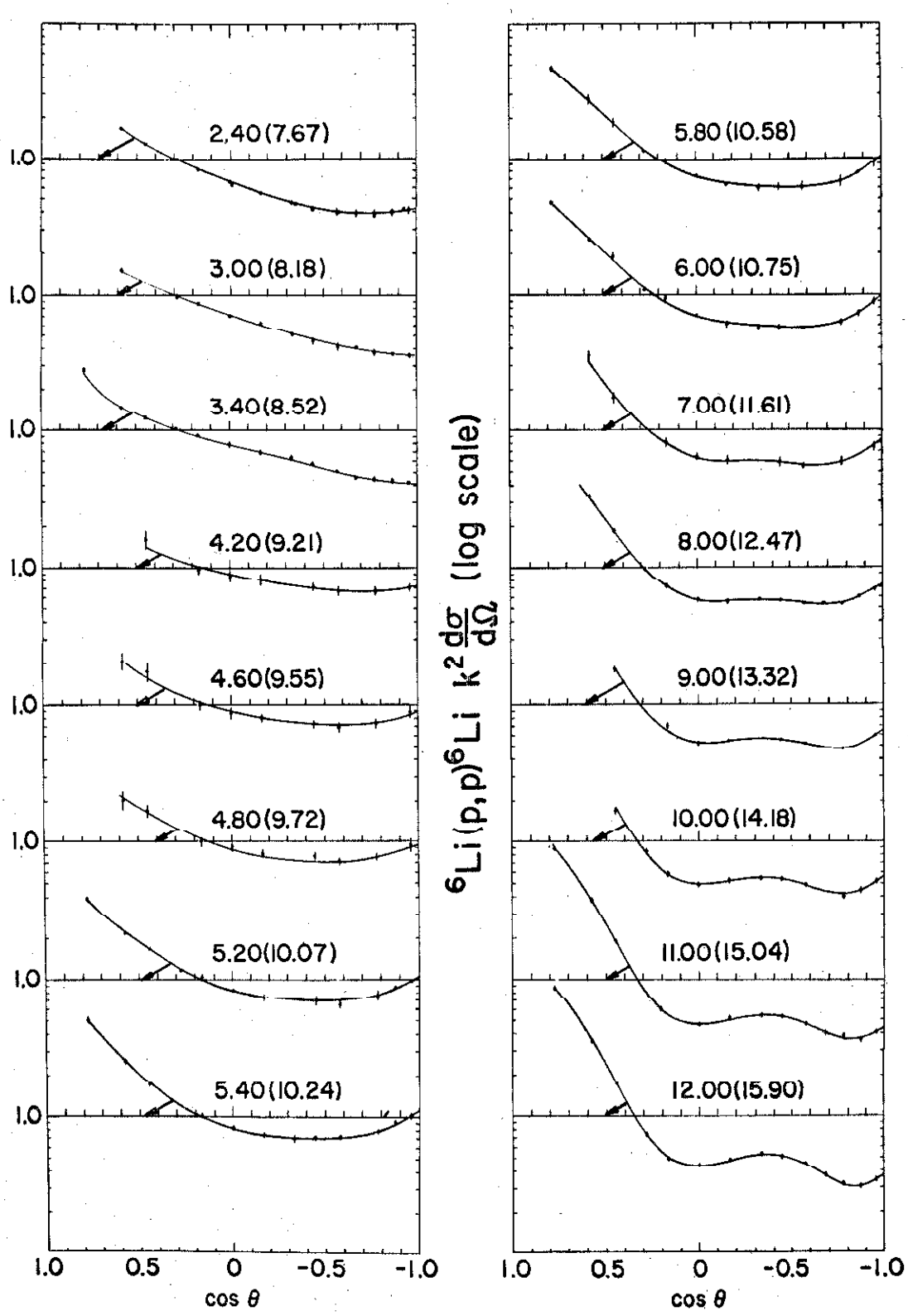
2.40(7.67)
3.00(8.18)
3.40(8.52)
4.20(9.21)
4.60(9.55)
4.80(9.72)
5.20(10.07)
5.40(10.24)
5.80(10.58)
6.00(10.75)
7.00(11.61)
8.00(12.47)
9.00(13.32)
10.00(14.18)
11.00(15.04)
12.00(15.90)
1.0
0.5
0
-0.5
-1.0
cos θ
^{6}Li(p,p)^{6}Li k^2 dσ/dΩ (log scale)

Figure 7
$^{6}Li(p, p)^{6}Li$ Excitation Functions

The data of McCray (1962) are represented by squares, and the present data (Harrison and Whitehead 1963) by circles. The center-of-momentum angles are given. The 180^{O} data were obtained by extrapolation. (Pages 9, 52, 54 and 72)

FIGURE 7 138

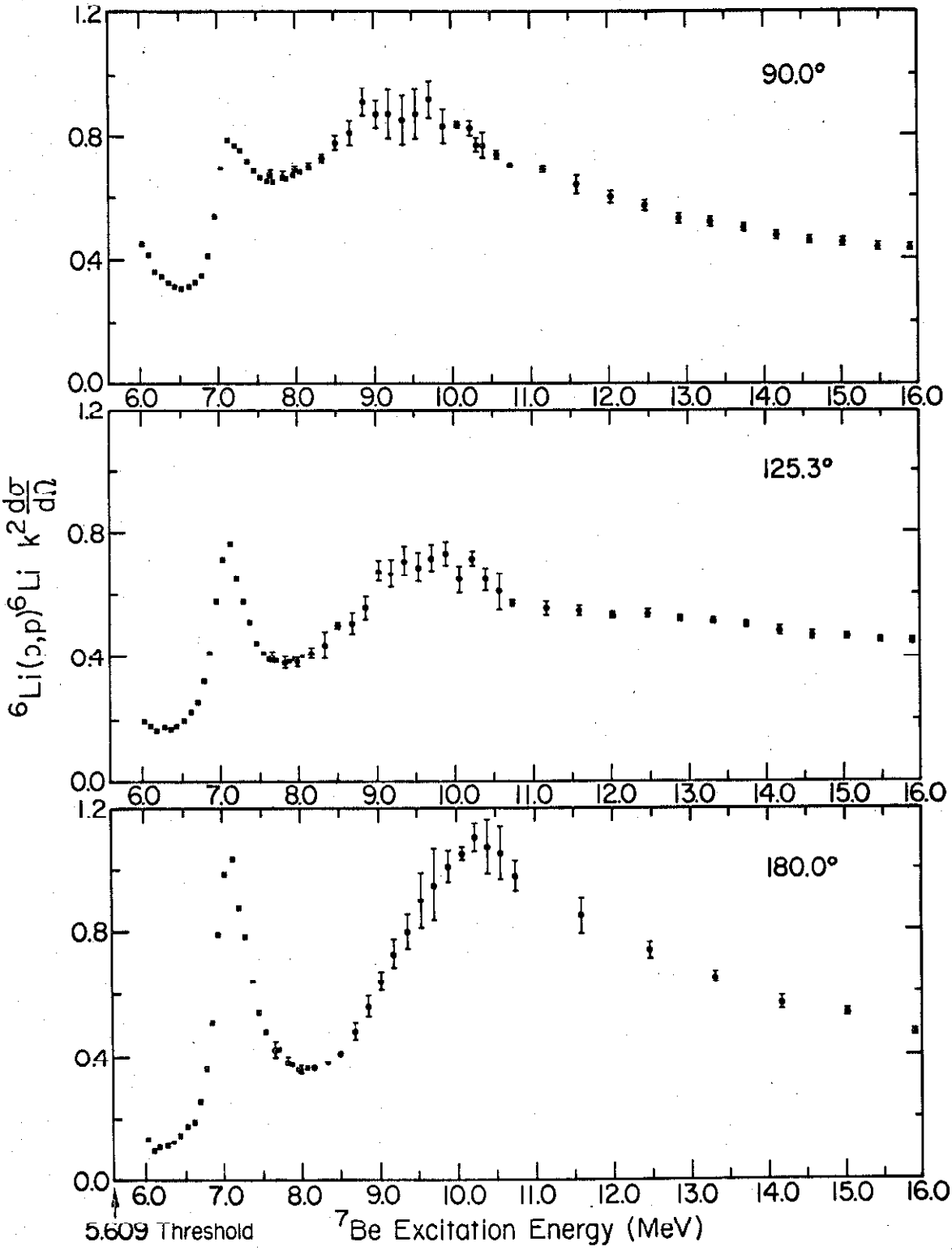
90.0°
125.3°
180.0°
$^6Li(p,p)^6Li\ k^2\frac{d\sigma}{d\Omega}$
5.609 Threshold
^7Be Excitation Energy (MeV)

Figure 8

Particle Spectrum Obtained with Surface Barrier Detector

The spectrum was obtained from the bombardment of a ^{6}Li target with 6.60-MeV protons. The counter was at a laboratory angle of 80.5^{o}. One channel is approximately 16.7 keV. (Page 13)

FIGURE 8 140

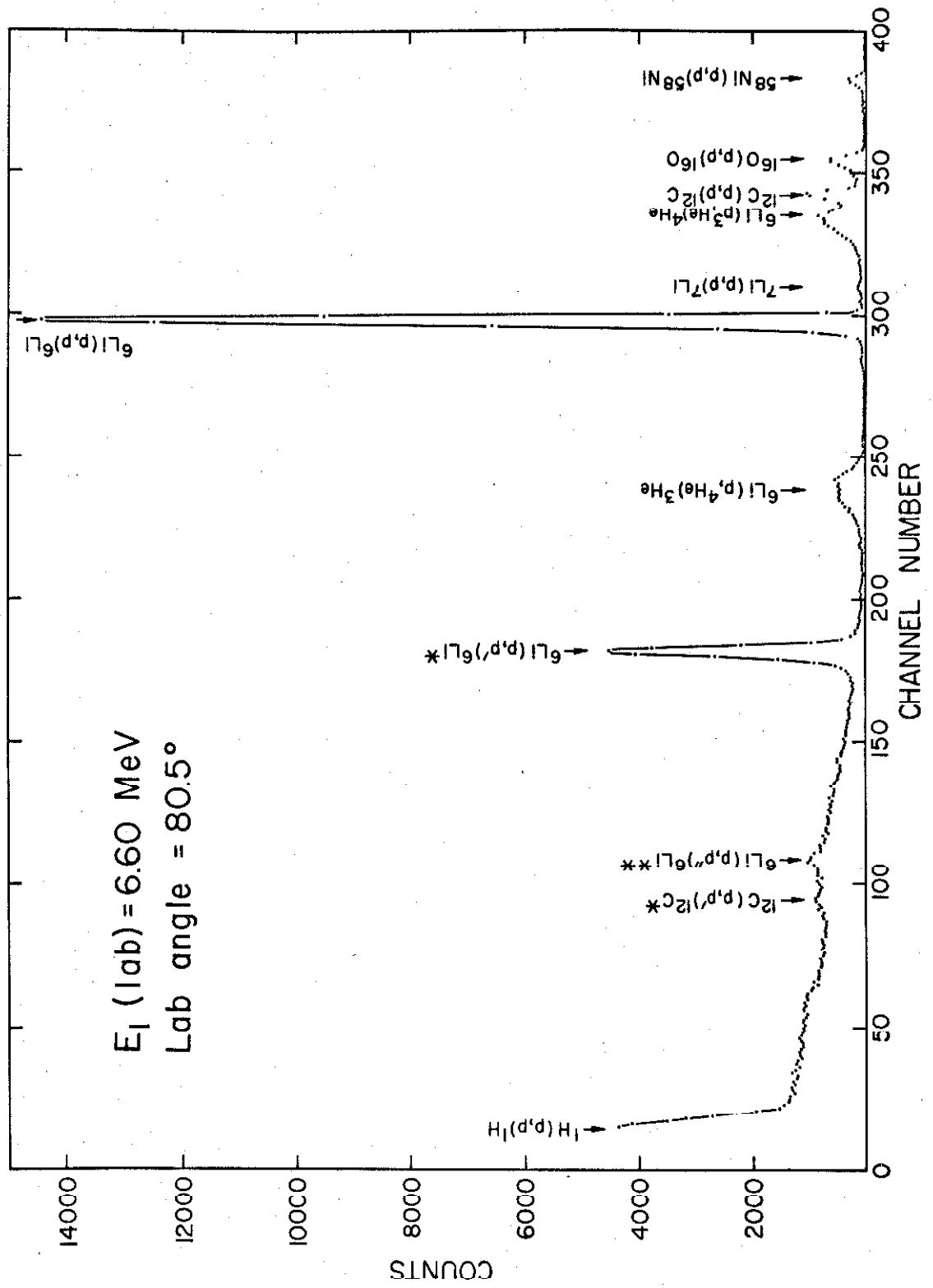
E_l (lab) = 6.60 MeV
Lab angle = 80.5°
COUNTS
CHANNEL NUMBER
$^{1}H(p,p)^{1}H$
$^{12}C(p,p')^{12}C^{*}$
$^{6}Li(p,p'')^{6}Li^{**}$
$^{6}Li(p,p')^{6}Li^{*}$
$^{6}Li(p,^{4}He)^{3}He$
$^{6}Li(p,p)^{6}Li$
$^{7}Li(p,p)^{7}Li$
$^{6}Li(p,^{3}He)^{4}He$
$^{12}C(p,p)^{12}C$
$^{16}O(p,p)^{16}O$
$^{58}Ni(p,p)^{58}Ni$

Figure 9
$^{6}Li(p, p')^{6}Li^{*}$ Angular Distributions

The differential cross section in millibarns per steradian is plotted as a function of the cosine of the center-of-momentum angle. The incident proton laboratory energy and the corresponding ^{7}Be excitation energy are given. Polynomial series stopping at P_2 and at P_4 were used in fitting the curves in Figures 9a and b respectively. (Pages 14 and 16)

FIGURE 9 142

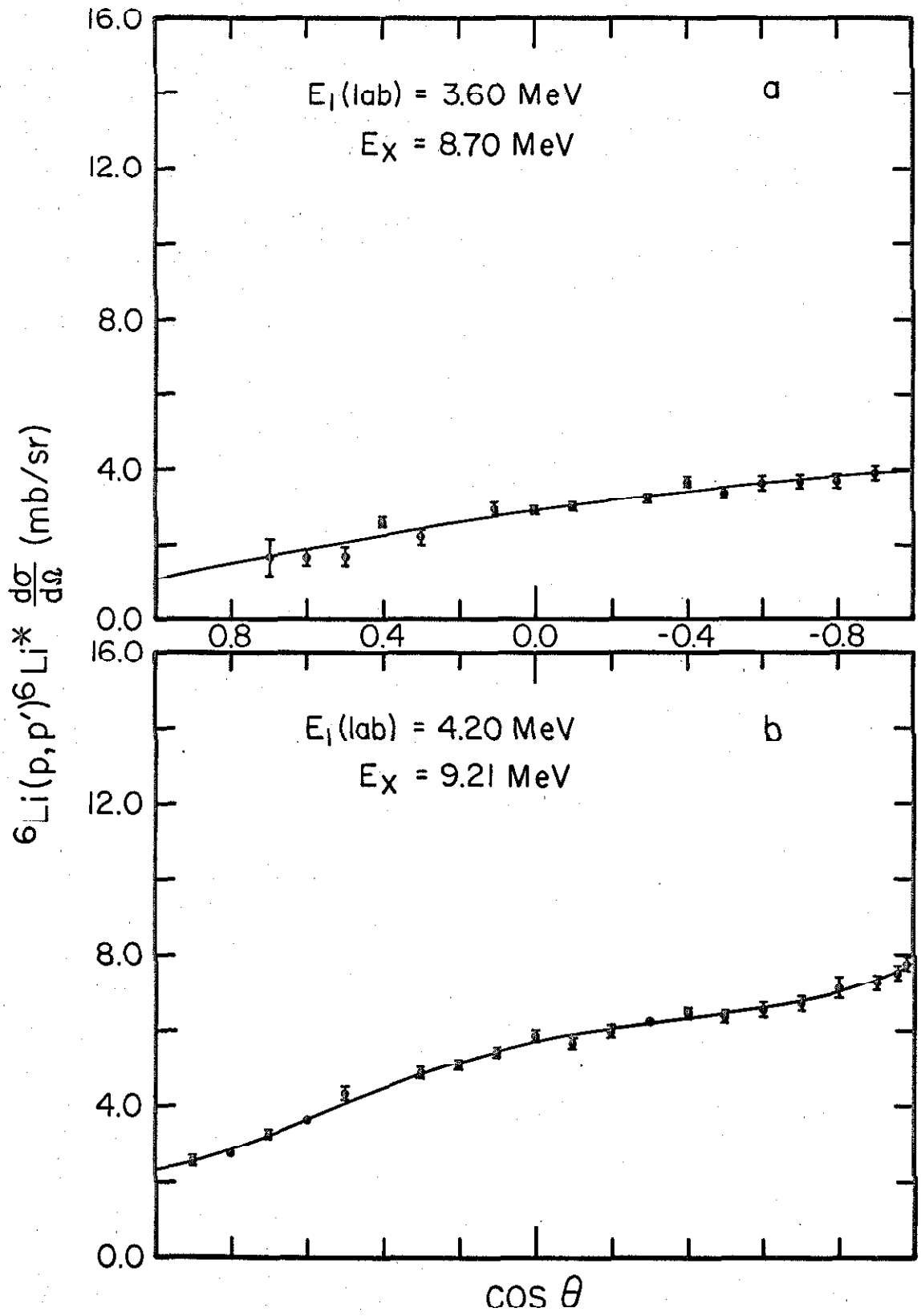
16.0
12.0
8.0
4.0
0.0
E_1(lab) = 3.60 MeV
E_X = 8.70 MeV
a
0.8
0.4
0.0
-0.4
-0.8
E_1(lab) = 4.20 MeV
E_X = 9.21 MeV
b
^{6}Li(p,p')^{6}Li* $\frac{d\sigma}{d\Omega}$ (mb/sr)
cos θ

Figure 10
$^{6}Li(p, p')^{6}Li^{*}$ Angular Distributions

Polynomial series stopping at P_4 were used in fitting the solid curves in Figures 10a and b. A series stopping at P_3 was used in fitting the dashed curve in Figure 10b. (Pages 14 and 16)

FIGURE 10 144

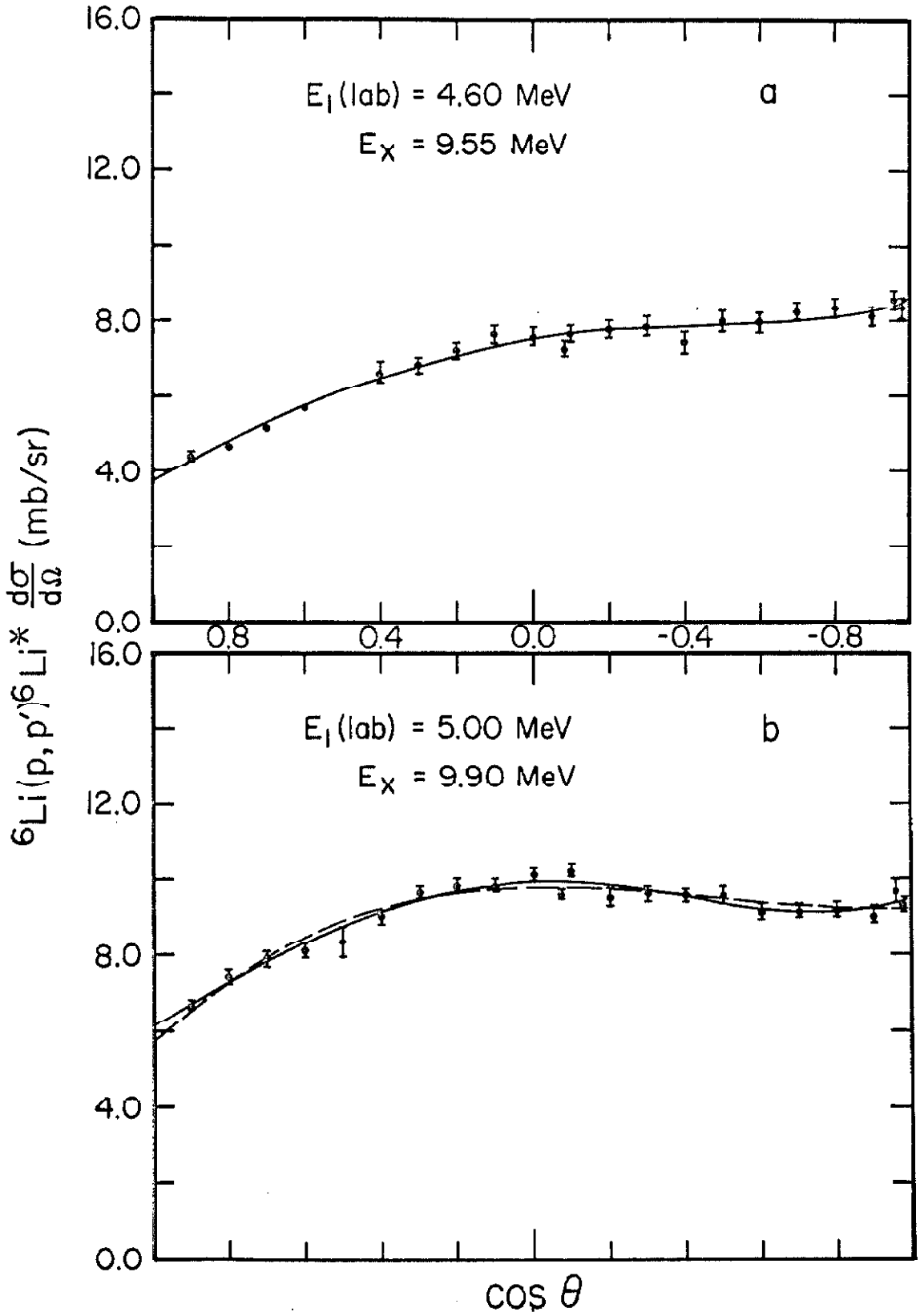

Figure 11
$^{6}Li(p, p')^{6}Li^{*}$ Angular Distributions

Polynomial series stopping at P_4 were used in fitting the curves in Figures 11a and b. (Pages 14 and 16)

FIGURE 11 146

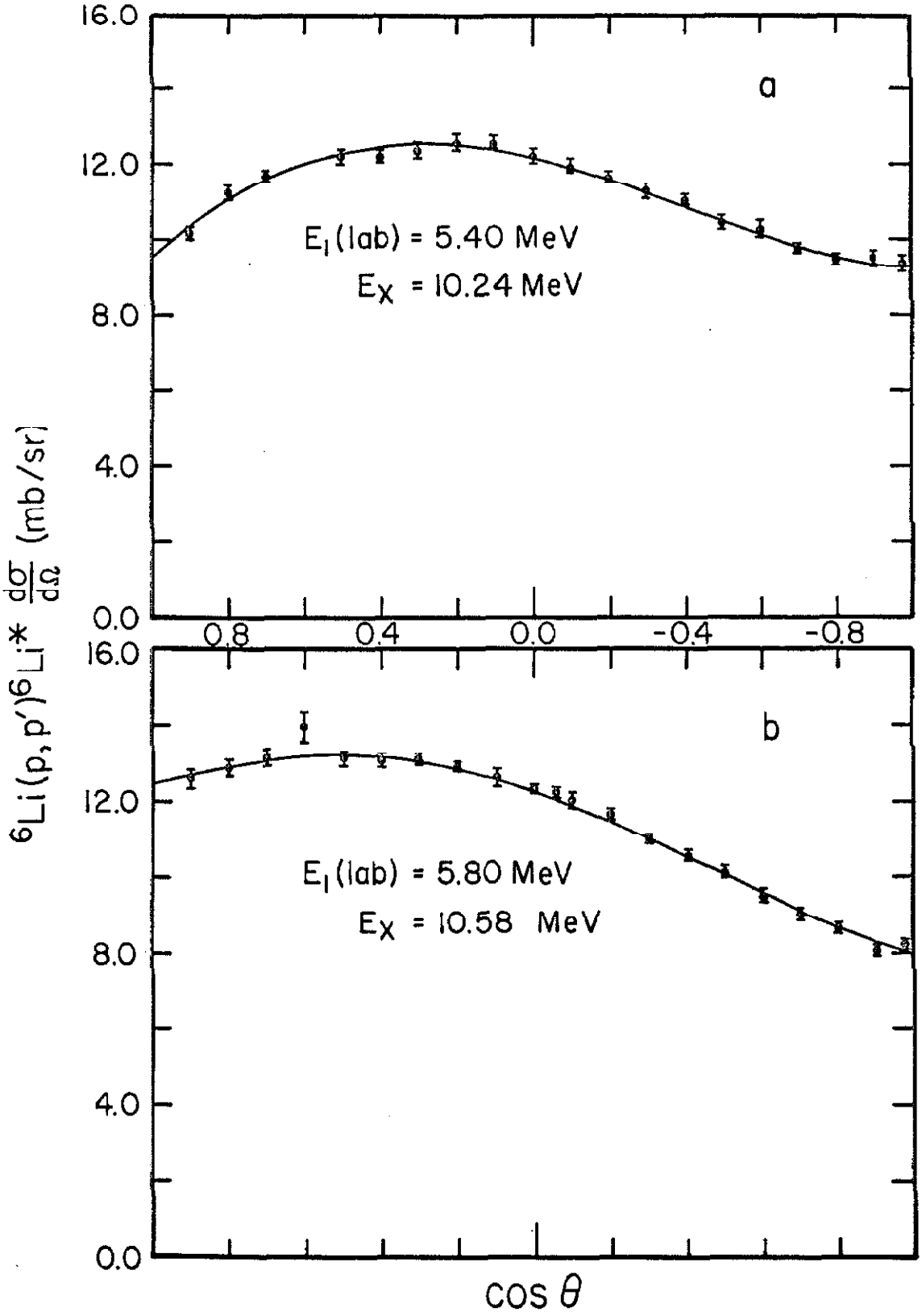

Figure 12
$^{6}Li(p, p')^{6}Li^{*}$ Angular Distributions

Polynomial series stopping at P_4 were used in fitting the curves in Figures 12a and b. (Pages 14 and 16)

FIGURE 12 148

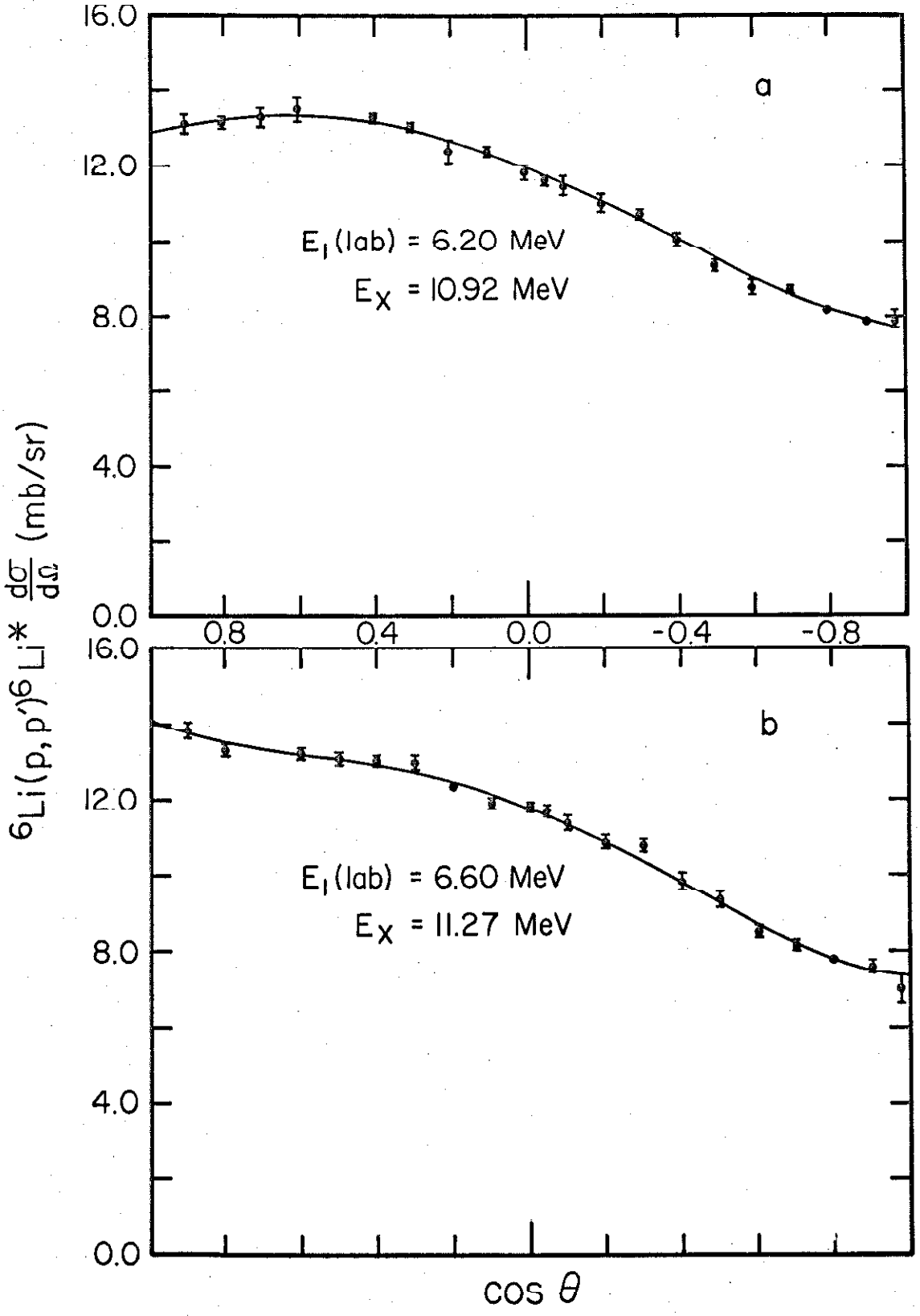

Figure 13
$^{6}Li(p, p')^{6}Li^{*}$ Angular Distributions

Polynomial series stopping at P_5 were used in fitting the solid curves in Figures 13a and b. A series stopping at P_4 was used in fitting the dashed curve in Figure 13b. (Pages 14 and 16)

FIGURE 13

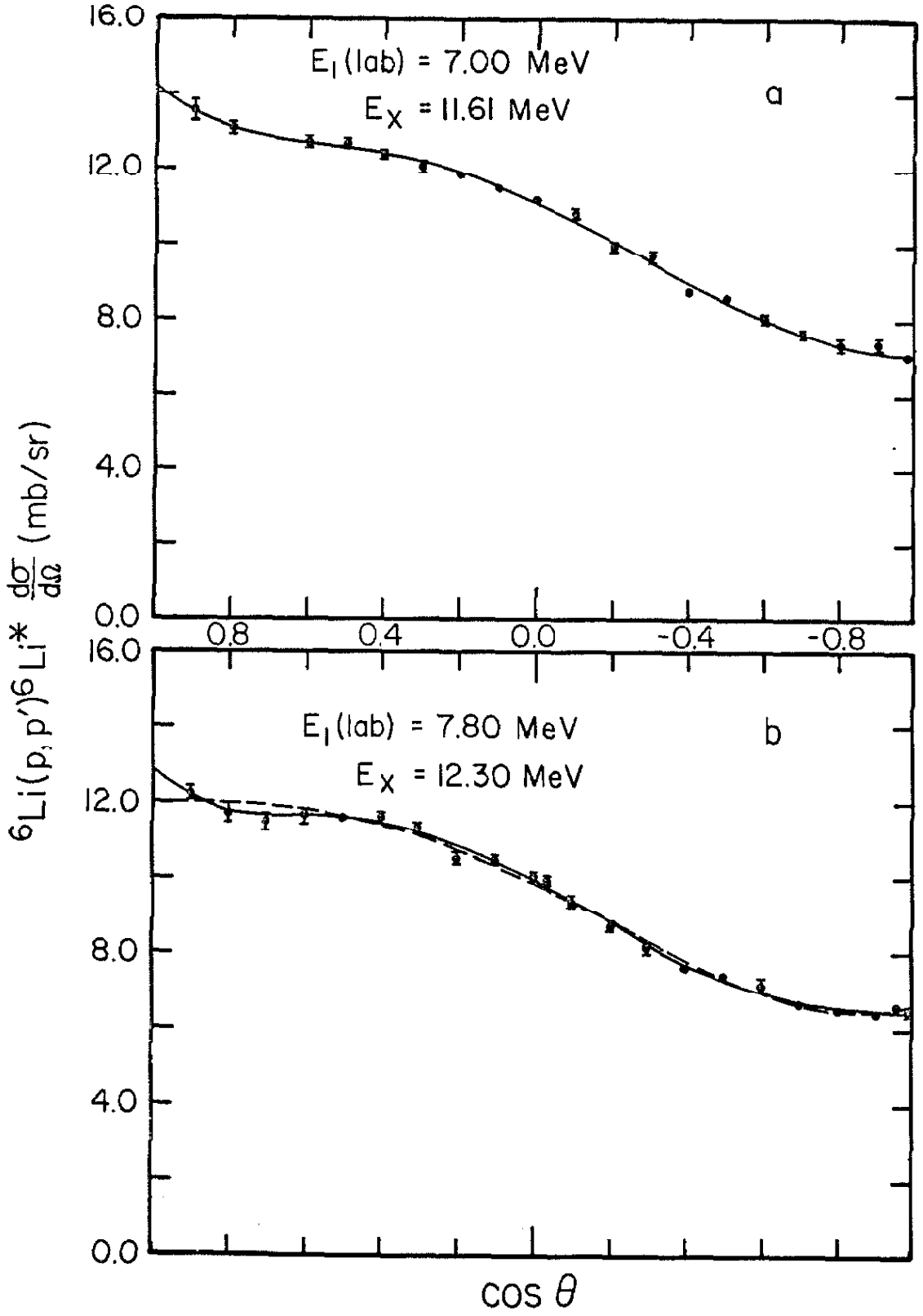
16.0
12.0
8.0
4.0
0.0
E_I (lab) = 7.00 MeV
E_X = 11.61 MeV
a
0.8
0.4
0.0
-0.4
-0.8
16.0
12.0
8.0
4.0
0.0
E_I (lab) = 7.80 MeV
E_X = 12.30 MeV
b
$^6Li(p,p')^6Li^*$ $\frac{d\sigma}{d\Omega}$ (mb/sr)
cos θ

Figure 14
$^{6}Li(p, p')^{6}Li^{*}$ Angular Distributions

Polynomial series stopping at P_5 were used in fitting the curves in Figures 14a and b. (Pages 14 and 16)

FIGURE 14 152

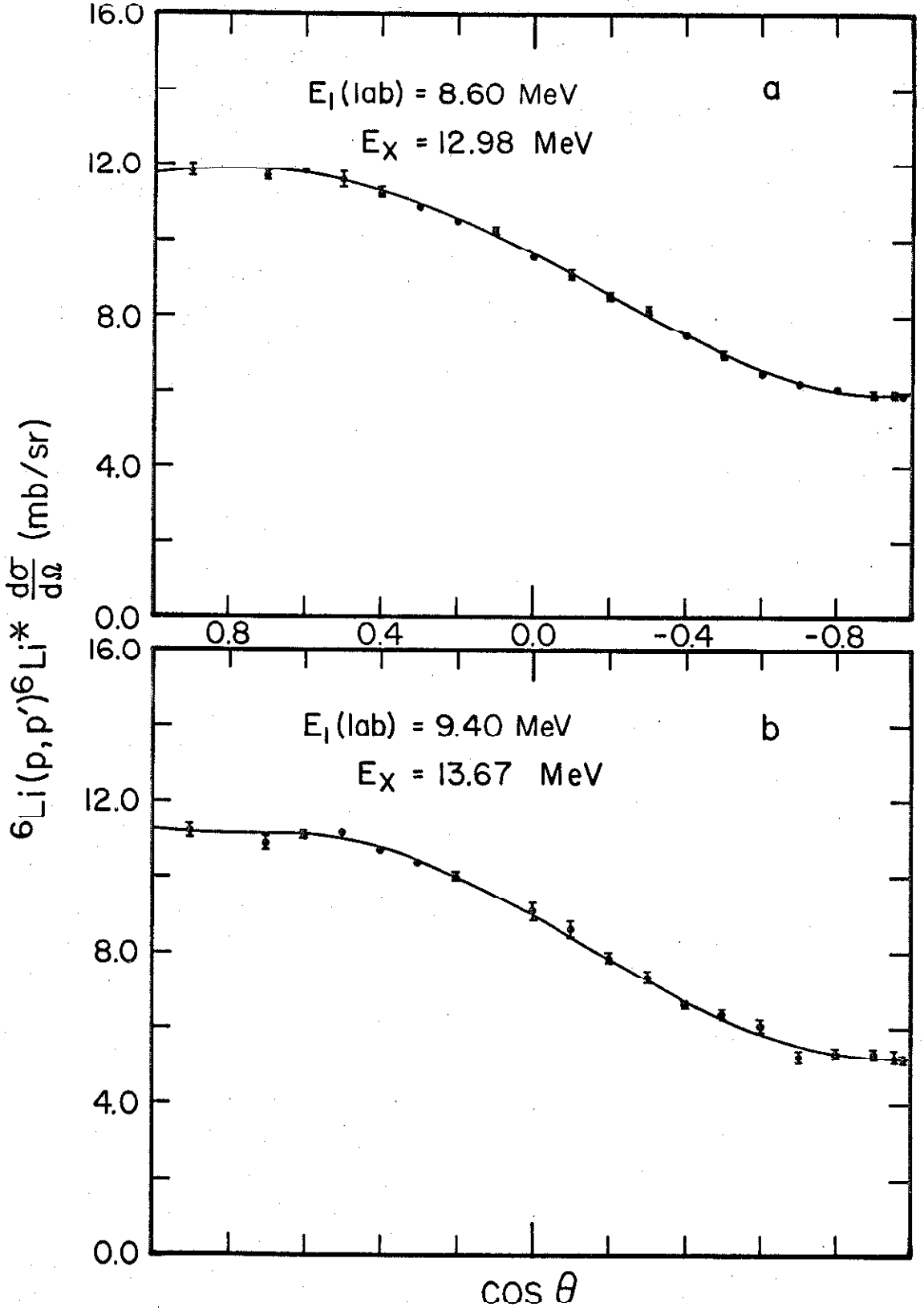

Figure 15
$^{6}Li(p, p')^{6}Li^{*}$ Polynomial Coefficients

The coefficients of the Legendre polynomials P_0 to P_5 and their standard errors are plotted. Each coefficient is labelled by the polynomial, and smooth curves have been drawn through some of the points. The coefficient of polynomial P_0 is equal to the total cross section σ divided by 4π. (Pages 16, 54, 61 and 64)

FIGURE 15

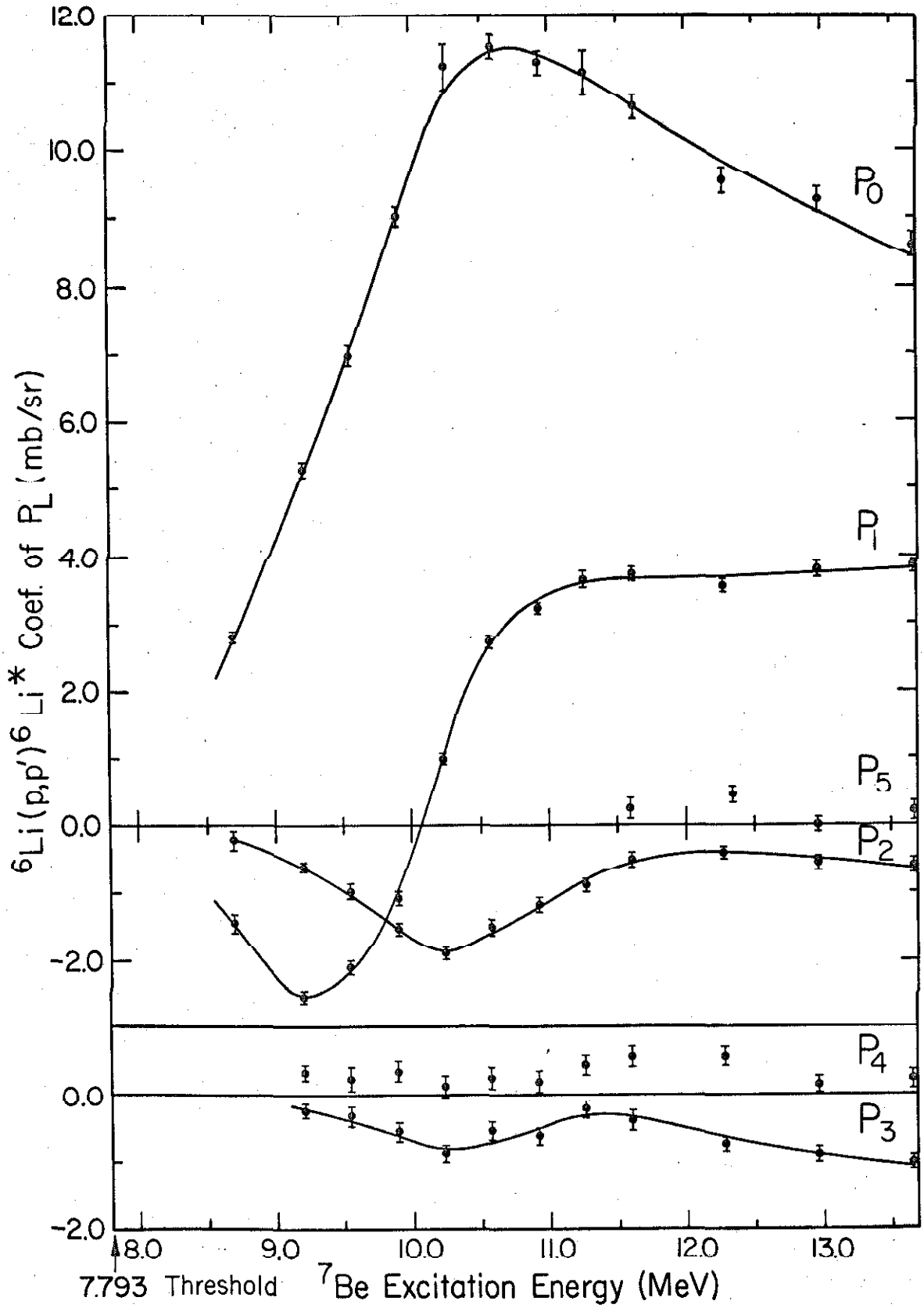
12.0
10.0
8.0
6.0
4.0
2.0
0.0
-2.0
0.0
-2.0
^{6}Li(p,p')^{6}Li* Coef. of P_L (mb/sr)
P_0
P_1
P_5
P_2
P_4
P_3
8.0
9.0
10.0
11.0
12.0
13.0
7.793 Threshold
^{7}Be Excitation Energy (MeV)

Figure 16

Gamma-Ray Spectra

Part of a γ-ray spectrum obtained from the bombardment of a ^{6}Li target with 6.20-MeV protons is shown in Figure 16a. A 7.62-cm long by 7.62-cm diameter NaI(Tl) detector was used at 90^{o} to the beam axis with its face about 17.5 cm from the target. In Figure 16b the 4.433-MeV γ ray from the ^{12}C contamination in the target has been subtracted from the spectrum. (Page 19)

FIGURE 16 156

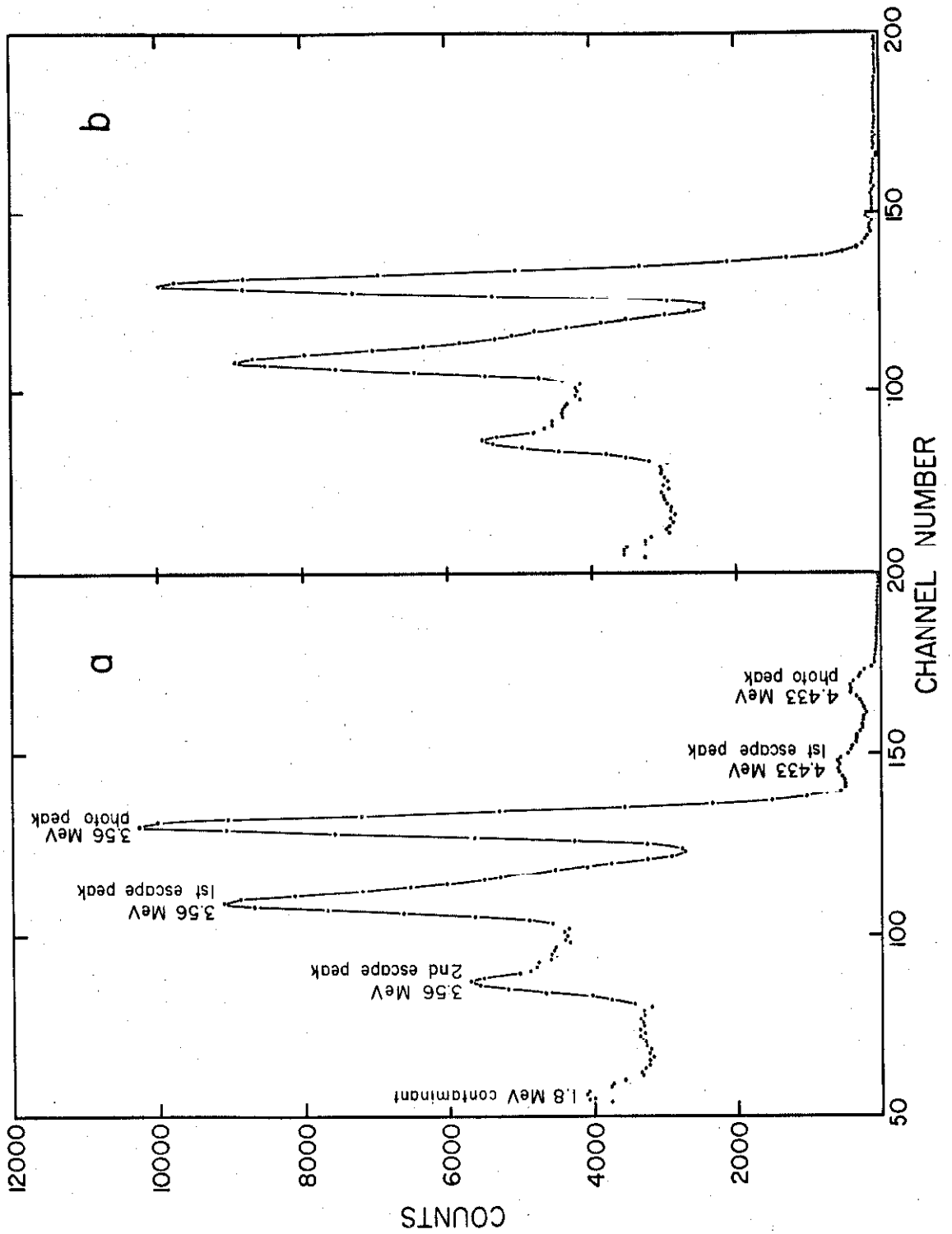

Figure 17

$^{6}Li(p, p'')^{6}Li^{**}$ Angular Distributions

The differential cross section in millibarns per steradian is plotted as a function of the cosine of the center-of-momentum angle. The incident proton laboratory energy and the corresponding ^{7}Be excitation energy are given. Polynomial series stopping at P_3 were used in fitting the curves in Figures 17a and b. (Pages 25 and 26)

FIGURE 17 158

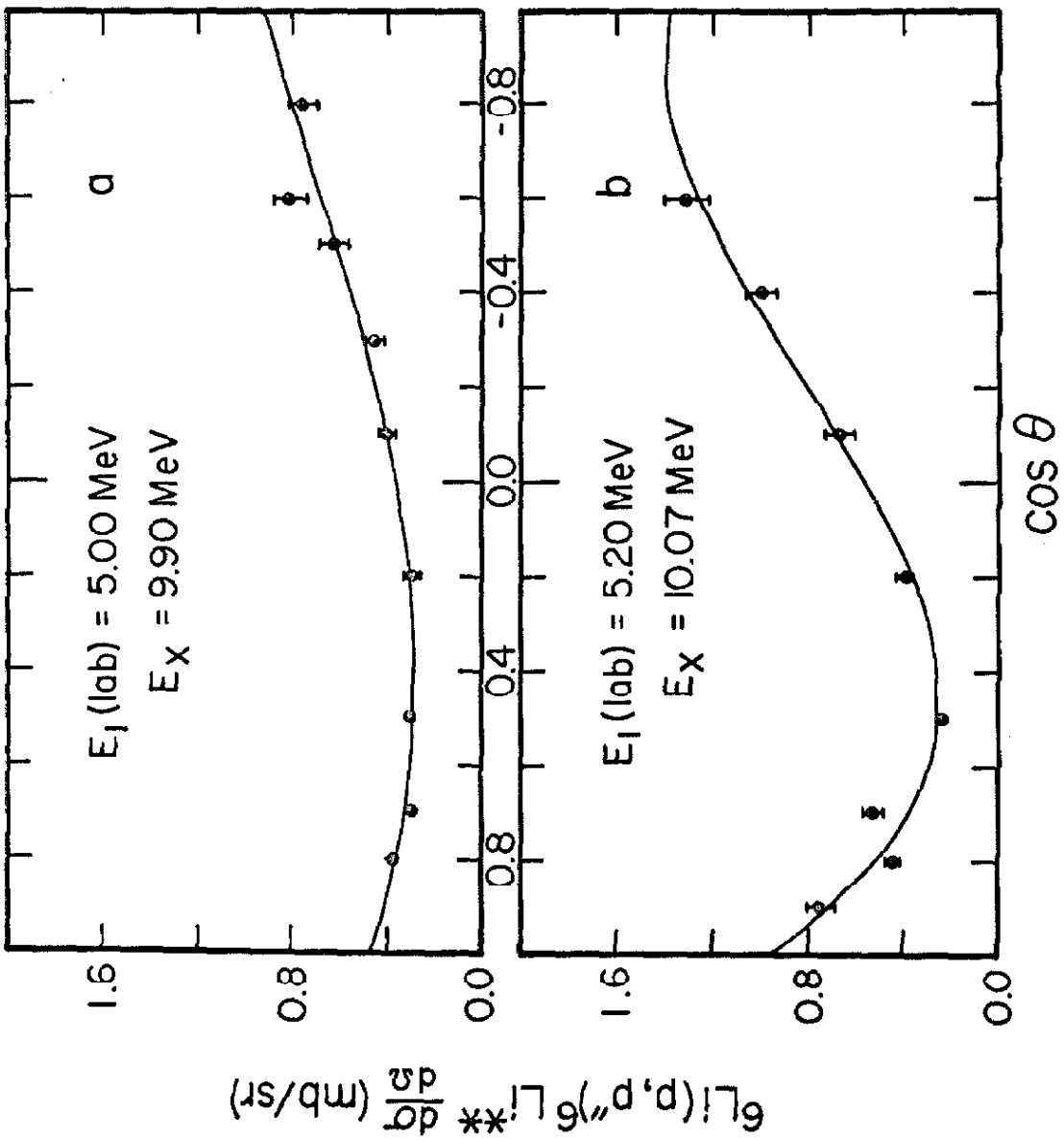

Figure 18
$^{6}Li(p, p'')^{6}Li^{**}$ Angular Distributions

Polynomial series stopping at P_3 were used in fitting the curves in Figures 18a and b. Two sets of data are shown in Figure 18b. The data obtained by the direct subtraction technique are represented by circles. The data obtained by the p-γ coincidence technique are represented by squares. (Pages 24, 25 and 26)

FIGURE 18 160

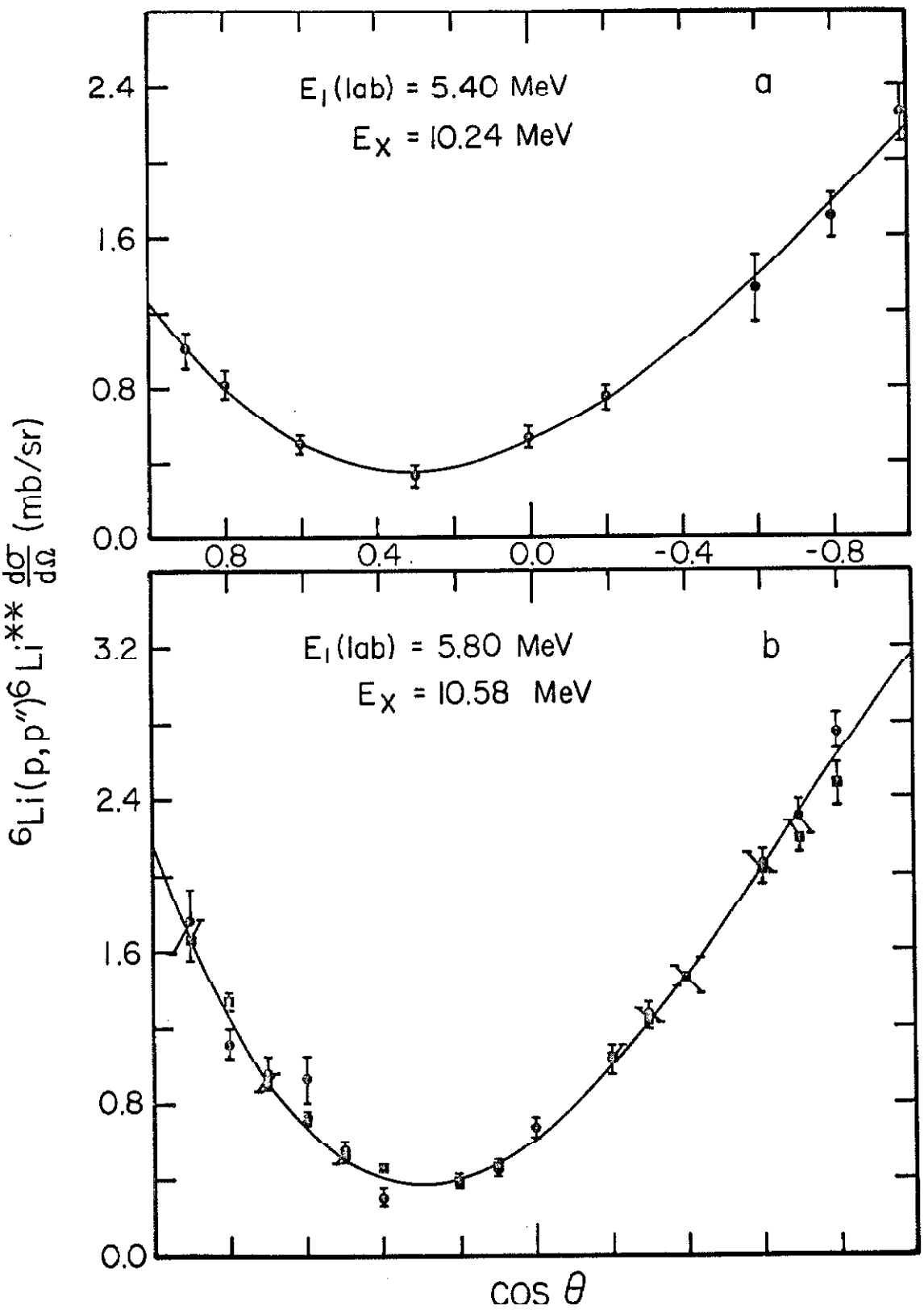

Figure 19
$^{6}Li(p, p'')^{6}Li^{**}$ Angular Distributions

Polynomial series stopping at P_3 were used in fitting the curves in Figures 19a and b. (Pages 25 and 26)

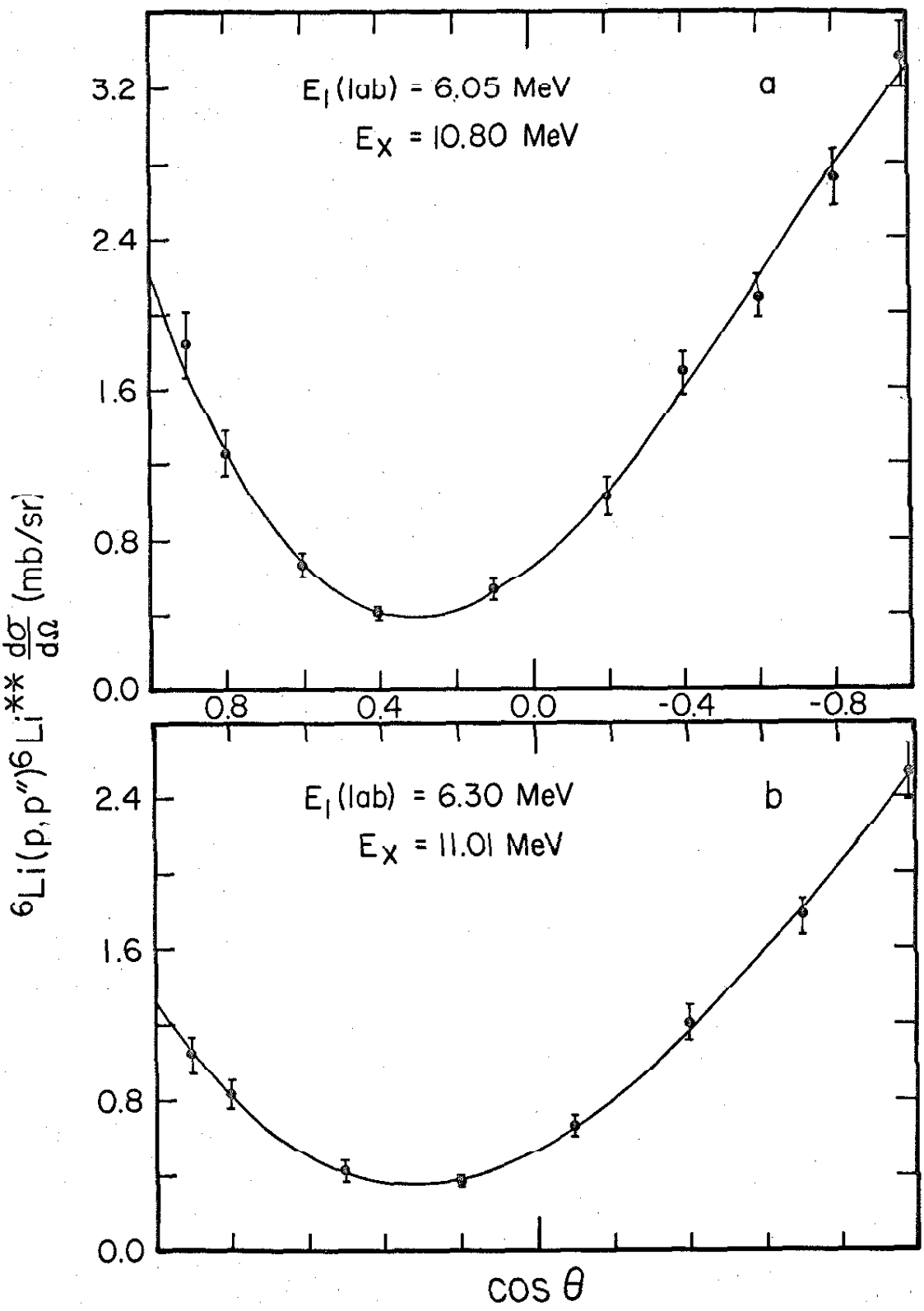
E_I(lab) = 6.05 MeV
E_X = 10.80 MeV
a
E_I(lab) = 6.30 MeV
E_X = 11.01 MeV
b
$^6Li(p,p'')^6Li^{**}$ $\frac{d\sigma}{d\Omega}$ (mb/sr)
cos θ
3.2
2.4
1.6
0.8
0.0
0.8
0.4
0.0
-0.4
-0.8

Figure 20

$^{6}Li(p, p'')^{6}Li$ Angular Distributions

Polynomial series stopping at P_3 were used in fitting the curves in Figures 20a and b. (Pages 25 and 26)

FIGURE 20 164

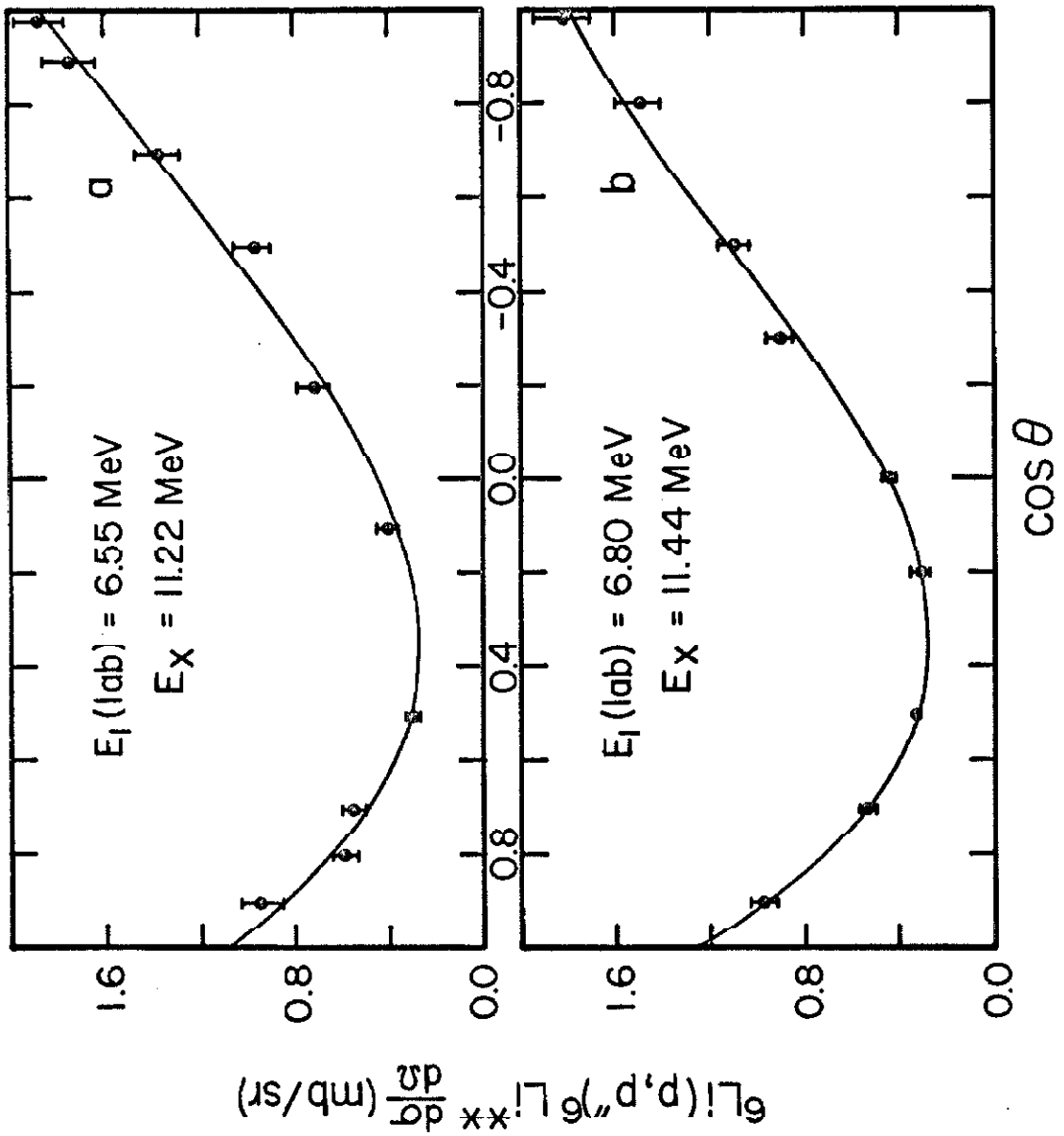

Figure 21

$^{6}Li(p, p'')^{6}Li^{**}$ Angular Distributions

Polynomial series stopping at P_3 were used in fitting the solid curve in Figure 21a and the dashed curve in Figure 21b. A polynomial series stopping at P_4 was used in fitting the solid curve in Figure 21b. (Pages 25 and 26)

FIGURE 21 166

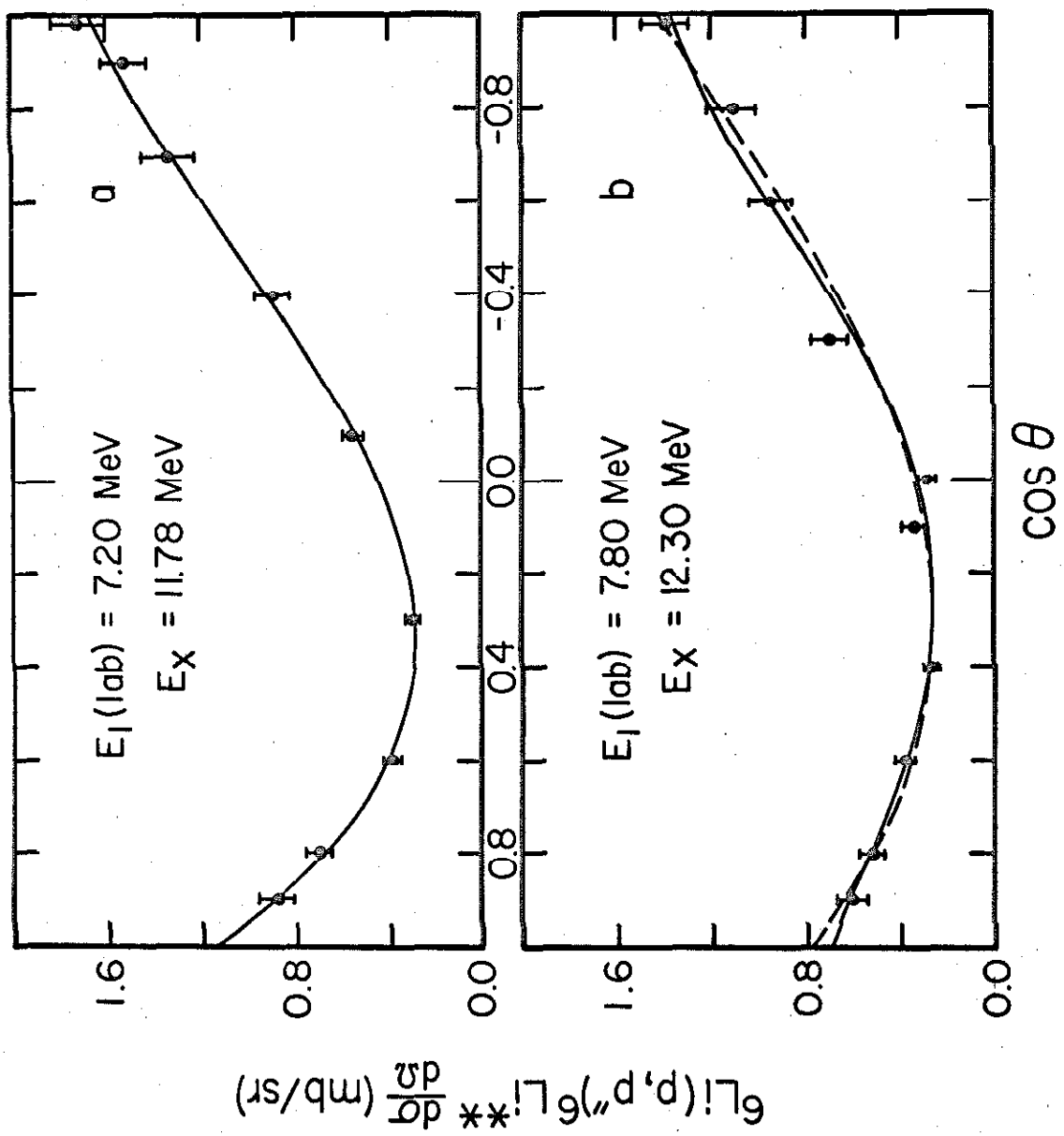

Figure 22

$^{6}Li(p, p'')^{6}Li^{**}$ Angular Distributions

Polynomial series stopping at P_4 were used in fitting the curves in Figures 22a and b. (Pages 25 and 26)

FIGURE 22 168

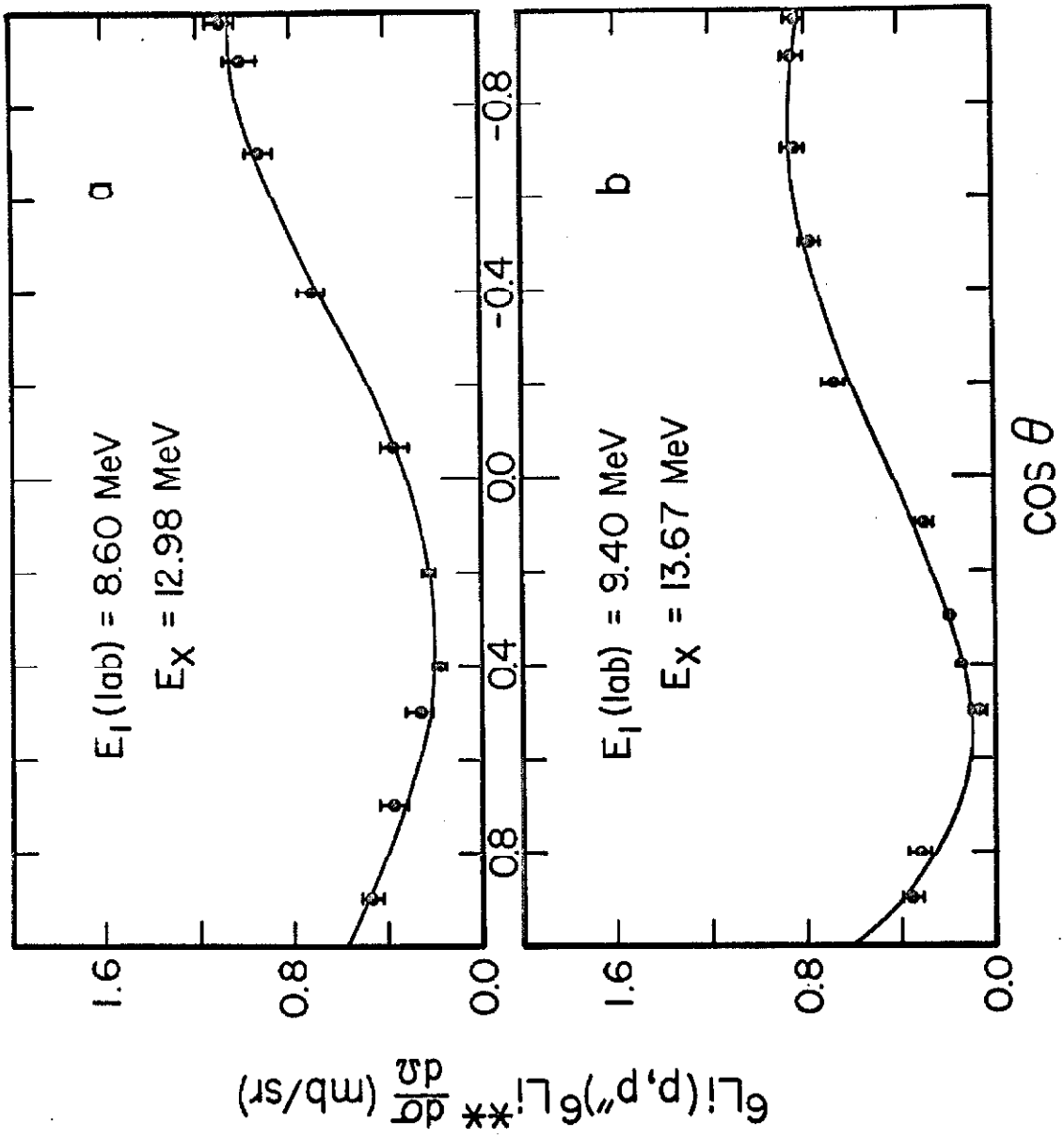

Figure 23
$^{6}Li(p, p'')^{6}Li^{**}$ Polynomial Coefficients

The coefficients of the Legendre polynomials P_0 to P_4 and their errors are plotted. Each coefficient is labelled by the polynomial. The data represented by circles were obtained from the angular distributions. The data represented by the squares and by the triangles were obtained from the γ-ray measurements with the 5.08- by 5.08-cm and 7.62- by 7.62-cm detectors respectively. The coefficient of polynomial P_0 is equal to the total cross section σ divided by 4π. (Pages 20, 26, 58 and 63)

FIGURE 23 170

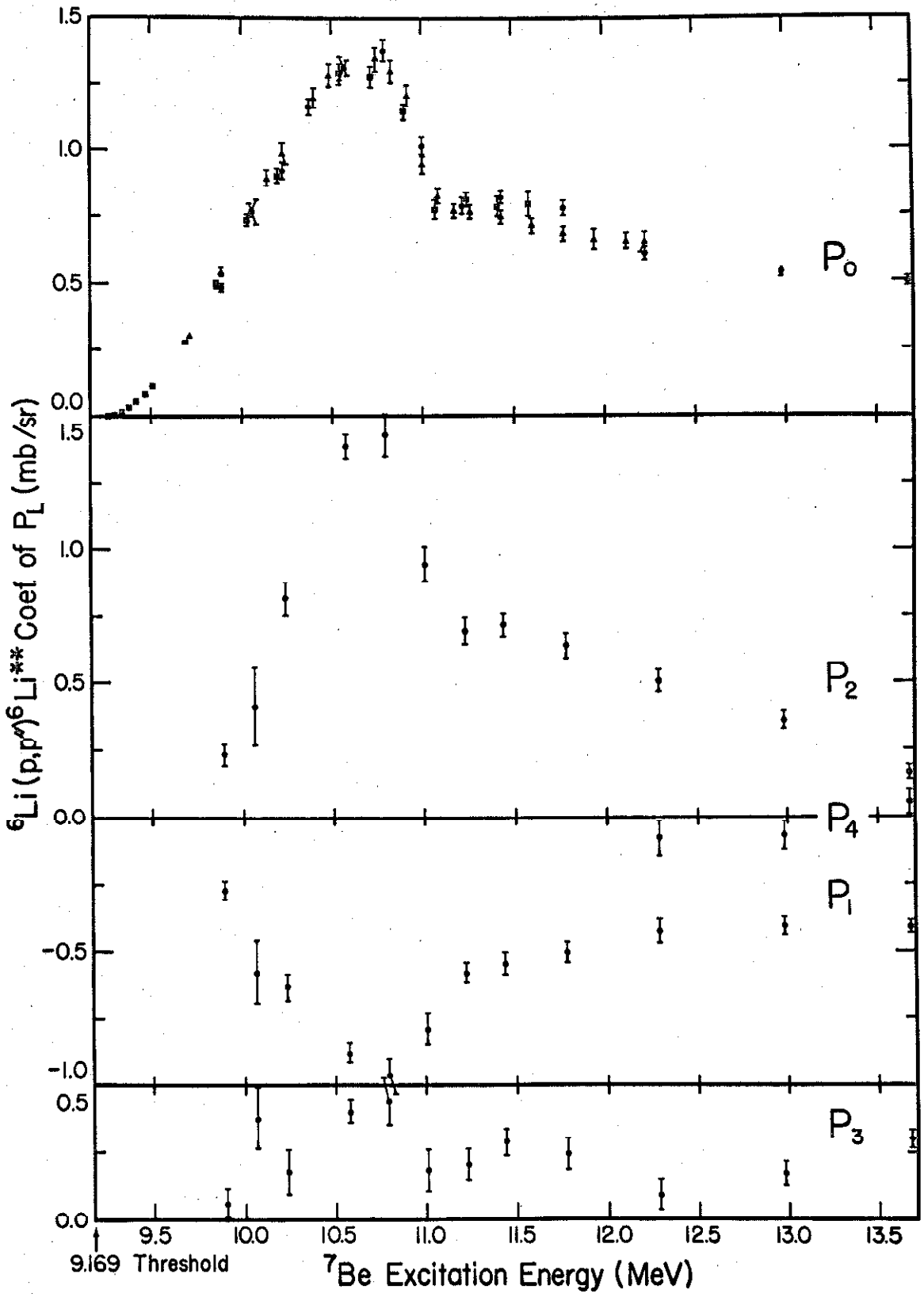

Figure 24
Apparatus Used to Study the $^{4}He(^{3}He, p'')^{6}Li^{**}$ Reaction

Essential components that have not been labelled in this assembly drawing are the collimating apertures (8) and (6), the anti-scattering baffle (7), and the 6250 Å nickel foil (23). The teflon insulator flange (3) contains an electron suppressor ring (12). This flange assembly is held together with nylon screws (27). (Page 26)

FIGURE 24 172

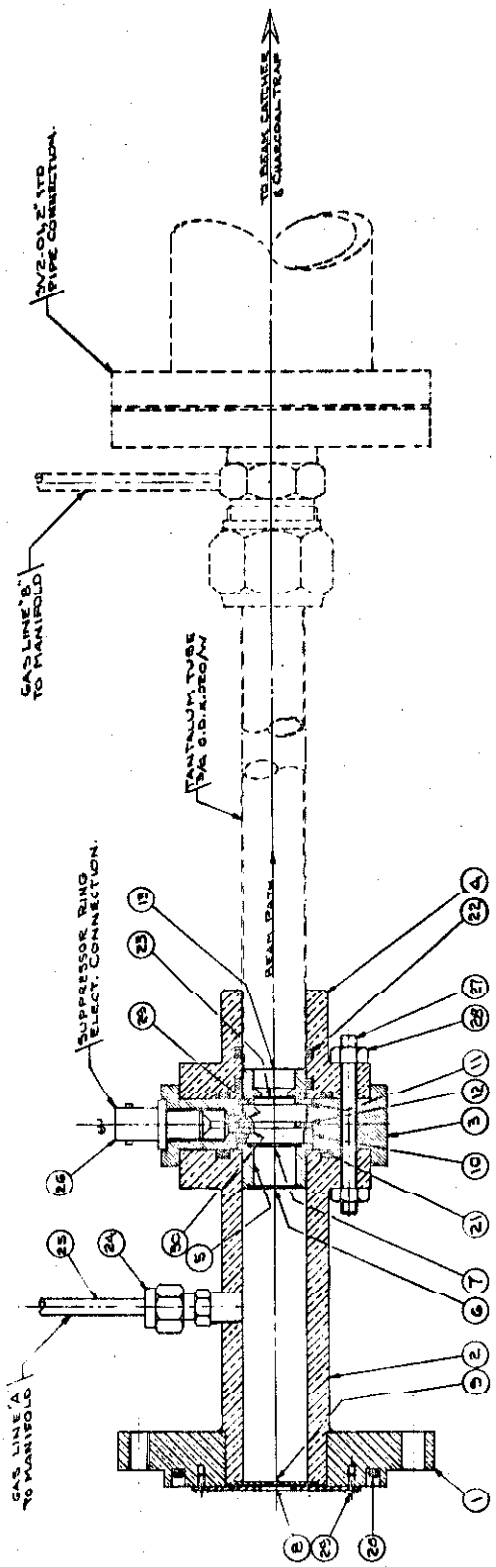

Figure 25

$^{4}He(^{3}He, p'')^{6}Li^{**}$ Data and Fit

The data are subject to an overall normalization error of about 20%. The solid curve represents a two-level fit over the entire range of data. Radius-dependent penetration factors with $\ell = \ell' = 1$ have been used and the arbitrary background represented by the dashed curve has been subtracted. The parameters of the fit are:

E_1 (MeV)	Γ_1	E_2	Γ_2	C_1 (MeV^2)	C_2	ζ	χ^2 ÷(degrees of freedom)
9.91	1.8	10.95	0.323	1.28	0.0103	180.9^{o}	7.0

(Pages 31, 64 and 65)

FIGURE 25 174

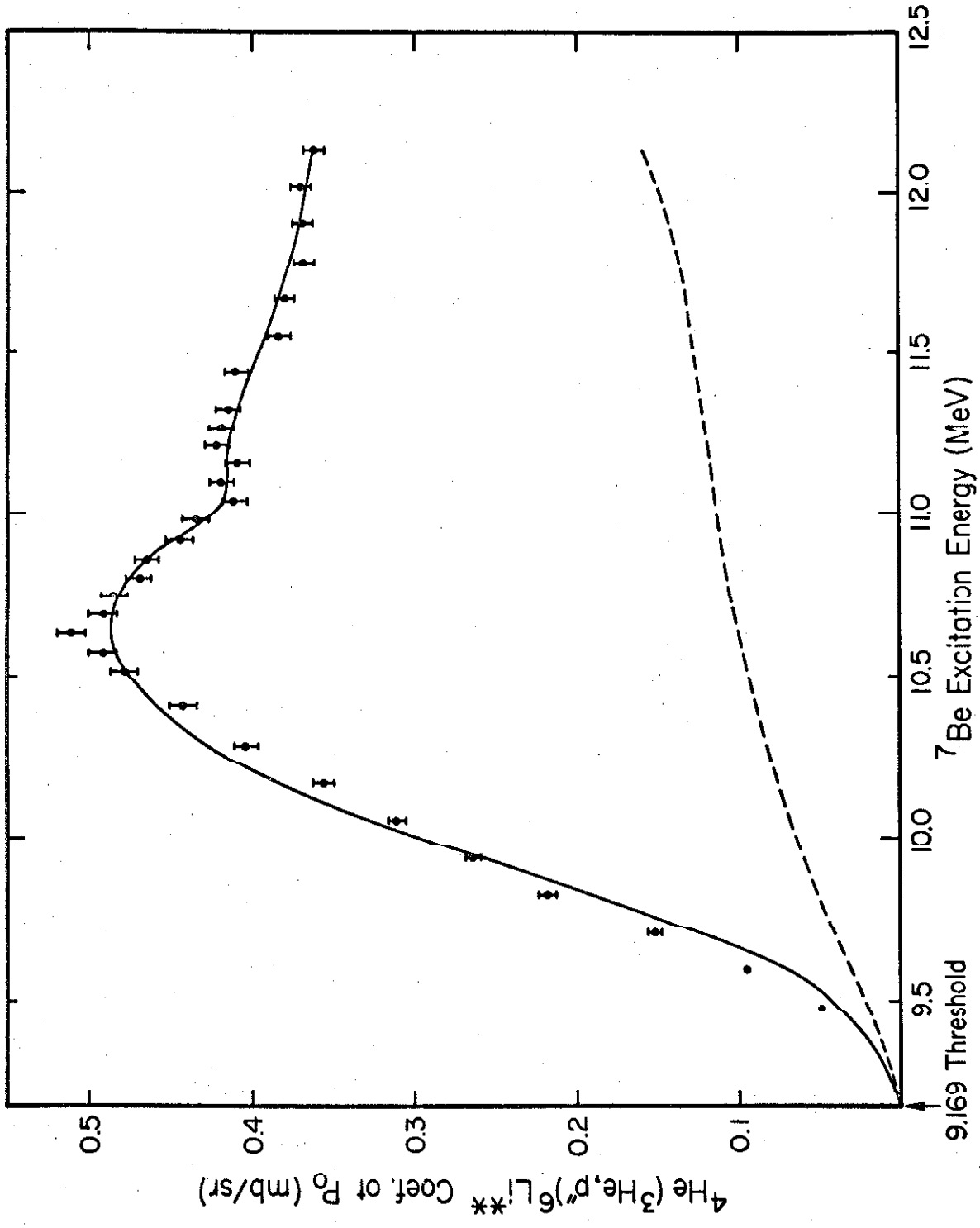

Figure 26
Relative Normalization of the $^{6}Li(p, ^{3}He)^{4}He$ and $^{4}He(^{3}He, p)^{6}Li$ Reactions

The data represented by squares were obtained from the ^{3}He groups in the particle spectra from the $^{6}Li + p$ induced reaction; the data represented by circles, from the ^{4}He groups. The normalization is the same as that of the $^{6}Li(p, p)^{6}Li$ data of McCray (1962), and a smooth curve has been drawn through the data points. The other data, obtained from the $^{4}He(^{3}He, p)^{6}Li$ reaction and the use of reciprocity, were normalized to the smooth curve. The data represented by x's were obtained in collaboration with Professor Tombrello; the data represented by triangles, by Spiger and Tombrello (1964). (Page 33)

FIGURE 26 176

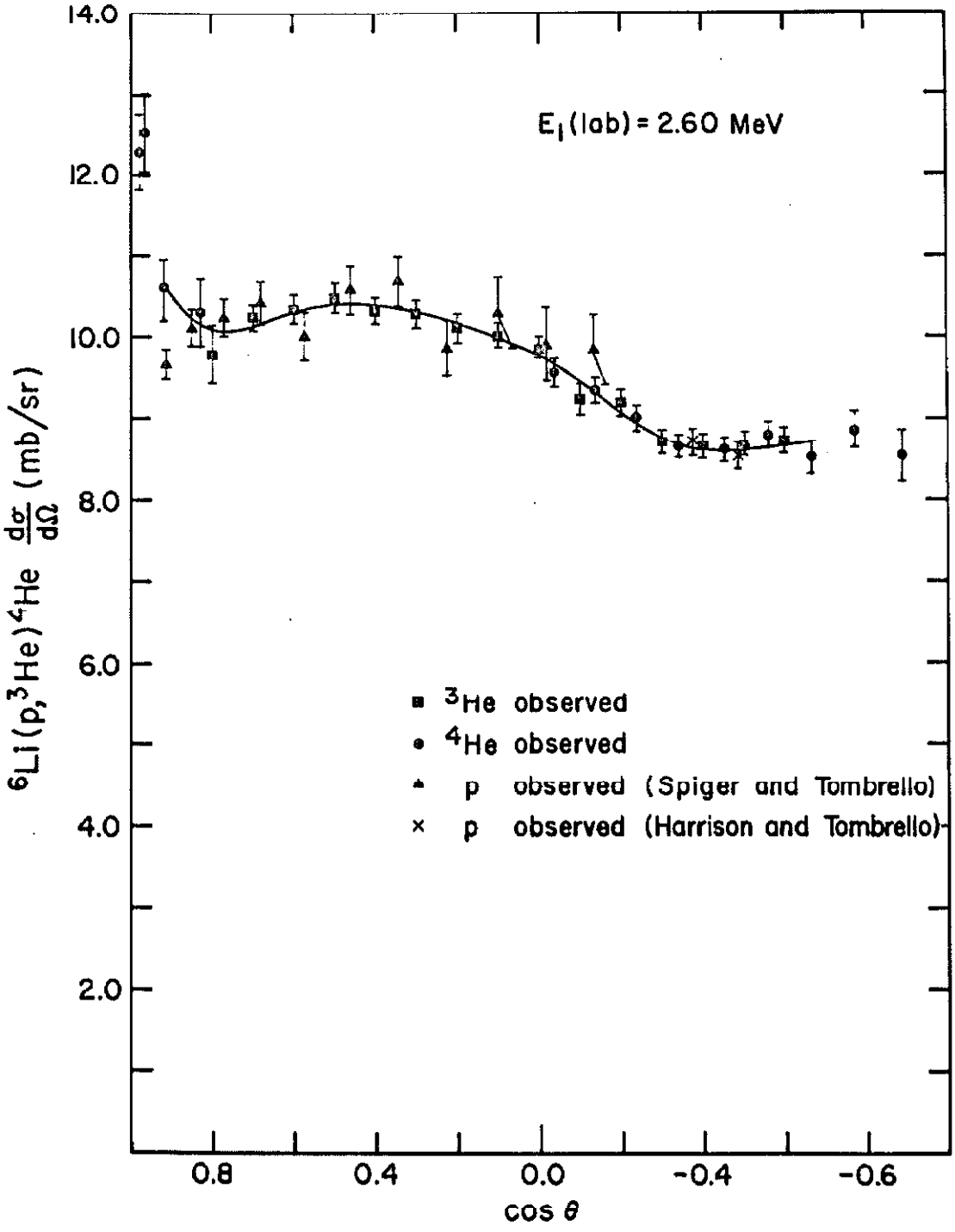

Figure 27

Penetration Factors

The radius-dependent (R-matrix) penetration factors, equation (9), and the radius-independent (Humblet-Rosenfeld) factors, equation (6), for $^{6}Li + p$ are shown on a logarithmic scale. The radius-dependent factors have been evaluated for a radius of $4.08\ 10^{-13}$cm. The radius-dependent factors are actually the factors defined by Humblet (1964a) multiplied by k. (Page 50)

FIGURE 27

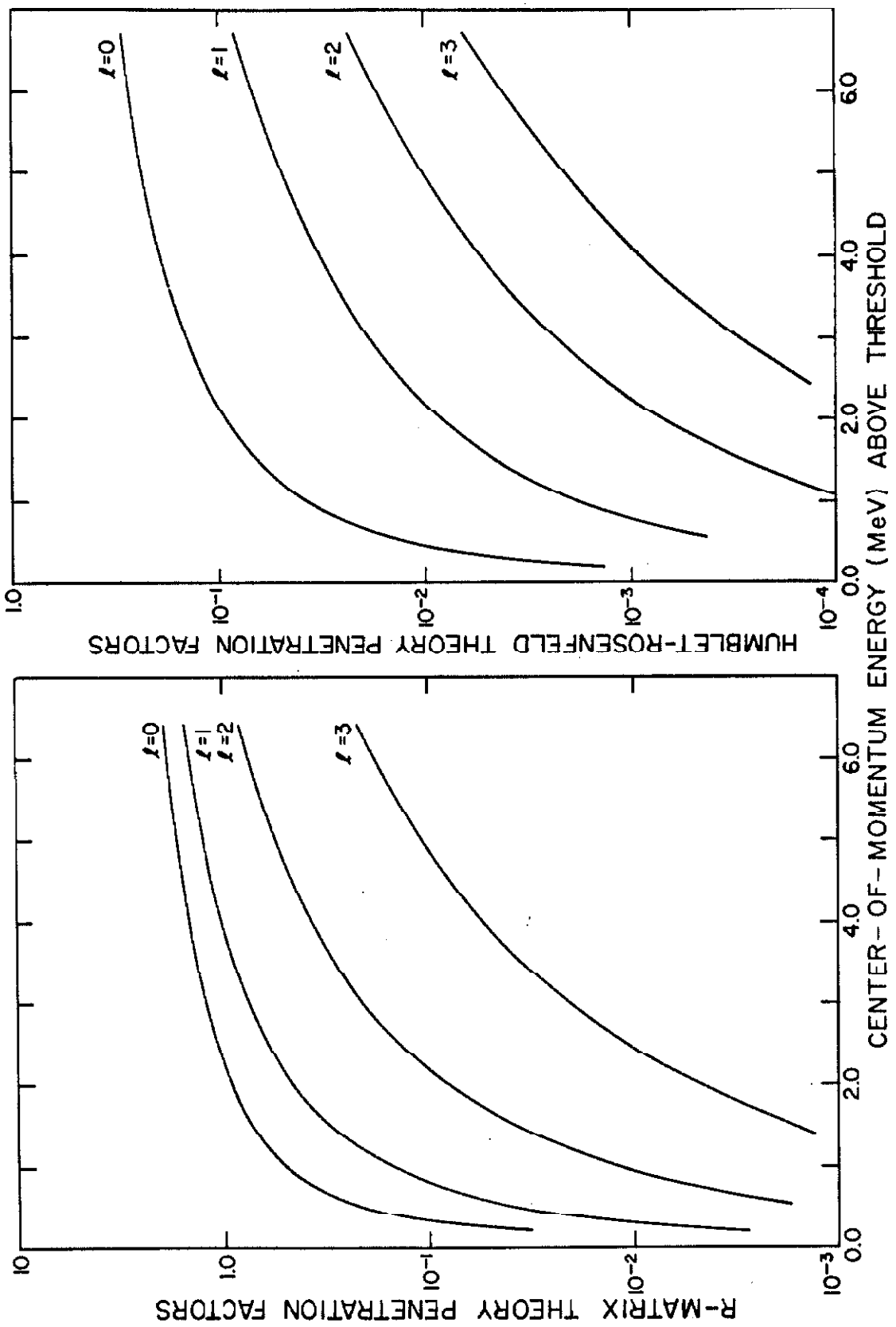
HUMBLET-ROSENFELD THEORY PENETRATION FACTORS
1.0
10^{-1}
10^{-2}
10^{-3}
10^{-4}
0.0
2.0
4.0
6.0
$\ell=0$
$\ell=1$
$\ell=2$
$\ell=3$
R-MATRIX THEORY PENETRATION FACTORS
10
1.0
10^{-1}
10^{-2}
10^{-3}
0.0
2.0
4.0
6.0
$\ell=0$
$\ell=1$
$\ell=2$
$\ell=3$
CENTER-OF-MOMENTUM ENERGY (MeV) ABOVE THRESHOLD

Figure 28

$^{6}Li(p, p')^{6}Li^{*}$ Single-Level Fits to the P_2 Coefficient

Radius-dependent and radius-independent penetration factors have been used in Figures 28a and b respectively. The solid curves are for $\ell = \ell' = 1$; the dashed curves, for $\ell = 3$, $\ell' = 1$. Fits are not possible for any other allowed combinations of ℓ values. The parameters of the fits are given in Table 11. (Page 57)

FIGURE 28

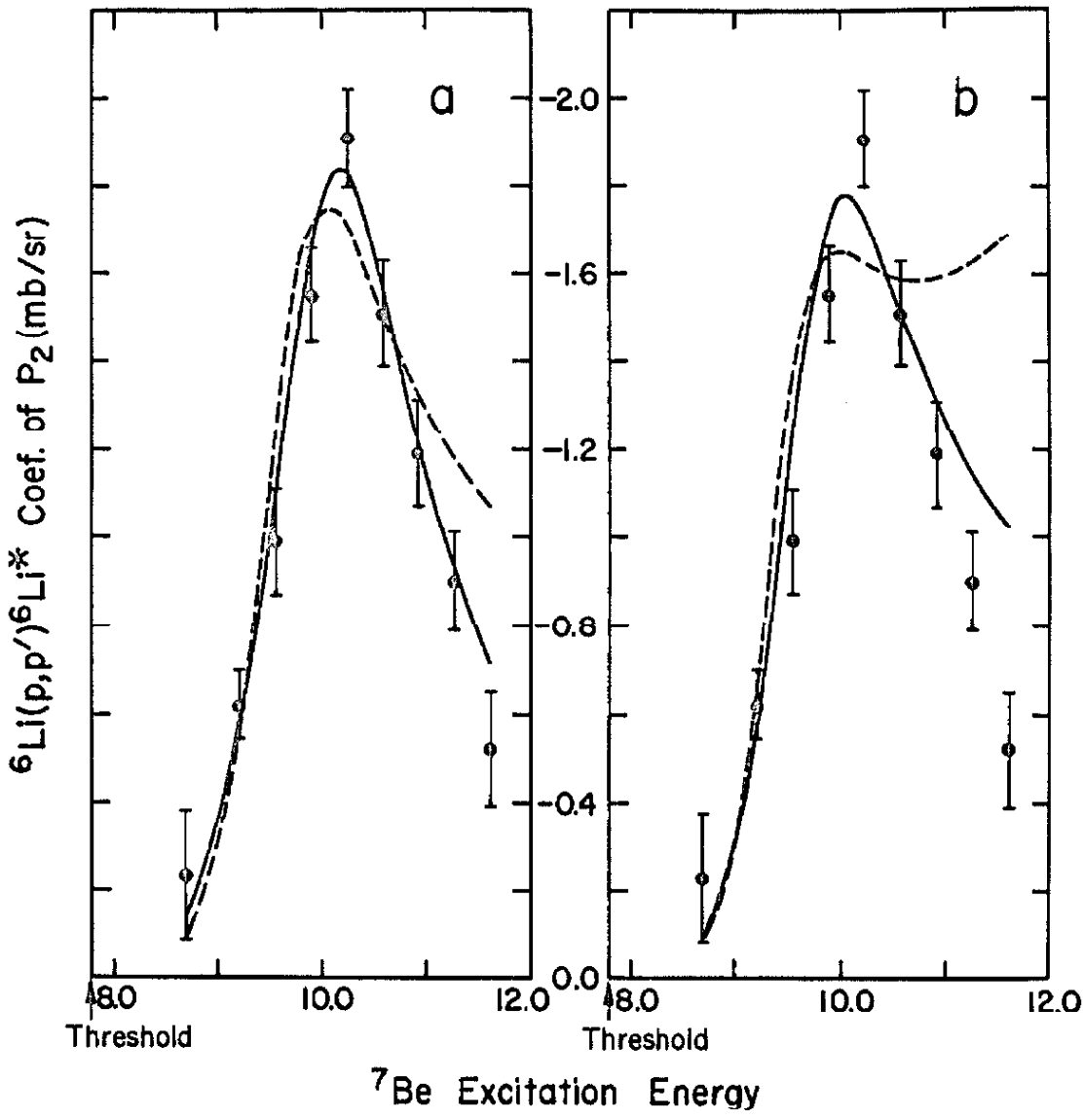
a
b
-2.0
-1.6
-1.2
-0.8
-0.4
0.0
8.0
10.0
12.0
Threshold
Threshold
^{6}Li(p,p')^{6}Li* Coef. of P$_2$(mb/sr)
^{7}Be Excitation Energy

Figure 29

$^{6}Li(p, p'')^{6}Li^{**}$ Fits to the P_0 Coefficient

The data have been fitted from 10.4- to 11.6-MeV ^{7}Be excitation energy. Radius-independent penetration factors have been used in a; radius-dependent factors in b to h. In all cases $\ell = \ell' = 1$. The extra curve in d represents approximately the contribution from the broad state alone. The parameters of the fits are

	E_1 (MeV)	Γ_1	E_2	Γ_2	D (MeV^3)	$\chi^2 \div$(degrees of freedom)
a	9.91	1.6	10.95	0.400	2.87	6.57
b	10.01	1.6	10.79	0.298	1.13	3.84
c	10.01	1.7	10.87	0.323	1.37	2.31
d	10.01	1.8	10.95	0.323	1.56	1.35
e	10.11	1.7	10.95	0.323	1.33	1.42
f	10.21	1.7	10.95	0.323	1.22	1.61
g	10.11	1.7	11.01	0.323	1.39	1.02
h	10.01	1.8	10.95	0.400	1.96	1.30

(Pages 62, 63, 76, 78 and 123)

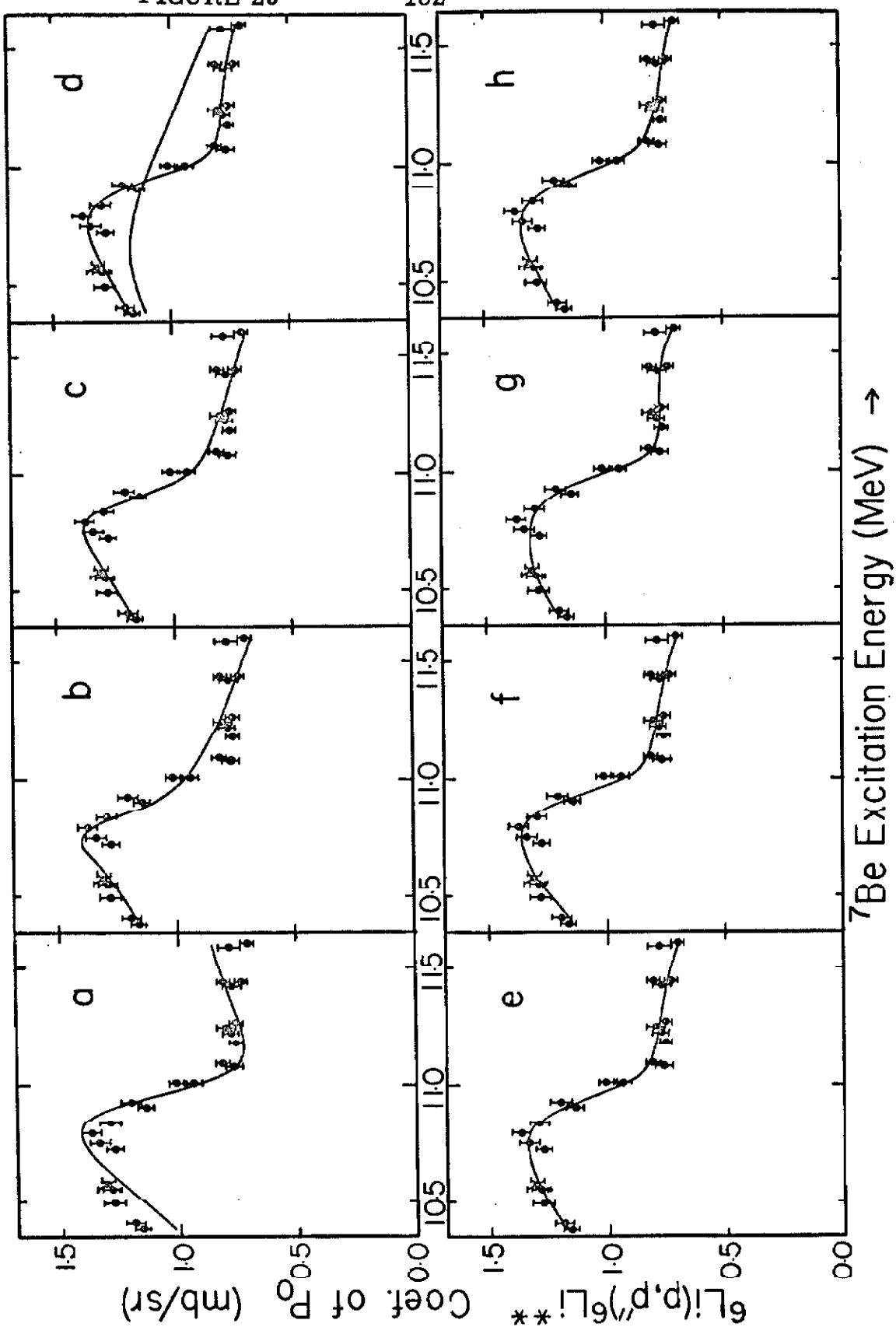
a
b
c
d
e
f
g
h
10.5
11.0
11.5
0.0
0.5
1.0
1.5
$^6Li(p,p'')^6Li^{**}$ Coef. of P_0 (mb/sr)
^7Be Excitation Energy (MeV) →

Figure 30

$^{6}Li(p, p'')^{6}Li^{**}$ Fits to the P_0 Coefficient

The data have been fitted from 10.4- to 11.6-MeV ^{7}Be excitation energy using radius-dependent penetration factors with $\ell = \ell' = 1$. The background shown has been subtracted in d to h. The parameters of the fits are

	E_1 (MeV)	Γ_1	E_2	Γ_2	D (MeV^3)	$\chi^2 \div$(degrees of freedom)
a	9.91	1.7	10.95	0.323	1.62	1.43
b	10.01	1.7	10.95	0.323	1.46	1.41
c	10.11	1.8	11.01	0.400	1.89	1.00
d	10.01	1.7	10.95	0.400	1.36	1.28
e	10.21	1.7	10.95	0.323	0.91	2.44
f	10.01	1.7	10.95	0.323	1.09	1.83
g	9.91	1.7	10.95	0.323	1.20	1.84
h	10.11	1.7	11.01	0.400	1.33	1.42

(Pages 62, 76, 78 and 123)

FIGURE 30

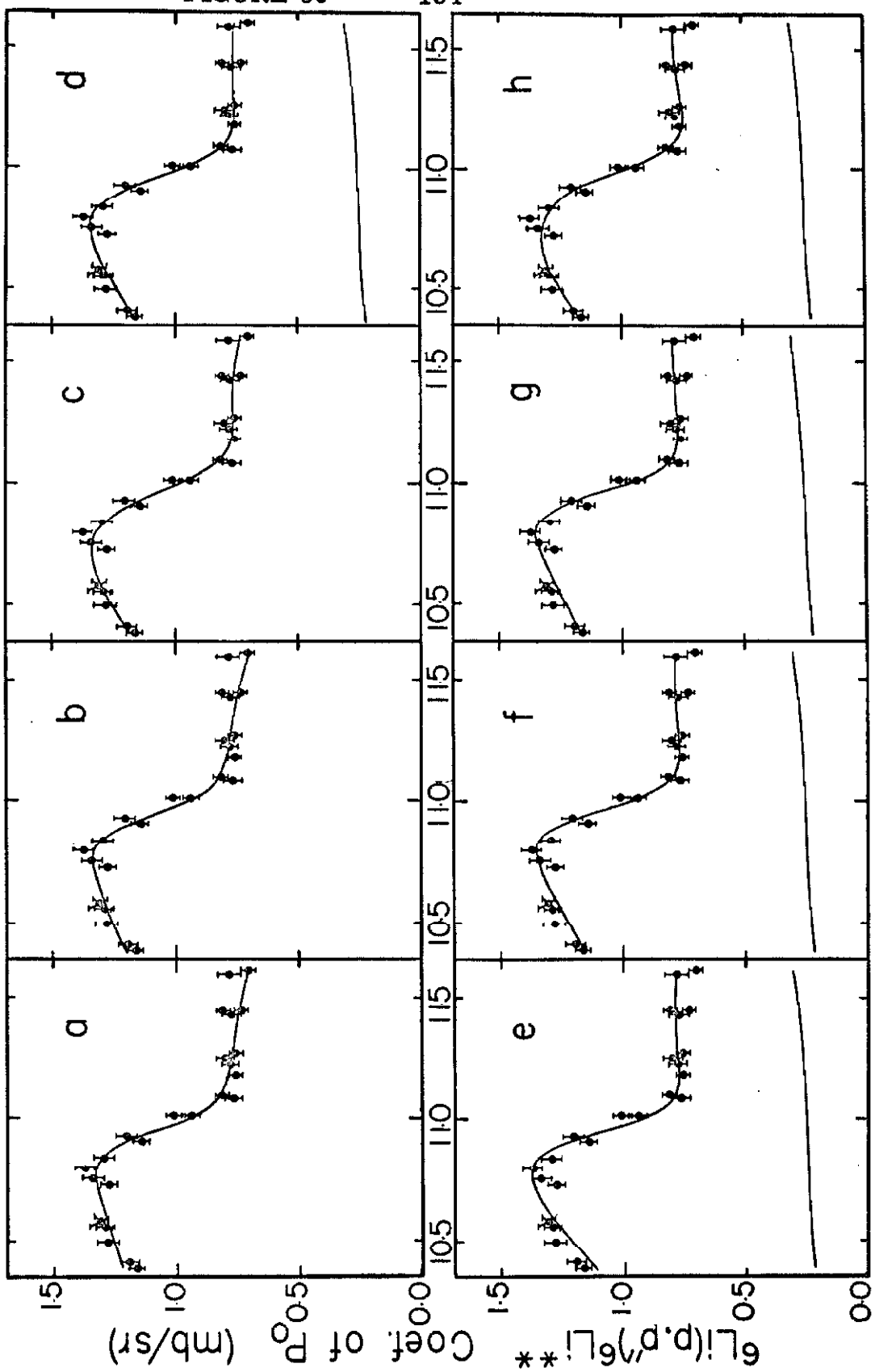
a
b
c
d
e
f
g
h
Coef. of P_0 (mb/sr)
$^6Li(p,p')^6Li^{**}$
^7Be Excitation Energy (MeV) →

Figure 31a

$^{6}Li(p, p'')^{6}Li^{**}$ Fit to the P_0 Coefficient

One of the curves in Figure 31a represents a two-level fit to the data from 9.52- to 12.12-MeV ^{7}Be excitation energy. Radius-dependent penetration factors with $\ell = \ell' = 1$ have been used. The parameters of the fit are

E_1 (MeV)	Γ_1	E_2	Γ_2	D (MeV^3)	χ^2 ÷(degrees of freedom)
9.91	1.8	10.95	0.323	1.7	6.1

The other curve in Figure 31a represents approximately the *contribution from the broad state alone.* *(Page 62)*

Figure 31b

$^{6}Li(p, p'')^{6}Li^{**}$ Fit to the P_2 Coefficient

The curve in Figure 31b represents a two-level fit to the data from 9.90- to 11.78-MeV ^{7}Be excitation energy. Radius-dependent penetration factors with $\ell = \ell' = 1$ have been used. The parameters of the fit are

E_1	Γ_1	E_2	Γ_2	χ^2 ÷(degrees of freedom)
10.41	1.6	10.95	0.323	0.73

(Page 62)

FIGURE 31 186

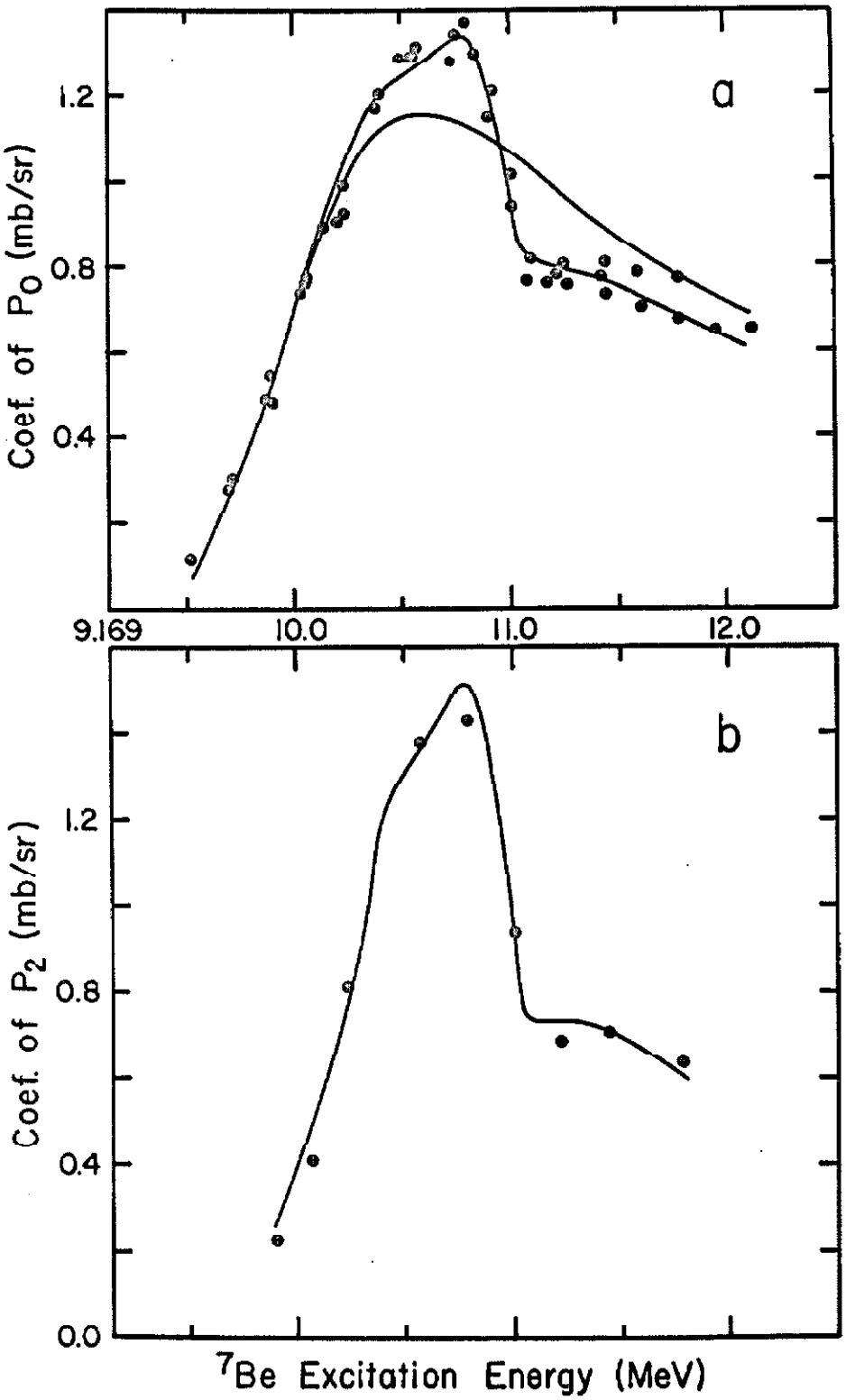

Figure 32

$^{4}He(^{3}He, p'')^{6}Li^{**}$ Fits to the P_0 Coefficient

The data have been fitted from 10.4- to 11.6-MeV ^{7}Be excitation energy using radius-dependent penetration factors with $\ell' = \ell = 1$. The background shown has been subtracted in f to h. The parameters of the fits are

	E_1 (MeV)	Γ_1	E_2	Γ_2	C_1 (MeV^2)	C_2	ζ	χ^2 ÷(degrees of freedom)
a	10.21	1.8	10.95	0.323	1.28	0.0148	220°	2.23
b	10.21	1.8	10.95	0.4	1.30	0.0194	222	1.89
c	10.21	1.8	11.01	0.323	1.28	0.0154	237	1.43
d	10.21	1.8	11.01	0.4	1.30	0.0198	239	1.12
e	10.21	1.8	11.09	0.4	1.28	0.0196	260	0.63
f	10.21	1.8	10.95	0.323	1.12	0.0170	186	1.05
g	10.21	1.8	10.95	0.4	1.12	0.0218	189	0.76
h	10.21	1.8	11.01	0.323	1.12	0.0168	204	1.30

(Pages 65, 79, 80 and 124)

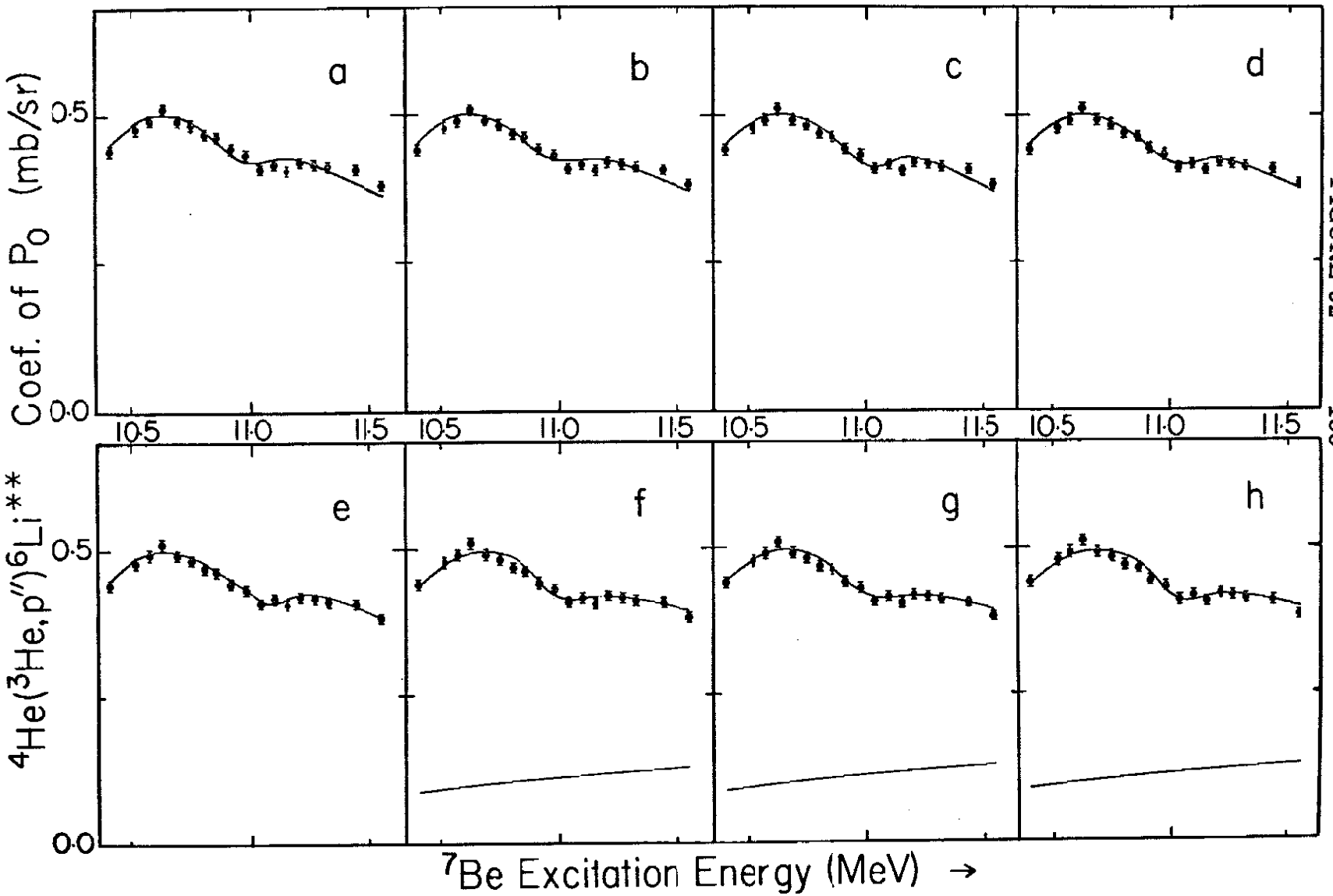
a
b
c
d
e
f
g
h
0·5
0·0
10·5
11·0
11·5
Coef. of P_0 (mb/sr)
$^4He(^3He,p'')^6Li^{**}$
^7Be Excitation Energy (MeV) →

FIGURE 32

Figure 33

$^{4}He(^{3}He, p'')^{6}Li^{**}$ Fits to the P_0 Coefficient

The data have been fitted from 10.4- to 11.6-MeV ^{7}Be excitation energy using radius-dependent penetration factors with $\ell' = \ell = 1$. The background shown has been subtracted. The parameters of the fits are

	E_1 (MeV)	Γ_1	E_2	Γ_2	C_1 (MeV^2)	C_2	ζ	$\chi^2 \div$(degrees of freedom)
a	10.11	1.8	11.01	0.4	1.18	0.0168	209°	0.88
b	10.21	1.8	11.09	0.4	1.14	0.0208	227	1.76
c	9.91	1.8	10.95	0.323	1.28	0.0116	186	1.17
d	10.11	1.7	11.01	0.323	1.12	0.0118	219	0.89
e	10.21	1.7	11.01	0.323	1.08	0.0144	216	0.75
f	10.11	1.8	10.95	0.323	1.16	0.0142	188	0.86
g	10.21	1.8	10.87	0.323	1.10	0.0170	160	1.11
h	10.11	1.8	10.79	0.323	1.14	0.0136	129	1.30

(Pages 65, 79, 80 and 124)

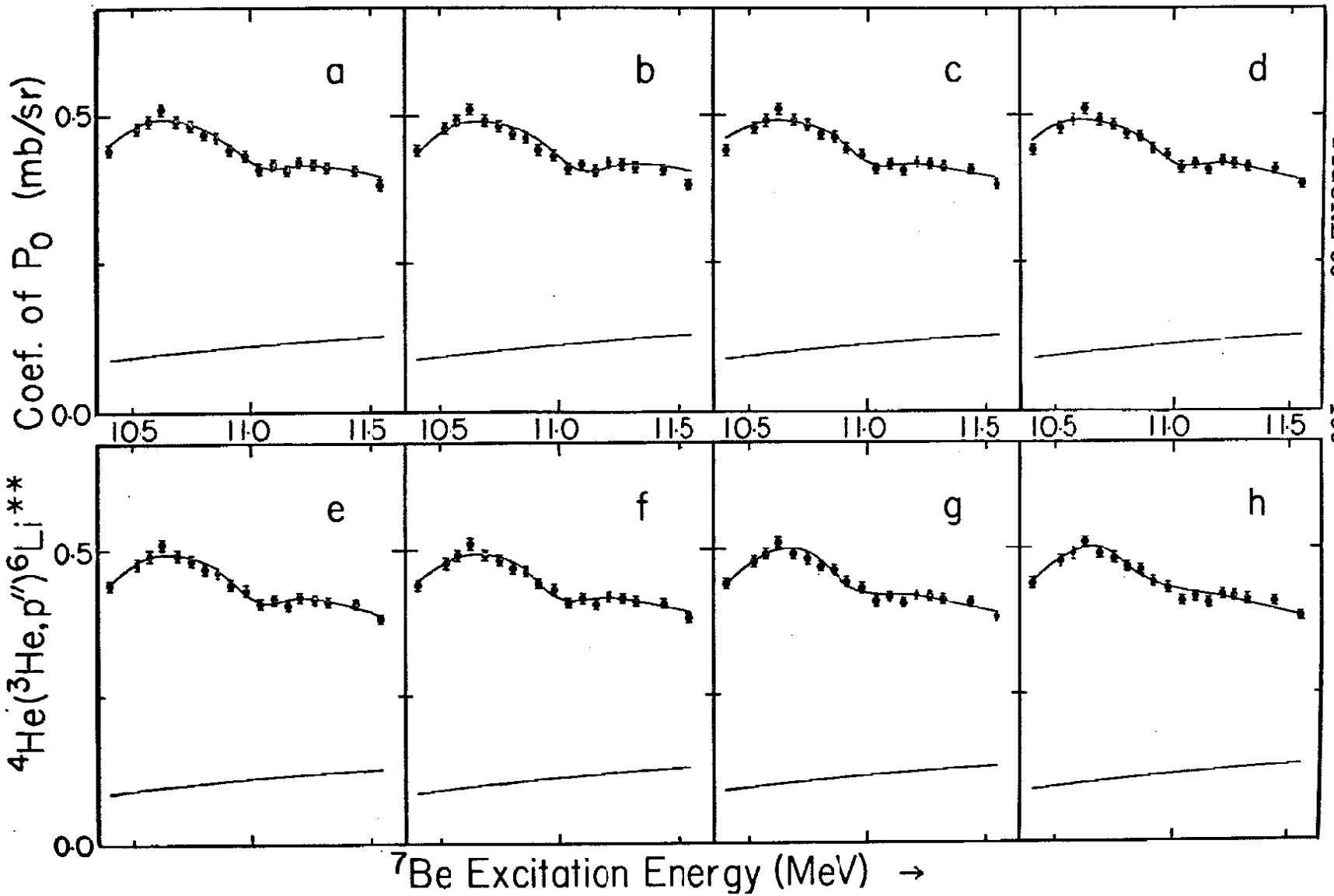
a
b
c
d
e
f
g
h
0·5
0·0
10·5
11·0
11·5
Coef. of P_0 (mb/sr)
$^4He(^3He,p'')^6Li^{**}$
^7Be Excitation Energy (MeV) →

FIGURE 33

Figure 34

Decomposition of the Two-Level Fit

The fitted curve a is the same as that in Figure 33f, and is the sum of the other four curves. Curves b and d represent the single-level contributions of the broad and of the narrower states respectively; curve e represents the contribution from their interference. Curve c represents an arbitrary, non-interfering background. A similar decomposition is obtained if no background is assumed.
(Pages 66 and 80)

FIGURE 34 192